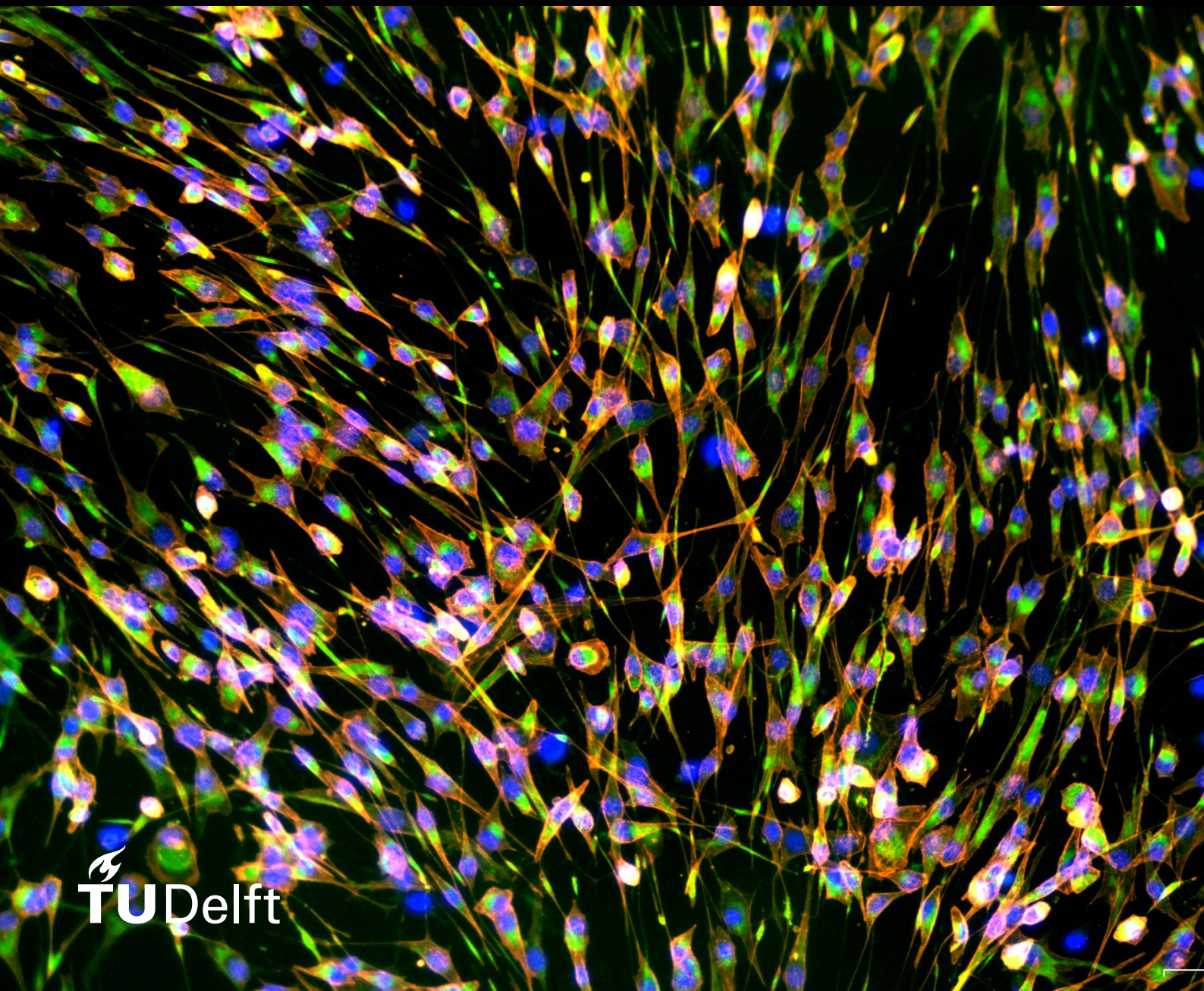


# Bioprinting of Zonal Cartilage Scaffolds Using Different Cell Densities

A biomimetic approach on cartilage regeneration

Angeliki Dimaraki





# 3D Bioprinting of Zonal Cartilage Scaffolds Using Different Cell Densities; A biomimetic approach on cartilage regeneration

By

**Angeliki Dimaraki**

in partial fulfilment of the requirements for the degree of

**Master of Science**

**in Biomedical Engineering**

at the Delft University of Technology,

to be defended publicly on Tuesday July 14, 2020.

Supervisory team: Prof. dr A. A. Zadpoor (chair)  
Assistant Prof. dr. ir. L. Fratila-Apachitei  
Dr. M. Mirzaali, TU Delft  
Dr. P. D. Payno, TU Delft, Erasmus MC  
Phd Candidate M. N. Ghouski, TU Delft

*This thesis is confidential and cannot be made public until July 14, 2023.*

An electronic version of this thesis is available at <http://repository.tudelft.nl/>.



# Preface

*Angeliki Dimaraki*  
*Delft, July 2020*

This thesis project was carried out at the department of Biomechanical Engineering of Delft's University of Technology as part of the curriculum of MSc Biomedical Engineering. The fabrication of the scaffolds was carried out in the Cytocompatibility and Biointerfaces Laboratory (TU Delft), while the histological experiments were performed in the Orthopaedics department of Erasmus MC.



# Abstract

The use of allografts for the treatment of critical size cartilage defects holds disadvantages including the limited number of donors and the compromised chondrocyte viability. These limitations have prompted researchers to explore different options, such as cartilage engineering. Bioprinting, a promising tissue engineering technique, could be used to fabricate biomimetic constructs that can potentially replace allografts. The present study explores the generation of a biomimetic chondrocyte density gradient in full-thickness bioprinted Alginate/NFC scaffolds with a PCL framework and investigates the effect of this zonal distribution of cells on the production of cartilage matrix within the scaffolds. To this end, two types of scaffolds were bioprinted; one with a graded three-zone distribution of cells (bottom zone:  $5 \times 10^6$  cells/ml, middle zone:  $10 \times 10^6$  cells/ml, top zone:  $20 \times 10^6$  cells/ml), and another with a homogeneous cell density ( $10 \times 10^6$  cells/ml) and cultured for 25 days. Furthermore, the mechanical properties of the multi-material scaffolds were evaluated. The results showed that a three-zone cell density gradient could be achieved using extrusion-based bioprinting. The gradient was maintained for 25 days in scaffolds cultured in non-chondrogenic media (absence of ascorbic acid) but was transformed into a two-zone gradient within the first 14 days, in cultures with chondrogenic media (presence of ascorbic acid in the medium), and maintained as such until the end of the experiment. The zonal distribution of cells led to a zonal distribution of sGAGs, after 14 days of culture, with the sGAGs deposition being increased in the areas of high cell density. However, there was no significant Collagen deposition within the scaffolds at any time point during the experiment. This study attempts to shed light into one of the gradients of the native cartilage tissue (cell density gradient), with the hope of contributing to the development of a biomimetic fully functional engineered cartilage scaffold in the future.



# Acknowledgements

I would like to express my sincere gratitude to my supervisor Assistant professor Dr.ir. E. Lidy Fratila-Apachitei who gladly helped me with the selection of the graduation project and trusted me enough to make me the first person to be working with the new bioprinter our lab had just acquired. For giving me this chance to work on such an interesting and important subject as the bioprinting of zonal cartilage scaffolds with a biomimetic cell density gradient, I cannot thank her enough. Together with PhD student Mahdiyeh Nouri-Goushki and Assistant professor Mohammad J. Mirzaali, they have been monitoring my progress, listening carefully to my ideas and concerns, and advising me regularly. During the months of the project they all stood by me with patience and understanding while providing me with feedback during the research process. Hence, their help has been of outmost significance for the completion of this project. Also, I owe a special thanks to Michelle Minneboo, who besides a very skilled lab technician who tended to my every need or question in the lab, has been a great company and friend during the long working hours in the lab, making things easier at times of stress or disappointment. I am also grateful to Prof. dr. Gerjo J.V.M. van Osch, Dr. Roberto Narciso and technician Nicole Kops from the Orthopaedics department of Erasmus MC who welcomed me to work there for the histological analysis of my samples and assisted me with the histological protocols and tests, by giving their expert opinion. Most of all, I would like to thank postdoc Pedro Diaz Payno. Ever since he joined our lab in December 2019, he has monitored my project during every step and has assisted me throughout the biochemical and histological procedures of the project. He made all the arrangements for me to work at Erasmus MC, taught me the tissue processing techniques and staining processes in practice, and helped me every way he could, during the long bioprinting experiments. I felt more secure working in the lab when he was around and I could always reach out to him for advice. I am so very thankful for our collaboration, as this project would have ended up a lot different if he was not around. Finally, I would like to thank my family without whom I would not have achieved my goals today. My parents and siblings - even though far away - they urged me to pursue this MSc degree and managed to give me strength and support whenever I needed it. A sweet text, two words over the phone, or an unexpected package here and there, was enough to renew my motive. Last but not least, a great thank you to all of my friends – the old ones and the ones I made here during my degree – who with their love and support helped me in this journey. Marianna, Dimitri, Thaleia, Shaiv, Marina, Ilia, your friendship has been an invaluable gift to me.



# Contents

Preface.....	ii
Abstract.....	i
Acknowledgements .....	iii
List of Figures.....	vii
List of Tables.....	xiii
Abbreviations.....	xv
<b>1. Introduction</b> .....	<b>1</b>
1.1 Articular Cartilage: Characteristics and Functions.....	1
1.2 Zonal Characteristics of Cartilage.....	2
1.3 Cartilage Injury & Treatment Strategies.....	4
1.4 Cartilage Engineering.....	7
1.4.1 Bioprinting Techniques.....	8
1.4.2 Gradient Scaffolds.....	10
1.4.3 Biomaterial Selection .....	11
1.5 Project Objectives.....	13
<b>2. Materials and Methods</b> .....	<b>14</b>
2.1 Experimental Procedures.....	14
2.1.1 Parametric Study – Optimization of Printing Parameters .....	14
2.1.2 Scaffolds Design .....	16
2.1.3 Cell Culture .....	18
2.1.4 Bioprinting.....	20
2.1.5 Mechanical Characterization of the Scaffolds.....	26
2.1.6 Immunohistochemical Evaluation of Cells and Scaffolds.....	27
2.1.7 Histochemical Evaluation of the Scaffolds .....	31
2.2 Data Analysis.....	35
2.2.1 Image Analysis .....	35
2.2.2 Statistical Analysis.....	39
<b>3. Results</b> .....	<b>40</b>
3.1 Design, Fabrication and Mechanical Characterization of the Scaffolds .....	40
3.2 Bioprinting of the scaffolds with different cell densities .....	42
3.3 ECM deposited by the cells embedded in the zonal scaffolds.....	49

<b>4. Discussion</b> .....	63
4.1 Design, Fabrication, and Mechanical Characterization of the Scaffolds .....	63
4.1.1 Cell Type Selection – Cell Culture .....	63
4.1.2 Scaffold Design.....	65
4.1.3 Bioprinting.....	66
4.1.4 Mechanical Characterization .....	67
4.2 Evaluation of the Cell Density Gradient’s Generation .....	69
4.3 Tissue Formation in the Cell-Embedded Scaffolds .....	70
4.3.1 Cell Density Gradient.....	70
4.3.2 ECM Deposition.....	72
4.4 Limitations of the Study – Future Recommendations .....	74
<b>5. Conclusion</b> .....	76
<b>Bibliography</b> .....	77
APPENDIX A: Optimization of Printing Parameters .....	85
APPENDIX B: 2D Chondrocyte Culture.....	89
APPENDIX C: Comparison of the Scaffold’s Designs .....	91
APPENDIX D: Images of the Bioprinted Scaffolds .....	93
APPENDIX E: Mechanical Characterization .....	94

# List of Figures

**Figure 1:** The main characteristics and functions of articular cartilage (adjusted from <https://www.arthritis-health.com/types/joint-anatomy/what-cartilage>). ..... 1

**Figure 2:** Illustration of a cartilage unit. The figure depicts the differences in cell morphology and cell density, as well as in extracellular matrix fiber arrangement along the cartilage's thickness (Ansari et al. 2019). ..... 3

**Figure 3:** Illustration of some of the most important gradients of the articular cartilage. As the cellular and molecular compositions of the articular cartilage vary from the superficial zone to the radial zone and porosity increases, a depth-dependent change is induced in the mechanical properties of the articular cartilage. A deeper color along the cartilage zones represents an increase of the included characteristics, while, conversely, a lighter color indicates a decrease of the included features (Ansari et al. 2019). ..... 3

**Figure 4:** (a) Healthy knee articular cartilage. (b) Damaged knee articular cartilage [from Mayo Clinic]..... 4

**Figure 5:** Images of the most common cartilage repair techniques used in the clinic. (a) Microfracture. (b) Autografting-Mosaicplasty. (c) Allograft implantation. (d) Autologous chondrocyte implantation. (e) Total joint replacement. Images (a) – (d) have been modified and reproduced from Getgood et al. 2009..... 7

**Figure 6:** A general process for bioprinting 3D tissues. . Cells are isolated from an organism, cultured in plates in order to proliferate and then are mixed with a biocompatible hydrogel. Then, the cell-embedded hydrogels are printed to create the scaffolds, which can then be used for transplantation into a patient, or for in vitro studies (Modified by Mandrycky et al. 2015)..... 9

**Figure 7:** Illustrations of the main different bioprinting methods. (a) Inkjet bioprinters deposit small droplets of hydrogel and cells to build tissue layer-by-layer. (b) Microextrusion bioprinters deposit a cell-laden liquid solution via pneumatic or manual force. (c) Laser-assisted bioprinting uses a laser to rapidly heat a donor layer (green), which forms a bubble propelling the bioink onto the substrate. (d) Stereolithography bioprinters use UV or visible light to selectively cross-link bioinks layer by layer to build a 3D construct (Foyt et al. 2018). ..... 10

**Figure 8:** Requirements for selecting a bioink for cartilage scaffolds using extrusion bioprinting (Gopinathan et al. 2018, Desimone et al. 2015, Parak et al. 2019)..... 13

**Figure 9:** Cellink's chart with the recommended pressures for PCL, according to the nozzle size and the print speed. The company recommends to use the above parameters during printing with PCL. It is also recommended to start printing with PCL with a temperature of 180°C (Cellink PCL Application Note, 15 February 2019). .... 14

**Figure 10:** Study design schematic. (a) The construct with the cell density gradient and the construct with the homogeneous cell distribution (control samples) were fabricated from bottom to top, using the corresponding cell densities for each of their zones. (b) Three cell seeding density groups ( $20 \times 10^6$ ,  $10 \times 10^6$ , and  $5 \times 10^6$  cell/mL) were used for the generation of the graded scaffolds and one cell seeding density group ( $10 \times 10^6$ ) was used for the generation of the homogeneous scaffolds.

These constructs were cultured in vitro and harvested at 0, 2, and 4 weeks for live/dead assay, and histological analysis. The pellets were generated using  $0.5 \times 10^6$  cells/ml, cultured for 0, 2, 4 weeks and used only for histology, while the empty scaffolds were cultured and harvested only at 0 and 4 weeks for histology. Ajusted from Ren et al.2016. .... 22

**Figure 11:** The steps of generating the cell-embedded hydrogel for each of the different cell densities. (a) The desired amount of material for each zone is placed in syringes. (b) The corresponding cell suspensions are added to the syringes containing the appropriate hydrogel volume. (c) With the use of a luer-lock and a second syringe the cells and the hydrogel are gently mixed together by mixing back and forth. (d) The final mixtures are concentrated in one syringe and transferred to new cartridges for bioprinting. .... 24

**Figure 12:** (a) Illustration of an unconfined compression test (Boschetti et al. 2004). (b) Configuration of the LLOYD LR5k machine used for the mechanical characterization of the scaffolds..... 27

**Figure 13:** In viable cells, the selective permeability of the membrane allows for calcein entry, but prevents EthD-1 from entering the cells (calcein+/EthD-1-). As a consequence, live cells appear green. During late apoptosis, membrane degradation creates pores in the plasma membrane allowing EthD-1 to enter the cells (calcein+/EthD-1+). Finally, the necrosis stage is characterized by membrane loss, so these last cells appear only red (calcein-/PI+) (Basmacıyan et al. 2017). .... 27

**Figure 14:** The procedure of cutting the scaffold in half, before Live-Dead staining, and imaging the cross section under the ZOE fluorescent microscope. The thicknesses of the three scaffold zones are not illustrated in their actual scale..... 28

**Figure 15:** The principle of direct and indirect immunofluorescence processes with the corresponding antibodies..... 30

**Figure 16:** Workflow of the tissue (or scaffold) processing steps during a general histological evaluation process. .... 31

**Figure 17:** Tissue embedded in paraffin (tissue block) with the cassette attached to it and the metallic mold in which it had been casted (adapted from <https://www.protocolsonline.com/histology/sample-preparation/paraffin-processing-of-tissue/>). .... 32

**Figure 18:** TWS pipeline for pixel classification. First, image features are extracted from an input image using Fiji-native methods. Next, a set of pixel samples is defined and represented as feature vectors, and a WEKA learning scheme is trained on those samples and finally applied to classify the remaining image data. The user can then interactively provide feedback by correcting or adding labels (Arganda-Carreras et al. 2017)..... 36

**Figure 19:** (a) H&E image ( $\times 10$  magnification) of is opend in Image J. (b) The brightness and the contrast of the image are each increased by 40%, to get a clearer distinction of the cell nuclei. (c) The image is transformed into an 8-bit (greyscale) image by splitting it into the three color channels (red, green, blue). The best channel which allows for better distinction of the nuclei from the background, is selected for further analysis (green channel). (d) The threshold is being adjusted in order to

achieve optimal object separation from the background. (e), (f), (g) The threshold color is shifted to black & white and the regions of interest corresponding to the three scaffold zones are set. (h) The three zones are analyzed separately for their cell number and the results of these images are evaluated by comparing them with the initial image, using the outlines of the distinct particles. The zones are defined from left to right starting from the bottom layer. The scale bars represent 0.2 mm. .... 37

**Figure 20:** (a) Alcian Blue image ( $\times 10$  magnification) is opened in Image J. (b) The Weka segmentation plugin is employed to classify the areas corresponding to cells, sGAGs and background stain. (c) The segmented image is transformed into a grayscale image by splitting it into the three channels according to the defined classes. The channel which allows for better distinction of the sGAGs from the background, is selected for further analysis. (d) The threshold is being adjusted in order to achieve optimal object separation from the background. (e), (f), (g) The regions of interest corresponding to the three scaffold zones (bottom, middle, top) are set. (h) The three zones are analyzed separately for their sGAGs content and the results of these images are evaluated by comparing them with the initial image, using the outlines of the distinct areas corresponding to sGAGs. Scale bars = 0.2 mm. .... 38

**Figure 21:** (a) Design of the PCL framework (left) and the full scaffold (PCL + hydrogel) (right) with their respective dimensions in mm. (b) Schematic representation of the PCL and the PCL + hydrogel parts with a  $0^{\circ}$ – $90^{\circ}$  infill pattern and a 10% infill density. The image illustrates the distinct layers of the scaffolds' parts with a highlight on the final printed zone (15<sup>th</sup> zone). (c) Compressive stiffness of the PCL and the PCL + hydrogel parts, respectively. (d) Viability data for the selected design, after bioprinting, at day 0. The images were obtained from the bottom and top planes of the printed scaffolds (N=2). The scale bars in the live/dead staining represent 100  $\mu\text{m}$ . 41

**Figure 22:** (a) Illustrations of the expected cell distribution patterns, graded (left) and homogeneous (right), throughout the zones of the designed scaffolds. (b) Live–dead images of a cross section of the scaffolds at days 0, 14 and 25. For the graded scaffolds the cross section is expected to yield an increasing amount of green fluorescent, when moving from the bottom to the top layers (when moving from left to right in the images), indicative of the increasing cell density. On the other hand, the cross section of a homogeneous scaffold is not expected to display any significant difference in the amount of green fluorescent between the scaffolds zones. The zones are divided from each other with a vertical blue line on the images and the scale bar represents 100  $\mu\text{m}$ . .... 43

**Figure 23:** H&E images of the bioprinted scaffolds cultured in medium without ascorbic acid after 0, 14 and 28 days showing the localization of the cell nuclei. The images shown in the box on the top left, illustrate a full stained slice of the scaffold (scale bar = 0.5 mm), while the higher magnification images on the bottom illustrate a specific region of interest of the slice, indicated by a rectangle on the top left image (scale bar = 0.2 mm). The dashed lines represent the borders of each of the scaffolds' three zones (bottom, middle, top). All images were acquired using a DM500 Leica optical microscope. .... 44

**Figure 24:** Graphs a, b, and c depict the mean and standard deviation of the 2D cell density (number of cells/ $\text{mm}^2$ ) as calculated for the two scaffold groups (graded and homogeneous), for the different scaffold zones (bottom, middle, top) and for days 0,

14 and 28, respectively. Each scaffold group was composed of N=2 samples, and the cell density calculation was obtained by image analysis of the H&E stained histological sections. The error bars show the standard deviation..... 45

**Figure 25:** Between-zones comparison of the cell density (cells/mm<sup>2</sup>) within the constructs with a cell density gradient and within the constructs with homogeneous cell distribution, for days 0, 14 and 28. The \*, \*\*, \*\*\*, and \*\*\*\* indicate significance of p<0.05, p<0.01, p<0.001 and p<0.0001, respectively, while the “ns” indicates a non-significant difference. The error bars show the standard deviation (n=2). ..... 46

**Figure 26:** Zone-by-zone comparison of the cell density (cells/mm<sup>2</sup>) between constructs with a cell density gradient and constructs with homogeneous cell distribution, for days 0, 14 and 28. The \*, \*\*, and \*\*\* indicate increasing significance levels (with p<0.05, p<0.01, and p<0.001, respectively), and the “ns” indicates a non-significant difference. The error bars show the standard deviation (n=2). ..... 46

**Figure 27:** Comparison of the initial cell density with which the cells were embedded in the hydrogel, before printing (theoretical cell density), and the cell density measured from the H&E histological images of the scaffolds at 0, 14 and 28 days after bioprinting (experimental cell density). The ns indicates no significant difference (p>0.05) between two values..... 48

**Figure 28:** Histological images of the bioprinted scaffolds cultured after 0, 14 and 25 days and stained for localization of the cell nuclei (Hematoxylin & Eosin), sGAGs (Alcian Blue) and Collagen (Picrosirius Red). The images shown in the box on the top left, illustrate a full stained slice of the scaffold (scale bar = 0.5 mm), while the higher magnification images on the bottom illustrate a specific region of interest of the slice, indicated by a rectangle on the top left image (scale bar = 0.2 mm). The dashed lines represent the borders of each of the scaffolds’ three zones (bottom, middle, top). All images were acquired using a DM500 Leica optical microscope..... 51

**Figure 29:** Between-zone comparison of the cell density (cells/mm<sup>2</sup>) within the constructs with a cell density gradient and within the constructs with homogeneous cell distribution, for days 0, 14 and 25. The \*, \*\*, \*\*\*, and \*\*\*\* indicate significance of p<0.05, p<0.01, p<0.001 and p<0.0001, respectively, while the “ns” indicates a non-significant difference. The error bars show the standard deviation (n=3). ..... 52

**Figure 30:** Zone-by-zone comparison of the cell density (cells/mm<sup>2</sup>) between constructs with a cell density gradient and constructs with homogeneous cell distribution, for days 0, 14 and 28. The \*, \*\*, and \*\*\* indicate increasing significance levels (with p<0.05, p<0.01, p<0.001 and p<0.0001, respectively, while the “ns” indicates a non-significant difference. The error bars show the standard deviation (n=3). ..... 53

**Figure 31:** Cell densities for each of the individual graded scaffolds for (a) day 0, (b) day 14 and (c) day 25. At day 0, all scaffolds were generated with the desired cell density gradient. At both days 14 and 25 there is one out of the three samples that maintains the cell density gradient (consisted of three different densities), throughout the scaffold’s zones. .... 54

**Figure 32:** Comparison of the initial cell density with which the cells were embedded in the hydrogel, before printing (theoretical cell density), and the cell density measured from the H&E histological images of the scaffolds at 0, 14 and 28 days after

bioprinting (experimental cell density). The ns indicates no significant difference ( $p>0.05$ ) between two values..... 55

**Figure 33:** Percentage of the total amount of sGAGs (total sGAGs area in a slice/slice area) within the constructs with a cell density gradient and within the constructs with homogeneous cell distribution, for days 0, 14 and 25. The \*, \*\*, \*\*\*, and \*\*\*\* indicate significance of  $p<0.05$ ,  $p<0.01$ ,  $p<0.001$  and  $p<0.0001$ , respectively, while the “ns” indicates a non-significant difference. The error bars show the standard deviation ( $n=3$ ). ..... 57

**Figure 34:** Between-zone comparison of the sGAGs percentage (sGAGs area in a zone/zone area) within the constructs with a cell density gradient and within the constructs with homogeneous cell distribution, for days 0, 14 and 25. The \*, \*\*, \*\*\*, and \*\*\*\* indicate significance of  $p<0.05$ ,  $p<0.01$ ,  $p<0.001$  and  $p<0.0001$ , respectively, while the “ns” indicates a non-significant difference. The error bars show the standard deviation ( $n=3$ ). ..... 58

**Figure 35:** Percentage of the total amount of Collagen (total Collagen area in a slice/slice area) within the constructs with a cell density gradient and within the constructs with homogeneous cell distribution, for days 0, 14 and 25. The \*, \*\*, \*\*\*, and \*\*\*\* indicate significance of  $p<0.05$ ,  $p<0.01$ ,  $p<0.001$  and  $p<0.0001$ , respectively, while the “ns” indicates a non-significant difference. The error bars show the standard deviation ( $n=3$ ). ..... 59

**Figure 36:** Between-zone comparison of the Collagen percentage (Collagen area in a zone/zone area) within the constructs with a cell density gradient and within the constructs with homogeneous cell distribution, for days 0, 14 and 25. The \*, \*\*, \*\*\*, and \*\*\*\* indicate significance of  $p<0.05$ ,  $p<0.01$ ,  $p<0.001$  and  $p<0.0001$ , respectively, while the “ns” indicates a non-significant difference. The error bars show the standard deviation ( $n=3$ ). ..... 60



# List of Tables

<b>Table 1:</b> Cellink’s table with the recommended pressures for Bioink, according to the nozzle size and the print speed. These values are the minimal extrusion values ( $\pm 2$ kPa) used for printing continuous filaments at 20–25°C <sup>with cells</sup> / <sub>without cells</sub> . ‘With cells’ assumes a mixture of one part cell suspension to ten parts hydrogel. For highly concentrated cell suspensions, the pressure needs to be increased towards the pressure used for the undiluted hydrogel. *Note: this is only a recommended reference of starting pressures. The actual pressure needed will vary depending on the amount and actual temperature of the bioink, as well as on the fitting of the piston in the cartridge and the leveling of the print surface (Cellink Bioink Bioprinting Protocol, 21 March 2019).....	14
<b>Table 2:</b> Approximate influence of printing parameters on printing objectives.....	15
<b>Table 3:</b> Design parameters determined through Slic3r software for all three biomaterials used in bioprinting.....	17
<b>Table 4:</b> A summary of the main characteristics of each of the three zones of the graded bioprinted scaffolds. The zones were designed based on to a biomimetic approach with the ultimate goal of achieving a cell density gradient within the volume of the scaffolds.....	20
<b>Table 5:</b> Experimental table of the study. Instead of day 0, pellets were evaluated at day 2 for the first time, because at an earlier time point they would be very delicate and frail to handle.....	21
<b>Table 6:</b> Calculation of the number of cells and the volume of the material needed for the bioprinting of scaffolds with graded and uniform cell densities.....	23
<b>Table 7:</b> Selected parameters for each material, used during bioprinting.....	25
<b>Table 8:</b> Primary and secondary antibodies used during direct (Actin) and indirect (Collagen II, Aggrecan) immunofluorescent staining. ....	30
<b>Table 9:</b> 3D cell density calculated from the 2D cell density of the H&E slices.....	47
<b>Table 10:</b> 3D cell density calculated from the 2D cell density of the H&E slices for the 2 <sup>nd</sup> experiment. ....	55
<b>Table 11:</b> Histological analysis of chondrocytes cultured in pellets, in differentiation medium, for 2 and 25 days, respectively. Pellets were stained for nuclei localization, sGAGs and Collagens.....	56
<b>Table 12:</b> Histological images for sGAGs and Collagen at days 0, 14 & 25, for graded (top zone) and homogeneous scaffolds. The 40x magnification allows for a visual assessment of these two ECM components as produced by the chondrocytes. The images were captured with the Leica DM500 optical microscope. Scale bar = 0.05 mm. ....	61



# Abbreviations

ACI : Autologous Chondrocyte Implantation  
CBM : Chondrocyte basal medium  
CCs : Chondrocytes  
CDM : Chondrocyte differentiation medium  
CGM : Chondrocyte growth medium  
DPBS : Dulbecco's Phosphate Buffered Saline  
DMSO : Dimethyl sulfoxide  
ECM : Extracellular matrix  
EthD – 1 : Ethidium homodimer - 1  
FBS : Fetal bovine serum  
FPSCs : Fat pad-derived stem cells  
GA : Gentamycin/Amphotericin  
GAGs : Glycosaminoglycans  
GelMA : Gelatin methacrylate  
H&E : Haematoxylin and Eosin staining  
HAMA : Methacrylated Hyaluronic Acid  
HEPES BSS : HEPES Buffered saline solution  
hr-FGF- $\beta$  : human recombinant fibroblast growth factor- $\beta$   
NFC : Nanofibrillated cellulose  
NHAC-kn : Natural human articular chondrocytes isolated from the knee  
OC tissue: Osteochondral tissue  
PBS : Phosphate Buffered Saline  
PCL : Poly-caprolactone  
PEG : Polyethylene glycol  
PEGMA : Polyethylene glycol methacrylate  
PFA : Paraformaldehyde  
PGs : Proteoglycans  
PSR : Picro-Sirius Red staining  
R3-IGF-1 : R3-Insulin-like growth factor-1  
RGD : Arg-Gly-Asp sequence  
sGAGs : Sulphated glycosaminoglycans  
TGF : Transforming growth factor



# 1. Introduction

## 1.1 Articular Cartilage: Characteristics and Functions

Articular cartilage is a subcategory of hyaline cartilage, and is an avascular, aneural, rubber-like, tissue that covers the ends of bones at the joints (Huber et al. 2000). The main functions of articular cartilage are the facilitation of the smooth movement of bones at the joints, and the protection of the bones from impacting during load-bearing activities (Roseti et al. 2017). The absence of blood vessels in cartilage leads in a very slow tissue turnover compared to other tissues, since the generation of hematoma -which is the first step in any biological healing process- is prevented (Huber et al. 2000). The living component of cartilage is solely made up of chondrocytes, a specialized, differentiated type of cells which produces and maintains the cartilage's ECM. The extracellular matrix (ECM) of cartilage is composed mainly of glycosaminoglycans (GAGs), proteoglycans (PGs) and collagen in the form of fibers, along which, the chondrocytes are orientated. Chondrocytes receive their nutrition through the diffusion of the synovial fluid, as a result of the tissue's mechanical movement (Getgood et al. 2009). The current thesis project focuses on the articular cartilage of the human femoral condyle. Figure 1 sums up the main characteristics and functions of the articular cartilage.

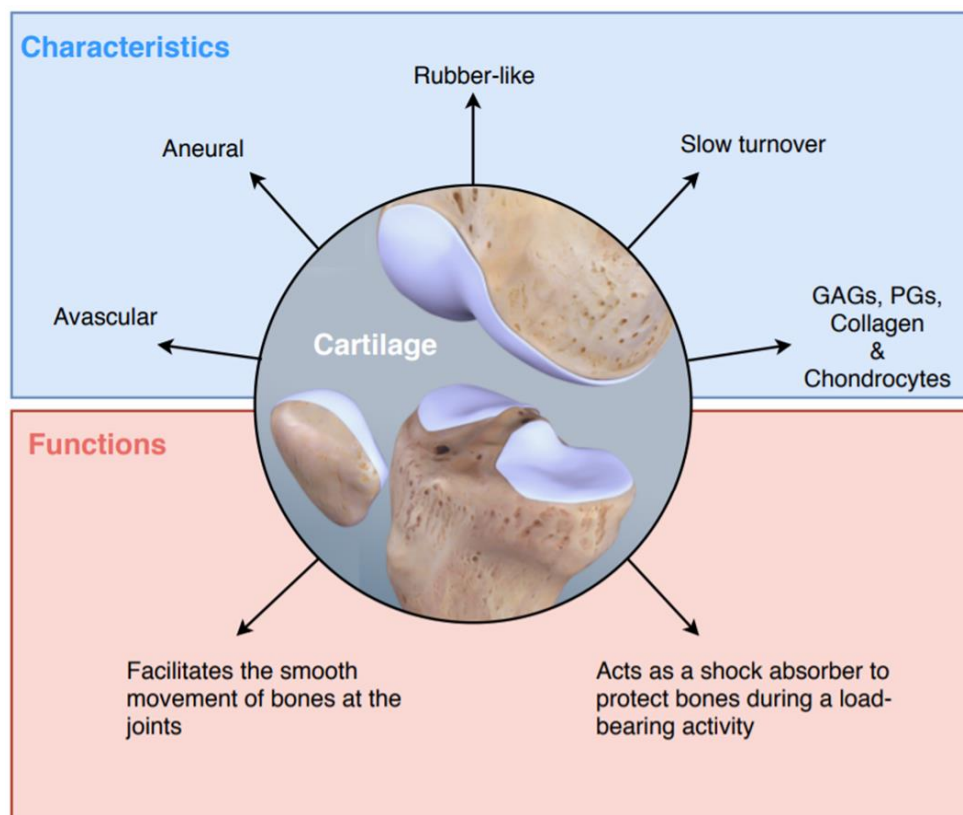


**Figure 1:** The main characteristics and functions of articular cartilage (adjusted from <https://www.arthritis-health.com/types/joint-anatomy/what-cartilage>).

## 1.2 Zonal Characteristics of Cartilage

Cartilage may macroscopically look like a dense, isotropic tissue; however, this is far from true. Cartilage is, in fact, a graded tissue that exhibits a regional organization of its components; both living and non-living. Based on this specific organization, cartilage is divided into three horizontal layers: the superficial layer, the middle layer, and the deep layer (Ansari et al. 2019). Underneath the deep layer, there is a layer of calcified cartilage that acts as an intermediate layer between the cartilage and the subchondral bone (Huber et al. 2000). Chondrocytes of each layer exhibit differences compared to the chondrocytes of other layers regarding the morphology (size and shape), the arrangement within the cartilage ECM, and the metabolic activity (Huber et al. 2000). Moreover, the cells' density changes between the three zones with the zone having the highest cell density, and the deep zone having the lowest cell density (Huber et al. 2000). Figure 2 depicts the cartilage structure described above. Each of the three cartilage layers can be distinguished from the others due to differences in collagen and proteoglycan content and in the alignment of collagen fibers (Daly et al. 2017). These variations in matrix composition and inner structure of the tissue bring upon zone-specific properties to the tissue and enable it to act as a shock absorber and a load distributor (Daly et al. 2017). The specific properties of each zone are described below.

The tangential zone (or superficial zone), which is in contact with the synovial fluid, is the thinnest zone of the articular cartilage taking up 10%-20% of the total cartilage thickness (Klein et al. 2009, Fox et al. 2009, Zhang et al. 2009). The chondrocytes in this region are elongated in the direction parallel to the surface, and the cell density is maximum compared to the other cartilage zones (Beck et al. 2013, Fox et al. 2009, Nooeaid et al. 2012). A characteristic example is the medial femoral condyle, where the number of chondrocytes per unit cartilage volume in the superficial zone is  $(24.0 \pm 7.5) \times 10^6$  cells/ml (Quinn et al. 2013). The collagen fibers in the region are thickly packed and arranged parallel to each other and to the cartilage surface, providing high tensile properties and resistance to shear stress (Huber et al. 2000).

The transitional zone (or middle zone) lies below the superficial zone and occupies 40%-60% (Ansari et al. 2019) of the total cartilage thickness (Klein et al. 2009). It is composed of rounded chondrocytes and a medium cell density. For the example of the medial femoral condyle, the cell density of the transitional zone is  $(10.3 \pm 1.1) \times 10^6$  chondrocytes/ml (Quinn et al. 2013). In this region, the collagen fibers are arched and randomly oriented, while the proteoglycan content is increased compared to the superficial zone (Huber et al. 2000). The mechanical properties of this zone are intermediate to those of the neighboring zones.

Finally, the radial zone (or deep zone) is the zone right above the calcified cartilage and takes up 30%-40% of the cartilage's total thickness. The chondrocytes occupying this layer are rounded or ellipsoid and are organized in columns perpendicular to the articular surface (Beck et al. 2013, Fox et al. 2009, Nooeaid et al. 2012). In this zone, the cell density is the lowest among the cartilage zones, with a value of  $(7.7 \pm 2.0) \times 10^6$  chondrocytes/ml, for the example of the medial femoral condyle (Quinn et al. 2013). According to an earlier study, the decrease of the chondrocyte density when moving from the tangential zone to the transitional and radial zones, is 59% and 67%,

respectively (Ducheyne et al. 2008). As far as the mechanical properties of the deep zone are concerned, the collagen network is oriented perpendicularly to the subchondral bone. This structure in combination with the high proteoglycan content provides the zone with high compressive strength (Huber et al. 2000, Klein et al. 2009). Figure 2 shows differences in cell morphology and orientation as well as in extracellular matrix fiber arrangement along the thickness of the cartilage (Ansari et al. 2019). Figure 3 shows the most important biochemical and mechanical gradients observed in the cartilage and how they fluctuate when moving from one cartilage zone to another.

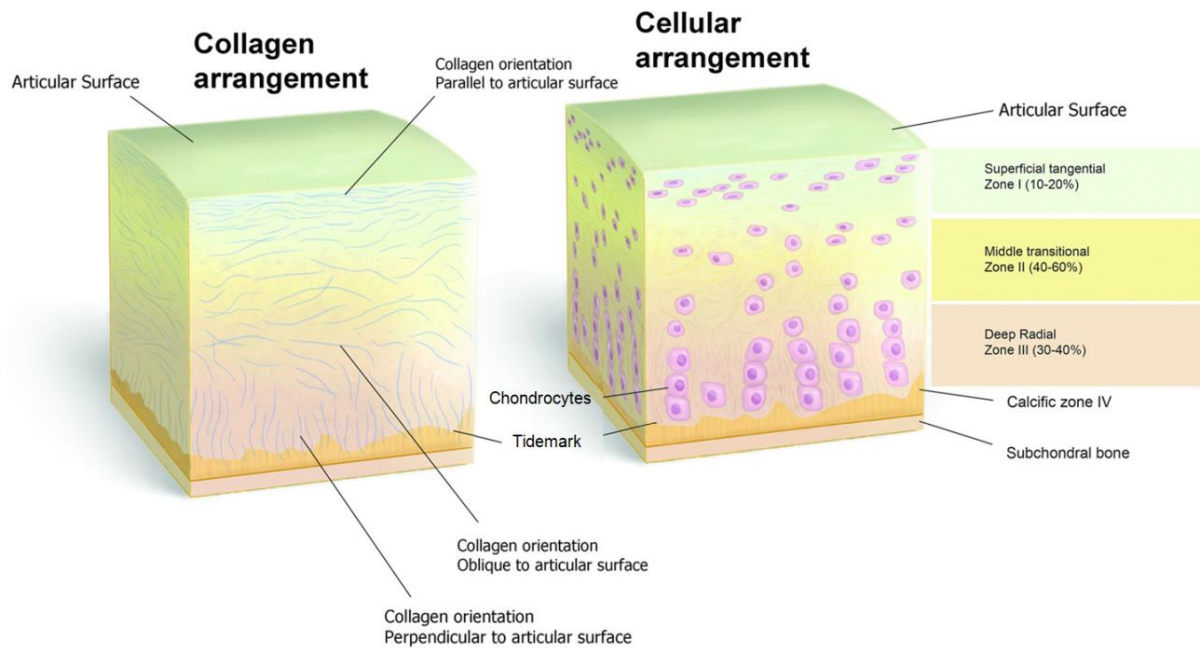


**Figure 2:** Illustration of a cartilage unit. The figure depicts the differences in cell morphology and cell density, as well as in extracellular matrix fiber arrangement along the cartilage’s thickness (Ansari et al. 2019).

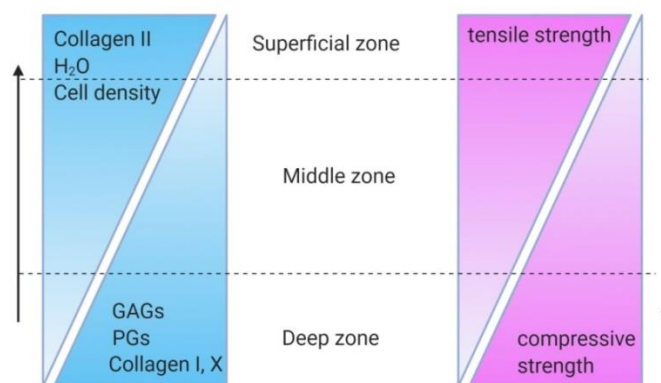


**Figure 3:** Illustration of some of the most important gradients of the articular cartilage. As the cellular and molecular compositions of the articular cartilage vary from the superficial zone to the radial zone and porosity increases, a depth-dependent change is induced in the mechanical properties of the articular cartilage. A deeper color along the cartilage zones represents an increase of the included characteristics, while, conversely, a lighter color indicates a decrease of the included features (Ansari et al. 2019).

### 1.3 Cartilage Injury & Treatment Strategies

Articular cartilage is damaged relatively often, either naturally over the course of time, or due to disease or focal trauma. Because of the cartilage's limited regenerative capacity, the surface of the injured tissue tends to be covered with a layer of fibrous, scar tissue, which is commonly inferior in quality to the original cartilage, with reduced mechanical and biochemical characteristics (Varady et al. 2016, Ahern et al. 2009). Moreover, without any nerves to "sense" the injury, the cartilage usually continues to wear-off without any pronounced symptoms, until the defect is extended to the full thickness of the cartilage, or even to the subchondral bone (Brittberg et al. 2016). Without proper treatment, these (osteo)chondral lesions can cause pain to the patients, deteriorating their life quality and mobility and could eventually lead to the development of osteoarthritis (OA) (Brittberg et al. 2016, Ahern et al. 2009). Figure 4 depicts a healthy knee joint versus a knee joint with an injury of the articular cartilage. Osteoarthritis, one of the main causes of cartilage degeneration worldwide, affected 303 million people globally in 2017 (James et al. 2018), and besides the effect on the individual patients, this situation deeply affects the health care system as well, resulting in enormous costs for health care (Roseti & Grigolo 2017).

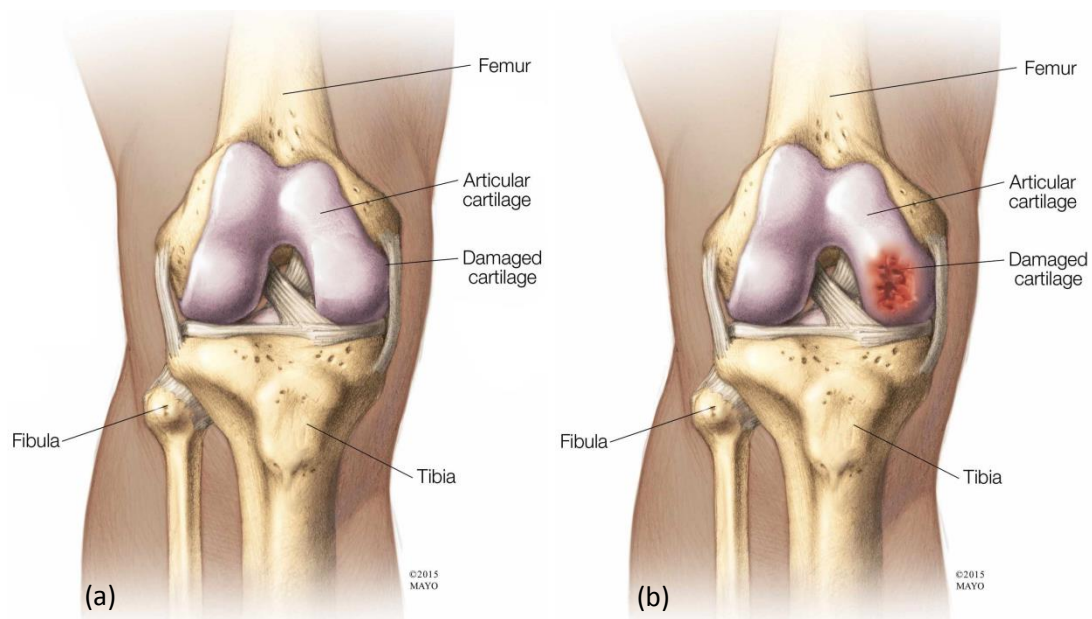


**Figure 4:** (a) Healthy knee articular cartilage. (b) Damaged knee articular cartilage [from Mayo Clinic].

Over the past years, various joint resurfacing treatments (surgical techniques and cell-based therapies) have been proposed in order to reverse the problems emerging from chondral damages. The most widely-known treatments include debridement with subsequent tissue stimulation, microfracture, implantation of autologous or allogenic osteochondral grafts, and autologous chondrocyte implantation (Ahern et al. 2009, Pettit et al. 2017, Monzon et al. 2018). If these treatments fail or the disease is diagnosed at a very late stage, the patients may need to be subjected to a total joint replacement surgery. A summary of the treatment methods can be seen in Figure 5.

**Debridement** and tissue stimulation is a two-step process which involves removal of the damaged piece of cartilage without replacing it, while stimulating the bone marrow to produce new chondrocytes for the production of cartilage ECM. This treatment is considered minimally invasive, but it has been shown to have the least predictable outcome and does not have a significant effect on the repair of larger defects (Nukavarapu et al. 2013, Getgood et al. 2009).

**Microfracture** is an invasive technique, used for small cartilage lesions, that causes controlled damage (3 – 4 mm deep holes) to the subchondral bone so that blood and MSCs can flow through it and initiate the healing process (Nukavarapu et al. 2013). Microfracture is relatively easy to perform, is cheap, and well tolerated by the patients, but tends to produce a fibrocartilagenous repair tissue, which mostly allows symptom relief for up to 2 years (Getgood et al. 2009). Therefore it is considered an effective solution for pain relief and it can slow down the cartilage damage at the joint, for a short period of time. On the other hand, it requires extensive postoperative rehabilitation and it may not provide a satisfying long-term prognosis, especially in young patients (Nukavarapu et al. 2013).

**Autologous osteochondral grafting** is a treatment method in which a healthy cartilage graft originating from the patient's body (isolated from a non-weight bearing cartilage area) is used to replace the injured cartilage. Even though this procedure can produce hyaline cartilage within the defect, the biomechanical and topographical properties between the graft and the recipient site cartilage tend to differ (Getgood et al. 2009). Although osteochondral grafts demonstrate satisfactory results, this method has many limitations, including the multiple wound sites that could risk the integrity of the joint (Nukavarapu et al. 2013), (Haene et al. 2012). Moreover, the defect size is a limiting factor for this process, when it comes to a single plug transfer, due to limited donor site availability. The transfer of multiple smaller plugs, to cover a larger defect area, has been investigated (mosaicplasty) but remains technically demanding and usually yields poor graft incorporation in the gaps between the plugs and native cartilage (Getgood et al. 2009).

**Allogeneic osteochondral grafting** is a strategy similar to the autologous grafting with the difference that the cartilage graft used to replace the injured cartilage, is now originating from the body of a donor. This technique is usually employed in cases of large (osteo)chondral defects, where there is substantial loss of bone and/or cartilage. Osteochondral allograft transplantation allows the implantation of biomechanically and topographically similar hyaline cartilage into a defect site and is particularly useful in young patients where joint replacement is not a viable option (Getgood et al. 2009). The reported results from the application of this treatment are good; however, the main limitations include the limited number of donors and the chondrocyte viability. To overcome the last limitation, fresh allografting has been preferred over frozen, but this raises the risk of rejection and disease transmission (Getgood et al. 2009), (Nukavarapu et al. 2013, Haene et al. 2012). As a result, in most countries the high cost and the scarceness of fresh donors (de Caro et al. 2015) has restricted this procedure to young patients with no other treatment options.

**Autologous chondrocyte implantation (ACI)** is used for medium and large-sized lesions, and is the only truly restorative method for cartilage damage. At first, an arthroscopic evaluation is

performed, followed by a biopsy in order to collect small pieces of the patient's own healthy cartilage (obtained from a non-weight bearing area), which contain autologous chondrocytes (Nukavarapu et al. 2013). After harvesting the tissue, the chondrocytes are isolated, and cultured in the lab for expansion. Finally, they are transplanted arthroscopically onto the injured area and are covered with a periosteal flap or a collagen membrane to prevent dislocation (Nukavarapu et al. 2013, Medvedeva et al. 2018, Omelyanenko et al. 2018, Getgood et al. 2009). This technique has been reported to have good to excellent results in a number of studies, while significantly less failures than the autografting after 10 years (Brittberg et al. 1994, Gillogly et al. 1998, Peterson et al. 2002), (Saris et al. 2009, Van Assche et al. 2011, Vanlauwe et al. 2011, Bentley et al. 2012, Katagiri et al. 2017). However, disadvantages still exist. Multiple surgeries are required, the availability of donor sites is limited and the risk of chondrocytes losing their natural phenotype during culture (de-differentiate into fibrocartilage) prevent this method from being applied effectively to larger-scale defects (Getgood et al. 2009). Moreover, there is a high probability of periosteal hypertrophy which requires debridement of the graft and the cost is increased compared to other alternatives (Getgood et al. 2009).

Despite the large number of potential treatments for cartilage repair, obstacles such as the formation of fibrocartilage and the lack of donors make it challenging to achieve a clear therapeutic effect. As a result, many patients need to undergo a **total joint replacement**, a long, heavy and expensive surgery during which parts of an arthritic or damaged joint are removed and replaced with a metal, plastic or ceramic device called prosthesis. The prosthesis is designed to replicate the movement of a normal, healthy joint and due to its lifespan (15-20 years for knee replacement (Fang et al. 2015) it is suggested mostly for older, less active patients (Fang et al. 2015). This treatment option cannot always guarantee the relief of symptoms or alleviate the need for repetition surgery, because of common issues related to infection, loosening or dislocation of the prosthesis.

Based on the available treatments listed above and their results, it can be concluded that pain reduction and partial restoration of small cartilage lesions have been achieved, to some extent. (Theodoridis et al. 2019). However, regarding the repair of large size defects, which are usually symptomatic and have a bigger impact on joint homeostasis, these methods have palliative effects and do not offer complete tissue regeneration. Therefore, treating the critical-size cartilage defects (defects that cannot heal on their own without medical intervention) is becoming the focus of increased interest from researchers who wish to relieve the patients from pain, improve the knee function and prevent the progression of degenerative diseases of the joint, stemming from this type of defects. An alternative approach, which holds the potential to improve the outcome of current therapies, is cartilage engineering and this study aims to shed some light to the engineering of scaffolds intended for use in critical-size cartilage defects.

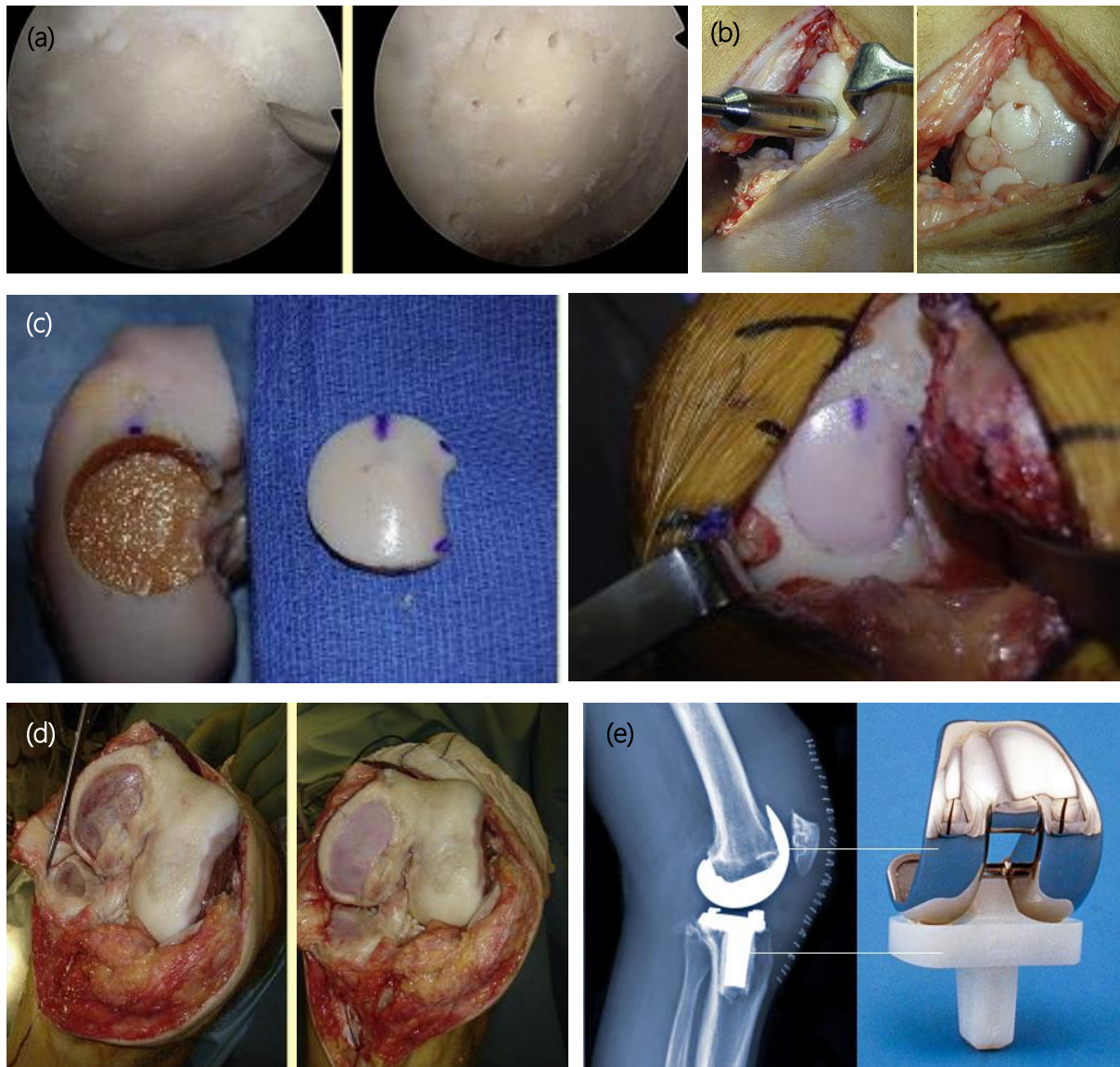


**Figure 5:** Images of the most common cartilage repair techniques used in the clinic. (a) Microfracture. (b) Autografting-Mosaicplasty. (c) Allograft implantation. (d) Autologous chondrocyte implantation. (e) Total joint replacement. Images (a) – (d) have been modified and reproduced from [Getgood et al. 2009](#).

## 1.4 Cartilage Engineering

Tissue engineering approaches for cartilage regeneration combine a support structure called "*scaffold*" with *cells* and a variety of *growth factors* which induce cell attachment, proliferation (and/or differentiation) and ECM production. This biomimetic approach aims to create a piece of artificial tissue which could eventually be implanted into the human body in order to replace the damaged tissue and ignite regeneration. To ensure that the implanted scaffolds achieve proper tissue regeneration, they must accurately reflect native tissue architecture and biological function ([Bittner et al. 2017](#)).

Many techniques have been proposed in the literature for the generation of cartilage scaffolds, such as freeze-drying ([Lukanina et al. 2018](#)), ECM decellularization ([Pati et al. 2017](#)), 3D printing ([Nowicki et al. 2016](#)), and bioprinting ([Ren et al. 2016](#)). The selection of the most suitable

technique depends on the desired scaffold properties each study aims for, and on the desired outcome (e.g. detailed and accurate architecture vs. fast fabrication, or introduction of cells to the scaffold via cell seeding vs. via cell bioprinting). Among the above techniques, bioprinting is the most recently developed one and it holds great advantages related to lower risk of rejection, and uniform tissue growth in vivo (Kačarević et al. 2017). The neo-tissue homogeneity rises from the homogeneously distributed cell-laden scaffolds, since cell placement is performed during the fabrication step and not post-fabrication, as is the case with cell seeding (Kačarević et al. 2017). A diagram of a typical bioprinting process, depicting all the necessary steps and components, is presented in Figure 6.

#### 1.4.1 Bioprinting Techniques

The most common bioprinting techniques currently used for patterning of biomaterials are: inkjet-based bioprinting, extrusion-based bioprinting, laser-assisted bioprinting, and laser-based bioprinting (stereolithography) (Murphy et al. 2014, Bittner et al. 2017, Kačarević et al. 2017). A summary of the techniques is presented in Figure 7.

*Inkjet bioprinting* is the most commonly used printing method, during which small droplets of bioinks are deposited onto a substrate base with the help of a print head. This method has the advantage of printing clinically relevant size scaffolds fast and with high resolution and thus it can be used in a variety of applications such as cell and DNA printing (Bittner et al. 2017). Cell viability after printing with this method remains at high levels because the shear stress imposed on cells can be avoided by using a nozzle-free ejection system (Murphy et al. 2014). A downside to the inkjet technology is the need for a tradeoff between the viscosity of the biomaterial and maximum ejecting force applied from the machine, and which limits the number of materials that can be used (Murphy et al. 2014). As an example of publication using this method, Li et al. 2015 generated a stable multilayered hydrogel scaffold of millimeter-scale using the inkjet printing of two different bioinks. The resulting scaffolds were geometrically uniform and demonstrated high cell viability and normal cellular functions.

*Microextrusion* is a common and affordable technique according to which a robotically controlled printing head facilitates the extrusion of a material, which is deposited onto a substrate by a microextrusion head. Typical microextrusion bioprinters use one or more printing heads for the handling of several materials at the same time. Their resolution and speed are not as good as in bioprinters utilized by other methods, but a variety of materials can be printed using this technique (Murphy et al. 2014). The materials compatible with microextrusion printers include hydrogels and some biocompatible polymers, like PCL. An important advantage of the microextrusion method is the ability to seed the printed scaffolds with very high cell densities close to those of the native tissue. Cell viability after microextrusion bioprinting depends on the extrusion pressure and the nozzle size and is lower than that of inkjet bioprinting, due to the shear stresses inflicted on cells during printing (Chang et al. 2008). Low pressure and large nozzle sizes can maintain cell viability at acceptable levels for tissue functionality (>70%), but that, in turn, decreases the resolution and printing speed (Murphy et al. 2014). Lately, many studies have reported high cell viability after scaffold bioprinting, but viability alone is not a reliable measure since besides being alive it is also

important for the cells to perform their essential functions within the generated scaffold (Murphy et al. 2014). Gao et al. 2018 utilized thermal-assisted extrusion in order to print the high strength PNT hydrogels with a chemical gradient. TGF- $\beta$ 1 and  $\beta$ -TCP particles were printed in the top and bottom layers of the scaffolds, respectively. The generated gradient scaffolds exhibited desirable mechanical properties and managed to maintain high fidelity and architecture. In vivo implantation in rats further verified that the generated scaffold could promote regeneration of osteochondral tissue, rendering microextrusion as a reliable tool in tissue engineering.

*Laser-assisted bioprinting* uses a pulsed laser beam to heat a solution containing biological material (e.g., growth factors, cells, etc.), and then it transfers the vaporized material to the scaffold, where it deposits it without any damage from the laser (Bittner et al. 2017, Murphy et al. 2014). This scaffold-free technique yields very high cell viabilities (>95%) and a resolution between 10–50  $\mu$ m (Murphy 2014), with some studies ever reporting an accuracy of a singular cell per droplet (Keriquel 2017). This method could be used for the generation of spatially gradated or chemically gradated constructs, but it is expensive and faces serious limitations regarding the stability and the size of the scaffolds that can be created, which render it inappropriate for osteochondral or cartilage tissue engineering (Bittner et al. 2017, Kačarević et al. 2017).

Lastly, *stereolithography* is an additive manufacturing method which is used to fuse together a bed of small particles using a high energy laser. The particles aimed by the laser melt and fuse together in a two-dimensional plane (Bittner et al. 2017). A 3D structure is generated by adding each layer on top of the previous one and sintered both layers together (Bittner et al. 2017). This nozzle-free technology can create high resolution, complex, internal architectures, ideal for specific applications, without the negative effects of shear pressure. However, this method can exhibit cell damage due to the use of UV light and the adverse cytotoxic effects of photoinitiators. Intra-layer heterogeneity is hard to achieve due to the mixing of particles after the addition of new powder on top of an already existing one (Bittner et al. 2017). Du et al. 2017 used this method to create an osteochondral scaffold using PCL and HA microspheres. The scaffolds derived using this method supported cell adhesion and proliferation in vitro, while exhibiting excellent biocompatibility.

Given its accessibility and the wide range of biomaterials that can be used with extrusion bioprinting, the current research project used this method to fabricate the cartilage scaffolds.

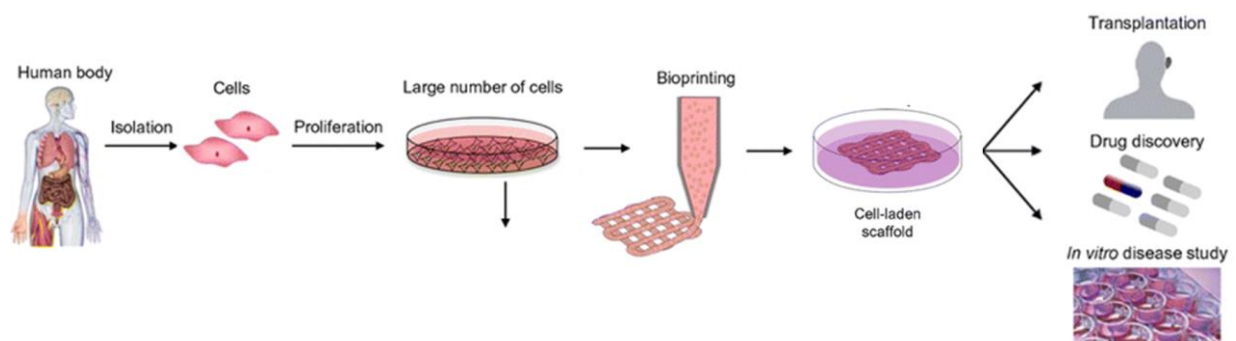


**Figure 6:** A general process for bioprinting 3D tissues. . Cells are isolated from an organism, cultured in plates in order to proliferate and then are mixed with a biocompatible hydrogel. Then, the cell-embedded hydrogels are printed to create the scaffolds, which can then be used for transplantation into a patient, or for in vitro studies (Modified by Mandrycky et al. 2015).

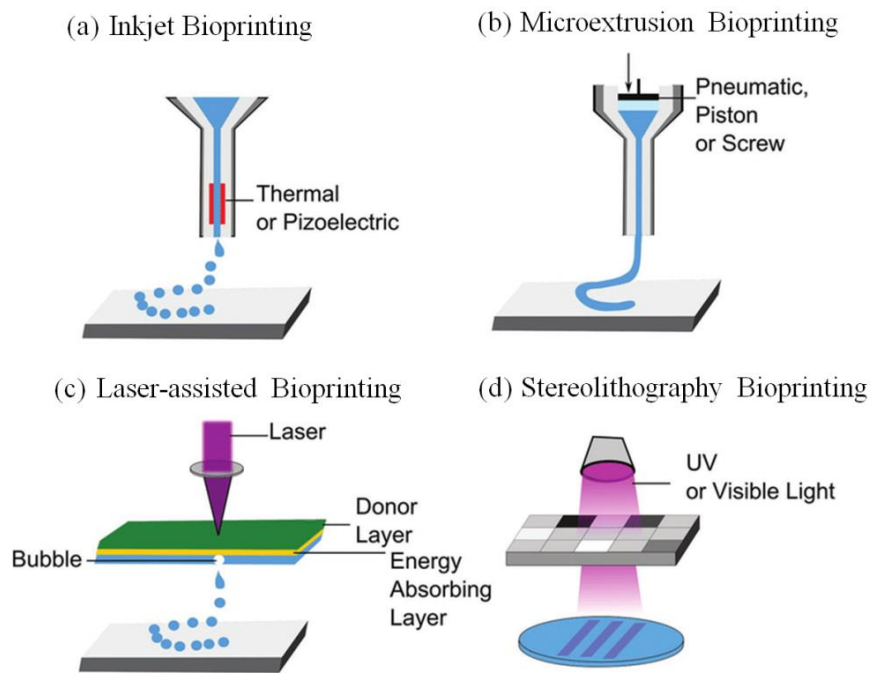


**Figure 7:** Illustrations of the main different bioprinting methods. (a) Inkjet bioprinters deposit small droplets of hydrogel and cells to build tissue layer-by-layer. (b) Microextrusion bioprinters deposit a cell-laden liquid solution via pneumatic or manual force. (c) Laser-assisted bioprinting uses a laser to rapidly heat a donor layer (green), which forms a bubble propelling the bioink onto the substrate. (d) Stereolithography bioprinters use UV or visible light to selectively cross-link bioinks layer by layer to build a 3D construct (Foyt et al. 2018).

#### 1.4.2 Gradient Scaffolds

It is essential that the existing gradients between the cartilage zones, described before, be studied and introduced to the modern tissue engineering approaches for the generation of scaffolds suitable for cartilage reconstruction.

Graded scaffolds aim to mimic the native tissue as closely as possible and for that they need to include the tissue's highly graded organization, chemical gradients, and mechanical properties in their structure (Bracaglia et al. 2017). Tissues such as the cartilage tissue are associated with a gradient of chemical composition and cell phenotypes which result in complex physical and mechanical properties (Bracaglia et al. 2017). The main gradient types can be classified into three categories: the physical gradients (Nowicki et al. 2016), the biological gradients (Levato et al. 2017), and the chemical gradients (Gao et al. 2018, Chen et al. 2018, Bracaglia et al. 2017). These gradient types can also be combined to generate a more complicated structure which mimics the native tissue as closely as possible. For example, Jeon et al. 2013 used a combination of biochemical and physical gradients to control stem cell behavior. The stiffness gradient was achieved by photocrosslinking the agent's microparticles using two different degrees of methacrylation, while the chemical gradient was achieved by mixing both TGF- $\beta$ 1 and BMP-2 growth factors in the hydrogel, before crosslinking. These gradients proved capable of regulating the number of encapsulated hMSCs and their differentiation towards bone or cartilage producing cells.

From the many studies introducing a gradient to their respective scaffolds, only one study (Ren et al. 2016) – to our knowledge – has attempted to investigate the cell density gradient using bioprinting. However, the study only focused on the biological effects of the density gradient, while the mechanical properties of the resulting graded scaffolds were not evaluated. Based on the above observation, it appears that there is a “gap” in the literature regarding research that focuses the effects of a cell density gradient and at the same time evaluates the mechanical properties of the scaffolds. The current project aims to investigate whether it is possible to generate a cell density gradient in engineered scaffolds using bioprinting, and the effect of such a gradient in tissue formation.

### 1.4.3 Biomaterial Selection

The first step into bioprinting a cartilage scaffold is the selection of the appropriate biomaterials for the specific application. Over the years, with the evolution of bioprinting, much research has been conducted in the field of biomaterials. Different biomaterials are constantly tested to create biomimetic scaffolds that could be used inside the human body, in direct contact with living cells, and provide these cells with the appropriate physical and mechanical cues for tissue biosynthesis. The most widely accepted requirements a biomaterial must fulfil to be considered a good candidate for bioprinting tissue scaffolds are printability, permeability, biodegradability, cytotoxicity, viscoelasticity, and bioactivity (Figure 8).

A large group of biomaterials, which has been proven appealing for cartilage engineering, is hydrogels. Most hydrogels are biocompatible, show low cytotoxicity, and their high water content allows the easy encapsulation of cells and provides a physical similarity to the native extracellular matrix of cartilage (Mouser et al. 2020). Some hydrogels even possess lubricating and load-transferring properties, and are capable of maintaining the natural chondrocyte phenotype (Mouser et al. 2020). However, in most cases hydrogels exhibit low shape fidelity, due to low viscosity, and insufficient mechanical properties. Therefore, the hydrogels’ properties need to be tuned to meet the requirements for accurate printing and support of the biological processes. This could be achieved by mixing together natural polymers and synthetic materials seems to diminish the disadvantages of every single component, while achieving better results than when the materials are used separately (Yang et al. 2017, Gopinathan et al. 2018, Unterman et al. 2012). Many studies have used dual-material scaffolds with different combinations of hydrogels and thermo-polymers to benefit from the advantages of both materials (Ruiz-Cantu et al. 2020, Lee et al. 2014, Daly et al. 2016, Kang et al. 2016, Shim et al. 2016, Castilho et al. 2018). The main hydrogel materials currently used for regenerative medicine purposes are based either on natural polymers isolated from animal tissues (such as alginate, collagen, and hyaluronic acid) or on synthetic polymers (such as GelMA and PEGMA). Natural polymers are more similar to animal or human ECM, while synthetic polymers can be synthesized with specific properties to fit specific applications (Murphy et al. 2014).

Alginate, the most common natural hydrogel, exhibits great biocompatibility and low immunogenicity, but its printing is challenging because it highly depends on the printing temperature. An Alginate/nanocellulose composite has been tested to improve the printability and

shape fidelity of Alginate (Mouser et al. 2020, Apelgren et al. 2017, Markstedt et al. 2015). Nanocellulose increased the viscosity of the blend and induced a pseudo-plastic behavior to it which resulted in constructs with higher shape-fidelity, while at the same time promoting cell adhesion, and cartilage-specific matrix deposition (Mouser et al. 2020, Apelgren et al. 2017, Ávila et al. 2016, Markstedt et al. 2015).

Another hydrogel which has been widely studied in cartilage engineering is collagen. Collagen constitutes the main component of the cartilage ECM, and collagen-based hydrogels exhibit great biocompatibility and biodegradation, without causing inflammation. Collagen scaffolds have been reported to promote MSCs adhesion and chondrogenesis, and maintain CCs phenotype, but their poor mechanical properties render chemical cross-linking necessary (Ren et al. 2016, Ibusuki et al. 2009). Hyaluronic acid (HA) is a new biomaterial which has gained much attention lately due to its remarkable results regarding neo-cartilage formation (Levett et al. 2014). HA supports cell attachment through surface receptors (Neuman et al. 2015) and recent studies have shown that stem cells embedded in HA hydrogels are able to maintain their multipotency and can differentiate towards the chondrogenic phenotype (Sakai et al. 2018). In order to enhance the mechanical properties of HA cartilage scaffolds, HA-based bioink was co-printed with polylactic acid (PLA) and was found to increase the expression of chondrogenic markers and the deposition of cartilage-specific matrix. These results indicate that it is a promising bioink candidate for cartilage tissue engineering based in 3D bioprinting (Antich et al. 2020).

An alternative to the natural polymers mentioned above is GelMA, which has been used a lot in literature, due to its ability to mimic ECM (Du et al. 2015). This can be indicated by the large number of studies using GelMA for their respective scaffolds (Ruiz-Cantu et al. 2020, Castilho et al. 2018, Levato et al. 2017, Daly et al. 2016). GelMA is a great alternative because it has better printability and – contrary to alginate – it is bioactive, in the sense that it promotes the cells' attachment in the material; even though some studies indicated that this property, combined with its higher stiffness, promotes a more fibroblastic phenotype for chondrocytes (Daly et al. 2016). The incorporation of HAMA in gelMA/gellan bio-ink has been proven to increase filament stability, and allow the chondrogenic differentiation of ACPCs and MSCs (Mouser et al. 2020).

From the soft hydrogels presented above, Collagen had already been tested as a bioink for the generation of a cell density gradient by (Ren et al. 2016). According to this study the cell density gradient could not be maintained in scaffolds of 3 mm height (thickness of human articular cartilage), which indicates that collagen might be too soft to maintain a zonal structure and allows the fusion of the different bioprinted zones of the hydrogel, even after crosslinking. Therefore, this material is not ideal for the purpose of the present study and was excluded. At the same time, the selection of a bioink compatible with our Cellink BIO-X bioprinter was very important for achieving optimal results during the biofabrication process. Hence, the use of biomaterials that were produced by the same company as the printer was decided. Pure hyaluronic acid was not available by Cellink, so the final choice was made between an **Alginate-based** hydrogel (CELLINK Bioink, Cellink) and a **GelMA-based** hydrogel (GelMA C, Cellink). Both hydrogels contained highly hydrated cellulose nanofibrils (nanocellulose) for enhanced printability. The final selection between

the two bioinks was made based on the cell phenotype each of the hydrogels induced. According to abovementioned findings (Daly et al. 2016) and preliminary bioprinting tests using both hydrogels, it was demonstrated that the Alginate-based hydrogel maintained a round chondrocyte phenotype, while the GelMA-based hydrogel promoted a more elongated one. Hence, the Alginate/nanocellulose hydrogel was selected over the GelMA/nanocellulose, for the encapsulation of the chondrocytes.

To reinforce the scaffolds' mechanical properties, researchers have used meshes or frameworks made of thermoplastic polymers which were printed together with low-stiffness hydrogels. Alginate's mechanical properties have been enhanced in multiple studies with the use of PCL (Daly et al. 2016, Lee et al. 2014). Similar PCL reinforcements have also been tested to different hydrogels such as Agarose (Daly et al. 2016), Collagen II (Ren et al. 2016), GelMA (Daly et al. 2016, Castilho et al. 2018), and PEGMA (Daly et al. 2016). Also, a study working with a HA-based bioink, co-printed the hydrogels with polylactic acid (PLA) to enhance their mechanical properties (Ansari et al. 2020). Therefore, to tackle the poor stiffness of the selected hydrogel and its average nozzle fidelity, the use of polycaprolactone (PCL) was decided, due to its great stability and mechanical properties which allow PCL to maintain the shape of the scaffolds, much like a skeleton gives shape and support to the human body.

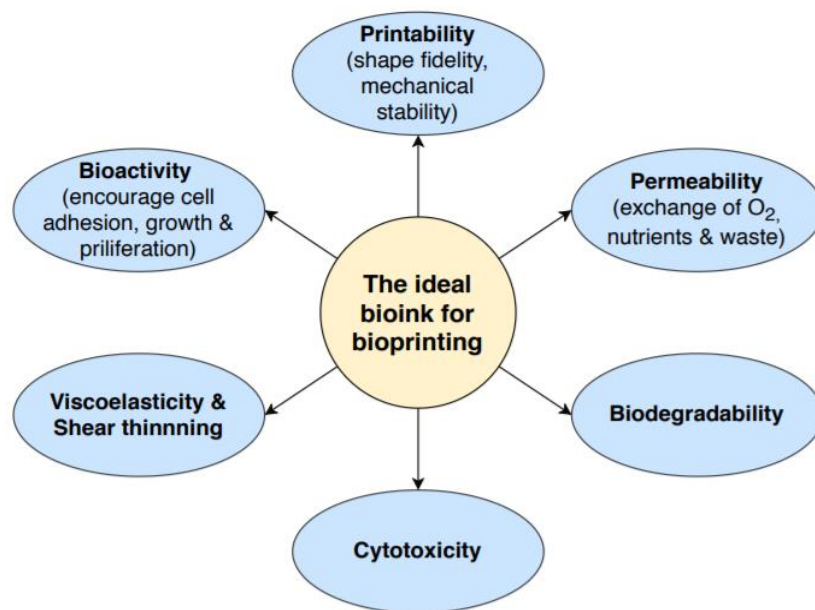


**Figure 8:** Requirements for selecting a bioink for cartilage scaffolds using extrusion bioprinting (Gopinathan et al. 2018, Desimone et al. 2015, Parak et al. 2019).

## 1.5 Project Objectives

All in all, the main objective of the current project is the fabrication of a graded cartilage scaffold with a biomimetic cell density gradient and enhanced mechanical properties, using extrusion bioprinting. Following the successful generation of the gradient, a second objective is the investigation of the effect the gradient has on the biosynthesis of cartilage ECM.

# 2. Materials and Methods

## 2.1 Experimental Procedures

### 2.1.1 Parametric Study – Optimization of Printing Parameters

Before starting to print, an optimization of the printing parameters (temperature, pressure and speed) for the selected materials was necessary. The nozzle size had been determined as the smallest possible (i.e. 0.2 mm) based on some preliminary results regarding the resolution and thickness of the printed fibers. A first estimation of the parameters' values can be obtained from the materials application sheet provided by the manufacturer (Cellink). The suggested values provided by Cellink are presented in Figure 9 (PCL) and Table 1 (Bioink).

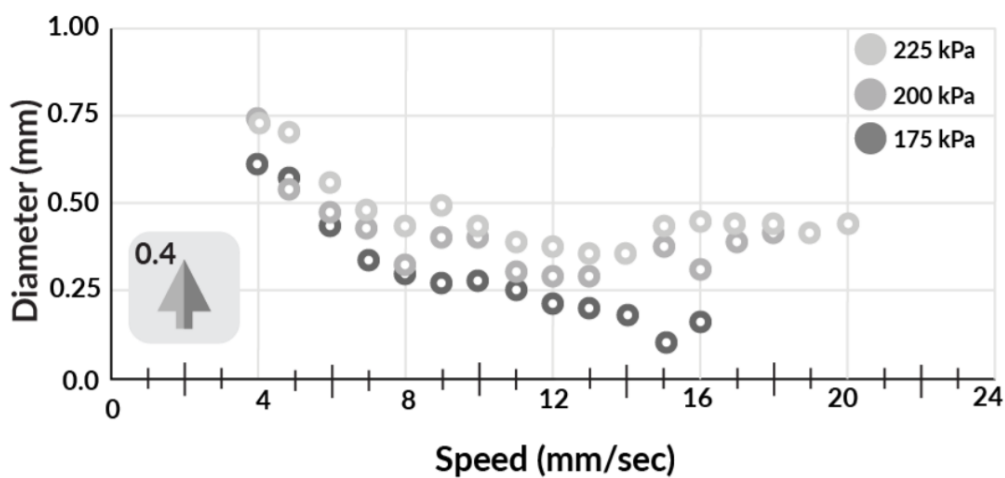


**Figure 9:** Cellink’s chart with the recommended pressures for PCL, according to the nozzle size and the print speed. The company recommends to use the above parameters during printing with PCL. It is also recommended to start printing with PCL with a temperature of 180°C (Cellink PCL Application Note, 15 February 2019).

**Table 1:** Cellink’s table with the recommended pressures for Bioink, according to the nozzle size and the print speed. These values are the minimal extrusion values ( $\pm 2$  kPa) used for printing continuous filaments at 20-25°C with cells/without cells. ‘With cells’ assumes a mixture of one part cell suspension to ten parts hydrogel. For highly concentrated cell suspensions, the pressure needs to be increased towards the pressure used for the undiluted hydrogel. \*Note: this is only a recommended reference of starting pressures. The actual pressure needed will vary depending on the amount and actual temperature of the bioink, as well as on the fitting of the piston in the cartridge and the leveling of the print surface (Cellink Bioink Bioprinting Protocol, 21 March 2019).

Printing speed (mm/sec) →	5		10		15		20	
Nozzle size (G) ↓								
22	6	11	8	13	9	14	11	17
25	8	12	10	15	11	17	12	17
27	10	13	14	15	15	17	16	20

Each of the PCL structures was assigned a different combination of pressure and temperature, with the printing speed constant at 4 mm/sec. Pressure values varied between 170 kPa – 200 kPa, with a 10 kPa increment, and temperature values varied between 210 °C – 250 °C, with a 10 °C increment. For the alginate-based structures, each one was printed with a different combination of pressure and speed, with the pressure varying between 15 mm/s – 30 mm/s, with a 5 mm/s increment, and the speed varying between 15 mm/s – 30 mm/s, with a 5 mm/s increment. The printing temperature was constant and since it was not controlled by the print head or the nozzle, it was considered as room temperature (RT). In order to achieve the highest resolution of the printed characteristics, the smallest available cylindrical nozzles were utilized for both designs ( $\varnothing$  0.2 mm). Based on the different combinations of printing parameters described above, a total number of 20 and 16 experimental conditions were tested for the PCL and the alginate-based hydrogel, respectively.

For the PCL parameters, an 8 mm by 8 mm object with a height of 0.4 mm was designed. The infill density was set at 10% in order to have enough empty space between the fibers, to measure their width. The height of 0.4 mm allowed for two layers to be printed so that a larger number of fibers' widths could be included in the measurements. For the Alginate-based hydrogel, a 40 mm long, 10 mm wide object with height of 0.2 mm, was designed, to test the printability of the ink in larger distances (Webb et al. 2017). An infill density of 5% was selected to convert the object in an alternating line before printing. Solidworks Student edition 2019-2020 software was used to design both objects. The .stl files were then converted into G-Code files using Slic3r. All structures were printed using the BIO-X bioprinter (Cellink). After printing, the images of the printed lines with a scale bar were acquired using the Keyence VHX-5000 microscope, and the thickness of each line was measured at seventeen locations (for the PCL structures) and fourteen locations (for the hydrogel structures) using ImageJ (NIH, USA).

The parameter optimization for the PCL was performed based on the best trade-off between the highest geometrical accuracy (the dimensions of the printed constructs closest to the dimensions of the designed construct) and uniform thickness of the fibers along their length. On the other hand, the parameter optimization for the bioink was performed using the parameter optimization index (POI), as described in Webb et al. 2017. The calculation of the POI was used for the assessment of the bioprint results, from a range of printing parameters, in a standardized manner. The POI calculation is based on the idea of minimizing the shear stress applied on the bioink, and on the encapsulated cells, while ensuring maximum geometric accuracy. The correlation of printing accuracy and shear stress with the printing parameters (speed, pressure, temperature) can be seen in Table 2.

**Table 2:** Approximate influence of printing parameters on printing objectives.

	Accuracy (%)	Shear Stress (kPa)
Increase of printing speed	Increases	-
Increase of pressure	Decreases	Increases
Increase of nozzle diameter	Decreases	Decreases

Since POI aims to maximize the printing accuracy and minimize the theoretical shear stress (TSS), its calculation is described by equation (1):

$$POI = Accuracy \cdot \frac{1}{TSS} \quad (1)$$

Accuracy is inversely proportional to the line thickness and it can be expressed by equation (2):

$$Accuracy \propto \frac{1}{line\ thickness} \quad (2)$$

The theoretical shear stress cannot be directly calculated, but it can be minimized by decreasing the pressure and nozzle size, as seen in equation (3):

$$TSS \propto \frac{1}{pressure} \cdot nozzle\ diameter \propto \frac{nozzle\ diameter}{pressure} \quad (3)$$

Replacing the parameters of equations (2) and (3) in equation (1), gives:

$$POI = Accuracy \cdot \frac{1}{TSS} = \frac{nozzle\ diameter}{line\ thickness \cdot pressure} \quad (4)$$

Finally, the POI values across a range of printing parameters, were normalized relative to the maximum POI in the experimental configurations, as seen in equation (5). The maximum normalized POI is related to the combination of parameters that maximize the accuracy and minimize the TSS.

$$POI = \frac{POI_i}{POI_{max,n}} \quad (5)$$

## 2.1.2 Scaffolds Design

### Designing the Scaffolds

The upper threshold of the PCL volume included in the scaffolds, to enhance the stiffness of the alginate hydrogel, was determined as 7%. Based on this condition, two alternative designs were considered in which the PCL would act as an outer skeleton for the hydrogel, concentrating the cell-embedded volume of the hydrogel in the centre and maintaining its shape throughout its thickness.

In the first design the PCL skeleton is composed of a square shaped base on the bottom, with a thickness of 2 layers (0.4 mm), and four vertical struts at the corners of the square base running up to the full height of the scaffold. The second design was the same as the first one, with the addition of a square base of 0.4 mm thickness on the top of the scaffolds. In the first design, the majority of the cells would theoretically stay intact and unaffected from the hot nozzle and only minor thermal effects would take place to the cells located around the perimeter of the 2 bottom layers. In the second design, the thermal effect on the cells would theoretically be more evident due to the passing of the hot thermoplastic nozzle over the two top layers of the scaffolds. The effects of the two designs on cell viability were assessed in preliminary experiments.

As far as the geometry is concerned, the designed scaffolds had a cuboid geometry with a square base with a side of 8 mm and a height of 3 mm, while the PCL framework was 0.4 mm thick. The base dimensions (8 mm × 8 mm) were chosen to match a critical-size defect based on the equine animal model, which is the largest model used in cartilage defects and best approximates the size and depth of human cartilage defects (Chu et al. 2010). The height was set at 3 mm to match the thickness of the human articular cartilage at the femoral condyle (Shepherd et al. 1999). As far as the dimensions of the hydrogel part are concerned, to avoid overlapping between the hydrogel and the PCL base, the over-extrusion of the hydrogel was compensated through the design, by decreasing the dimensions of the hydrogel part by 400µm on both sides of the x and y direction.

On the first attempt of printing the designed scaffold, it became apparent that the fabrication of the four 400µm thick vertical struts on the corners would be a challenging job, since the hydrogel contained within the struts was quite soft and the struts would buckle inwards due to the tension exerted from the hydrogel to the extruded PCL during the movement of the print head from one strut to the other. For this reason, it was decided that an external support around the perimeter of the scaffold would enhance the stability of the struts and maintain their vertical geometry.

In order for the BIO-X bioprinter to use multiple materials together (i.e. the PCL, the bioink, and the support), for the construction of a single scaffold, each material needed to be assigned to a specific part of the object, which would be separate from other parts assigned to other materials. Therefore, the design of the scaffolds was divided into three parts: (1) the stiff skeleton part made of PCL (PCL, Cellink), (2) the inner cell-embedded part made of hydrogel (Bioink, Cellink), and (3) the outer support part made of Cellink START (Cellink START, Cellink); a polyethylene oxide-based gel that is water-soluble and works as an excellent sacrificial material. Each part was generated separately in Solidworks and then assembled together into the full object.

### Slicing Software

The Solidworks .stl files were processed with the Slic3r 1.3.0 software to generate the .gcode file. The .gcode file was later used by the bioprinter for the fabrication of the scaffolds. The .stl parts were loaded one-by-one on the software and then for each part the following parameters were set: the extruder number, the infill pattern, the infill density, the infill angle, the solid infill threshold area, the layer height, and the nozzle diameter for each extruder. Table 3 contains the above parameters and their values for each scaffold part.

**Table 3:** Design parameters determined through Slic3r software for all three biomaterials used in bioprinting.

	Extruder n°	Infill pattern	Infill density	Infill angle	Solid infill threshold area	Layer height (mm)	Nozzle diameter (mm <sup>2</sup> )
PCL	3	Rectilinear	100%	90°	10	0.2	0.2
Hydrogel	1	Rectilinear	10%	90°	10	0.2	0.2
Support	2	Rectilinear	100%	90°	10	0.2	0.2

As mentioned earlier, the infill pattern and infill angle were chosen as “rectilinear” and 90°, respectively, and the infill density was set at 10% because this was the higher density for which open pores could be fabricated within the scaffold using the Alginate-based hydrogel.

### 2.1.3 Cell Culture

Chondrocytes are the sole cellular component of healthy cartilage and specialize in the production and maintenance of the extracellular matrix of cartilage. Therefore, it is currently the best choice for a cell source to be used for cartilage tissue engineering.

#### Initiation of Culture Process / Thawing of Cells

The cells used in this study were human articular chondrocytes isolated from the hyaline cartilage in the knee (NHAC-kn, Lonza). The cells were bought in ampoules, each containing  $\geq 500.000$  cells with  $\geq 70\%$  viability at passage number 2. Before seeding the cells into vessels, the cryovials were quickly thawed in a  $37\text{ }^{\circ}\text{C}$  water bath until the ice melted. The cells were subsequently mixed using a micropipette and were dispensed in a density of  $10.000\text{ cells/cm}^2$  in T75 flasks, where they were cultured in 20 ml of chondrocyte basal medium (CBM™ Medium, Lonza) containing the following growth supplements: 1:20 Fetal bovine serum (FBS), 1:500 Insulin, 1:500 R3-Insulin-like growth factor 1 (R3 - IGF 1), 1:1000 Gentamicin/Amphotericin-B (GA), 1:1000 Transferrin and 1:200 human recombinant Fibroblast Growth Factor-Beta (hrFGF- $\beta$ ) (Clonetics™ CGM™ BulletKit™, Lonza). After seeding, the flasks were gently rocked to evenly distribute the cells and were allowed to equilibrate in a  $37\text{ }^{\circ}\text{C} \pm 1\text{ }^{\circ}\text{C}$ , 5%  $\text{CO}_2$ ,  $90\% \pm 2\%$  humidity incubator. Medium was changed the first day after seeding the cells, in order to remove the DMSO, and after that it was refreshed every other day using 20 ml of medium per flask. It is important to note that centrifugation was not performed to remove cells from the cryoprotectant cocktail, because this action would be more damaging than the effects of DMSO residue in the culture.

#### Cell Passaging

The cells were passaged when they reached 90% confluency. The medium was removed from each of the flasks and the cells were rinsed with 12 ml of HEPES-Buffered Saline Solution (HEPES-BSS, Chondrocyte ReagentPack™, Lonza). After removing HEPES-BSS, the cells were covered with 9 ml of Trypsin/EDTA Solution (Chondrocyte ReagentPack™, Lonza) and incubated at  $37\text{ }^{\circ}\text{C}$  for 2-5 minutes until the cells were detached from the bottom of the flasks. After the cells were released, the Trypsin was neutralized using 18 ml of Trypsin Neutralizing Solution (Chondrocyte ReagentPack™, Lonza) and the cell solution was transferred to a sterile 50 ml centrifuge tube. The flasks were rinsed once again using 6ml of HEPES-BSS to collect any residual cells and the solution was added to the 50 ml tube. The harvested cells were centrifuged at  $200 \times g$  for 5 minutes to suspend the cells into a pellet. The supernatant was subsequently discarded and the pellet was resuspended in 1 ml or 2 ml of fresh medium. The new suspension was used to count the cells using the Trypan Blue method. The cells were then seeded into new flasks with a seeding density of  $10.000\text{ cells/cm}^2$ . The number of flasks to be inoculated and the volume of cell suspension to be seeded into each flask, were calculated using the following equations, accordingly:

$$\text{Number of flasks} = \frac{\text{Total number of viable cells}}{\text{Growth area} * \text{Recommended Seeding Density}}$$

$$\text{Seeding Volume} = \frac{\text{Total volume of diluted cell suspension}}{\text{number of flasks (as determined in previous equation)}}$$

After passaging, the flasks were gently rocked to evenly distribute the cells and were allowed to equilibrate in a 37 °C±1 °C, 5% CO<sub>2</sub>, 90%±2% humidity incubator. Chondrocyte growth medium (CBM plus additives) was refreshed every other day using 20 ml of medium per flask. Chondrocytes were cultured and passaged until passage 3 before bioprinting.

### Cell Counting

For counting the number of cells in a cell suspension, 5 µl of suspension and 5 µl of Trypan Blue were added into a 0.5 ml tube and mixed gently using a micropipette. For more accurate results, the above mixture is always prepared in duplicates. The 10 µl mixture was then pipetted into the opening of one chamber on a counting slide. The counting slide was subsequently inserted into the slide slot of a TC20 cell counter (Biorad). The machine automatically initiates a cell count and the count results (total number of cells/ml, number of live cells/ml and cell viability percentage) appear on the screen. After the count the slide was removed from the machine and discarded into the biological waste bin.

### Freezing of Cells

In order to freeze the cultured cells at passage 3, a cryopreservation medium was prepared using 80% CGM™ without FBS, 10% DMSO and 10% FBS. The cells were harvested and suspended into a pellet as described in the *Cell Passaging* section. Then, they were re-suspended in cryopreservation medium in a concentration of 1×10<sup>6</sup> - 2×10<sup>6</sup> cells/ml. Aliquots of 1 ml suspension were then pipetted into cryo-vials, which were in turn insulated using an isopropanol freezing canister. The vials were stored at -80°C overnight and the next day were removed from the canister and stored in a box in the -80°C. The frozen passage 3 cells were thawed and cultured again in flasks (as described in the *Thawing* and *Cell Passaging* sections), in order to be used for bioprinting.

### Pellet Generation

The 2D cultured chondrocytes were first washed with PBS, trypsinized and centrifuged for 5' at 200\*g. Then, they were re-suspended in 2ml medium and counted. After counting, the cells were separated into 1.5 ml autoclaved Eppendorf tubes for the creation of the pellets. For each pellet, 250.000 cells were used, and thus, this amount of cells was transferred in each of the 1.5ml Eppendorf tubes. The tubes were subsequently centrifuged for 5' at 200\*g in the micro-centrifugation machine. After spinning down the cells, the pellets were created. The supernatant medium was then removed and 0.5 ml of fresh chondrocyte differentiation medium (CDM, Lonza) was carefully added to the pellets. After adding the medium, the lid of the tubes was carefully closed and was pierced twice (two holes were generated on top of the lid), using a 0.8 mm syringe needle, to allow the cells to breath. Finally, the pellets were incubated in a 37 °C±1 °C, 5% CO<sub>2</sub>, 90%±2% humidity incubator. The medium was carefully changed three times a week, just like it was for the cell-embedded scaffolds, with extra attention of not touching the holes of the lid with

the gloves to avoid contamination. Nine pellets were created in total, three per time point (day 2, day 14, day 28), which were used for histology analysis.

## 2.1.4 Bioprinting

### Cell Density Gradient

The cell density gradient within the volume of the fabricated scaffolds was created by bioprinting each of the three cartilage zones with a constant cell density, different from the cell densities of the other zones. To ensure better results regarding cell behaviour and tissue formation, the cell densities of the scaffolds' zones needed to mimic the cell densities of the native cartilage zones (Ren et al. 2016, Ansari et al. 2019). Thus, based on data from previous studies (Ren et al. 2016, Ansari et al. 2019, Hunziker 2002) the cell densities were determined as follows:  $20 \times 10^6$  cells/ml for the top (i.e. superficial) zone,  $10 \times 10^6$  cells/ml for the middle zone and,  $5 \times 10^6$  cells/ml for the bottom (i.e. deep) zone. This means that the top cell density was four times higher than the bottom density and twice as high as the middle layer. The thickness of the zones was set as 20%, 47%, and 33% of the total scaffold height for the superficial, middle, and deep zone, respectively. This decision was made based on the results of studies on the structural organization of the native cartilage and its zones, according to which the superficial zones takes up 10%-20% of the total volume of the cartilage, the middle zone takes up 40%-60% and the deep zone takes up 30%-40% (Klein et al. 2009, Hunziker et al. 2002). Based on the above, from the 15 layers making up the scaffold (the scaffolds is 3 mm in height and each layer has a height of 0.2 mm), 3 consist the top zone (high cell density), 7 consist the middle zone (medium cell density) and 5 consist the bottom zone (low cell density). A summary of these design parameters is presented in Table 4.

**Table 4:** A summary of the main characteristics of each of the three zones of the graded bioprinted scaffolds. The zones were designed based on to a biomimetic approach with the ultimate goal of achieving a cell density gradient within the volume of the scaffolds.

Zones of the graded scaffolds	Top	Middle	Bottom
Cartilage zones corresponding to scaffolds zones	Superficial	Middle	Deep
Zone/scaffold volume ratio	20%	47%	33%
Thickness	0.6 mm	1.4 mm	1 mm
Number of layers/zone	3	7	5
Cell density	$20 \times 10^6$ cells/ml	$10 \times 10^6$ cells/ml	$5 \times 10^6$ cells/ml

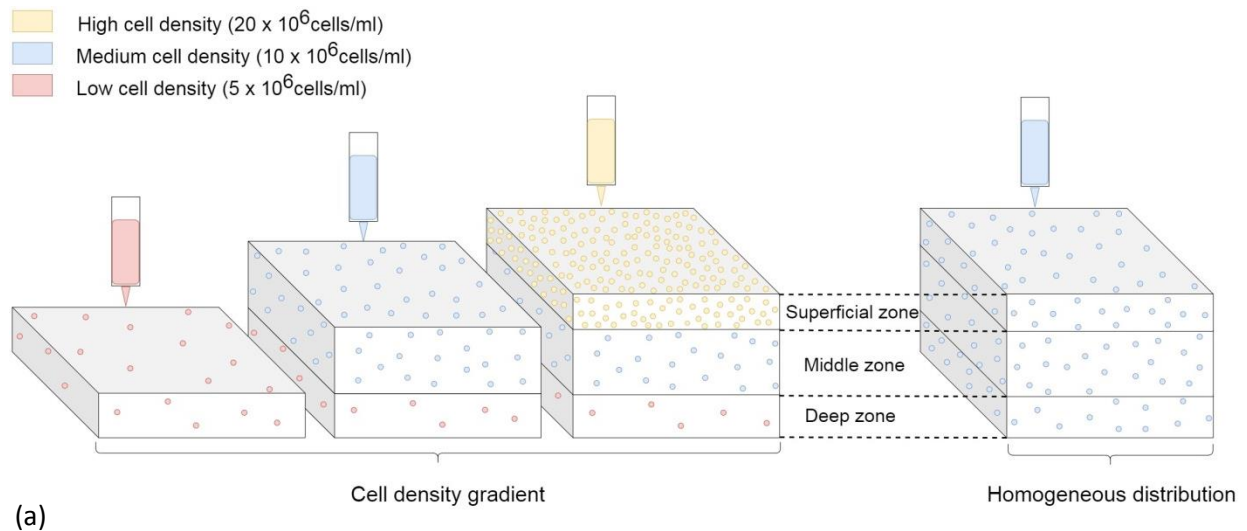
After determining the zonal specifications of the graded scaffolds it was necessary to define the appropriate control samples in order to be able to assess the results of the experiment. As a first control the fabrication of *homogeneous scaffolds* with a cell density of  $10 \times 10^6$  cells/ml, throughout the whole thickness of the scaffold, was decided. The  $10 \times 10^6$  cells/ml density is the same as the cell density used in the middle zone of the graded scaffolds and corresponds to the mean cell density in the human femoral condyle cartilage (Hunziker 2002). These scaffolds will be used as controls to evaluate the generation and maintenance of the cell density gradient in the graded scaffolds (using Live/Dead and H&E staining). Since homogeneously printed scaffolds

(fabricated with the same cell density throughout the whole construct) are not expected to show any difference in terms of cell numbers through their thickness, while graded scaffolds are expected to have an increase of cell density from the bottom to the top zones, this discrepancy would be the validation of a successful experiment. Regarding tissue formation (sGAGs and Collagen) an extra control was decided to be considered. A *3D culture of chondrocytes*, in the form of a pellet, under the same culture conditions as the cell-embedded scaffolds would allow for comparable histological results between pellets and scaffolds. This comparison could be useful in case the scaffold experiment does not yield the expected results (e.g. the cells within the scaffolds do not produce any matrix). In this case, a 3D culture of chondrocytes would be able to elucidate whether the cells themselves were problematic, or whether the bioprinting had a negative effect on them. Finally, regarding the different staining of the scaffolds, it was decided to fabricate *empty scaffolds* – made only from PCL and hydrogel, without containing any cells – which would act as controls to evaluate the staining of the substrate (material). The empty scaffolds were printed under sterile conditions and cultured under the same conditions as the cell-embedded scaffolds and, therefore, they were also used to determine the condition of the material (e.g. degradation or other visible changes in the cell-free material) over time, under culturing conditions.

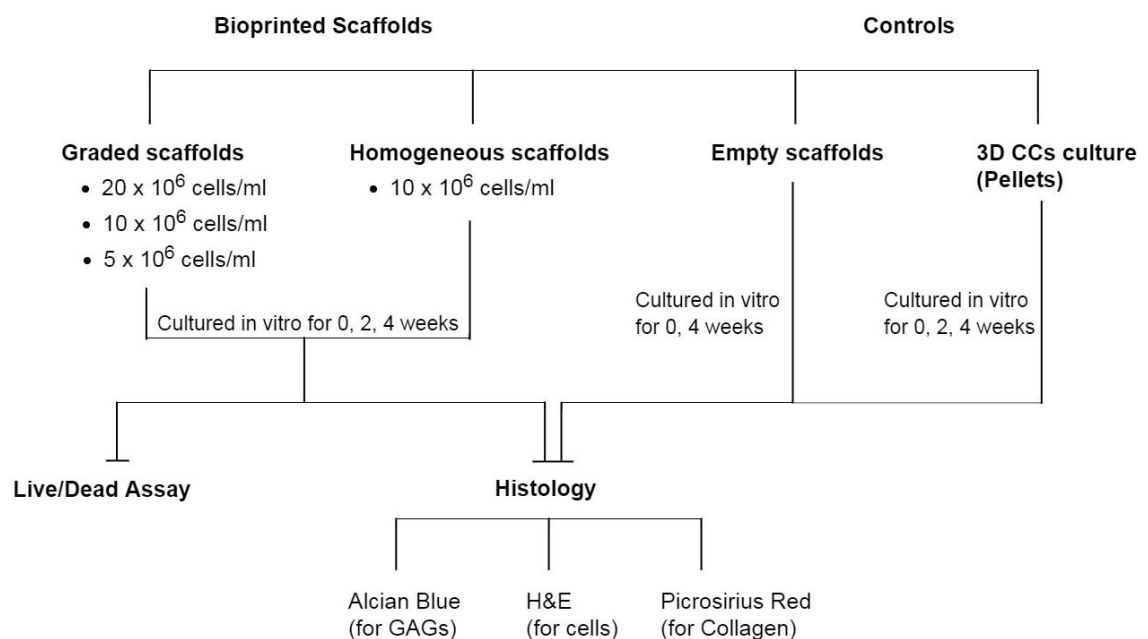
The bioprinting procedure of the current project was divided into two parts, with the first being used for the evaluation of the cell density gradient, and the second being mainly used for the assessment of the neo-tissue formation, even though a gradient analysis was performed to it, as well. The difference between the two parts lies in the sample number and the culture medium used for the scaffolds' culture. The number of scaffolds used for the gradient assessment were n=2, for each time point, and they cultured in differentiation medium without ascorbic acid, while the scaffolds used for the evaluation of ECM were n=3, for each time point, and were cultured in differentiation medium with ascorbic acid (to enhance the ECM production). Table 5 shows the suggested experimental table in terms of type and number of samples generated for each time point during the study and Figure 10 depicts the experimental configuration with the samples and controls described above.

**Table 5:** Experimental table of the study. Instead of day 0, pellets were evaluated at day 2 for the first time, because at an earlier time point they would be very delicate and frail to handle.

	Day 0	Day 2	Day 14	Day 25	Day 28
Graded (3 cell densities) – (assessment of the gradient)	2	-	2	-	2
Graded (3 cell densities) – (assessment of ECM deposition)	3	-	3	3	-
Homogeneous (control) – (assessment of the gradient)	2	-	2	-	2
Homogeneous (control) – (assessment of ECM deposition)	3	-	3	3	-
Pellets (control)	-	3	3	3	-
Empty scaffolds (no cells – control for staining)	3	-	-	3	-



(a)



(b)

**Figure 10:** Study design schematic. (a) The construct with the cell density gradient and the construct with the homogeneous cell distribution (control samples) were fabricated from bottom to top, using the corresponding cell densities for each of their zones. (b) Three cell seeding density groups ( $20 \times 10^6$ ,  $10 \times 10^6$ , and  $5 \times 10^6$  cell/mL) were used for the generation of the graded scaffolds and one cell seeding density group ( $10 \times 10^6$ ) was used for the generation of the homogeneous scaffolds. These constructs were cultured in vitro and harvested at 0, 2, and 4 weeks for live/dead assay, and histological analysis. The pellets were generated using  $0.5 \times 10^6$  cells/ml, cultured for 0, 2, 4 weeks and used only for histology, while the empty scaffolds were cultured and harvested only at 0 and 4 weeks for histology. Adjusted from Ren et al.2016.

### Cell Preparation for Bioprinting

Isolated chondrocytes are differentiated cells that, after serial expansion in monolayer culture, lose their differentiated phenotype and become fibroblast-like, thus, losing their ability to produce cartilage specific markers such as Collagen type II and Aggrecan. Therefore, chondrocytes expanded in culture will need to be re-differentiated in order to produce neo-tissue. By the 3rd passage, the cells are almost completely de-differentiated and the level of re-differentiation a

culture can reach decreases with increasing numbers of passages in an expansion medium in monolayer culture. According to that, passage 3 is the maximum passage number for chondrocytes to be able to fully re-differentiate to their natural phenotype. The Lonza NHAC-kn were bought at passage 2 and in order to reach the cell numbers needed to perform the experiment, they had to be expanded until passage 3. The trypsinization of the passage 3 chondrocytes before bioprinting, however, increased the passage number by 1, so the actual cells with which the bioprinting was performed were of passage 4. Therefore, passage 4 was chondrocytes for the bioprinting.

When the passage 3 chondrocytes reached 90%-100% confluence, the bioprinting process could begin. First, the medium was removed and the cells were rinsed, trypsinized, neutralized, put in 50ml tubes and centrifuged as described in the *Cell Passaging* section. The pellets were re-suspended in 2ml fresh CGM medium per tube, and the cells were subsequently counted. Next, all the different cell suspensions were combined together in a 50ml tube to collect the total number of cells. Subsequently, the final cell suspension was divided into three new tubes based on the number of cells that corresponded to each of the scaffolds' zones. The three tubes were centrifuged, again and this time each of the pellets (containing the total number of chondrocytes to be printed in each of the cartilage zones) was re-suspended in the correct amount of medium. The amount of culture medium added to re-suspend the cells should be equal to 1:10 of the bioink volume. Table 7 presents an example of the calculations performed for the cells and hydrogel, before bioprinting.

**Table 6:** Calculation of the number of cells and the volume of the material needed for the bioprinting of scaffolds with graded and uniform cell densities.

		Number of scaffolds	Number of layers per scaffold	Total number of layers	Material Volume	Number of cells
Graded	Superficial		3	27	0.42 ml	8.5x10 <sup>6</sup>
	Middle	9	7	63	1 ml	10x10 <sup>6</sup>
	Deep		5	45	0.70 ml	3.5x10 <sup>6</sup>
Uniform	Superficial		-	-	-	-
	Middle	9	15	135	2.1 ml	21x10 <sup>6</sup>
	Deep		-	-	-	-
<b>TOTAL</b>		<b>18</b>	<b>15</b>	<b>270</b>	<b>4.22 ml</b>	<b>43x10<sup>6</sup></b>

As mentioned before, the experiment included 3 scaffolds per condition (graded, homogeneous) per time point (day 0, 14 and 28), so the total number of cell-embedded scaffolds was 3x2x3=18 scaffolds. From preliminary tests it had been determined that 1ml of the Alginate-based bioink was enough to print 64 layers with dimensions of 8mm x 8mm x 0.2mm, and 10% infill density. The 18 scaffolds were composed of 18 scaffolds x 15 layers/scaffold = 270 layers and 270 layers/(64 layers/ml) ≈ 4.22 ml of bioink, in total. Likewise, the bioink volume for each of the zones of the graded scaffolds, as well as the corresponding number of cells, was calculated.

After the calculation of the number of cells and the volume of the material to be used during bioprinting, the three cell suspensions were mixed with the corresponding amount of material to create the three different mixtures of cell densities. This means that, for example, for the mixture intended for the superficial zone of the graded scaffolds, in 0.42 ml of hydrogel a suspension of 42  $\mu$ l containing  $8.5 \times 10^6$  cells (cell density of  $20 \times 10^6$  cells/ml) would be added. The generation of the hydrogel-cells mixture is illustrated in Figure 11. First, the right amount of hydrogel is taken up by a syringe, from the cartridge containing the material. Then the corresponding cell suspension is pipetted into the syringe containing the hydrogel, and then with the help of a sterile female-female luer-lock and a second syringe, the two components are mixed together by gently mixing back and forth between the syringes to homogenize the cells in the bioink. After mixing, the mixture is transferred in one syringe and any air bubbles are removed by gently tapping the syringe to concentrate them on top and pushing them out of the syringe. Finally, the mixture is transferred from the syringe to a new cartridge for bioprinting.

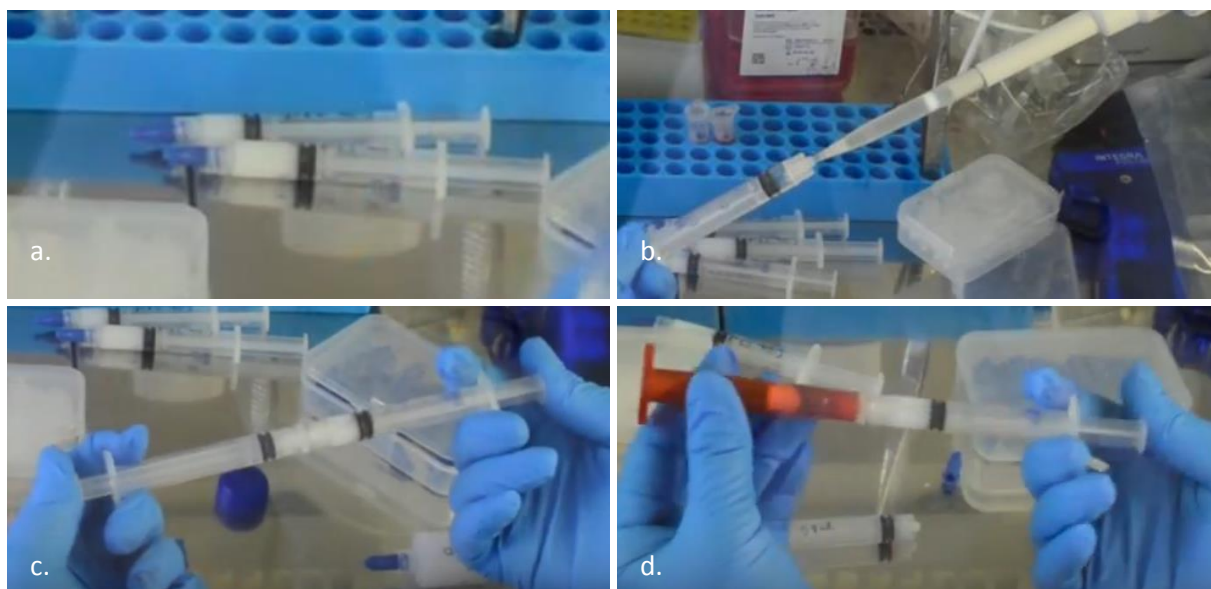


**Figure 11:** The steps of generating the cell-embedded hydrogel for each of the different cell densities. (a) The desired amount of material for each zone is placed in syringes. (b) The corresponding cell suspensions are added to the syringes containing the appropriate hydrogel volume. (c) With the use of a luer-lock and a second syringe the cells and the hydrogel are gently mixed together by mixing back and forth. (d) The final mixtures are concentrated in one syringe and transferred to new cartridges for bioprinting.

### Printer Setup

In order to set up the bioprinting procedure the printer was initially moved from the lab bench to the cell culture hood (laminar flow hood). The “UV sterilization” mode of the hood was turned on and when it was finished the “clean chamber” mode of the printer was initialized. The “clean chamber” mode utilizes UV light and a fan-filter system to selectively sterilize the surface and filter the air of the bioprinter chamber. This two-step sterilization procedure, of the hood and the bioprinter, ensured that bioprinting would run under sterile conditions. After the sterilization was performed, the printer was turned on and the correct .gcode file was selected from the connected USB stick. Once selected, the preview of the design was displayed on the bioprinter’s screen, with

all the layers and the extruders assigned to each one of them being visible. Next, the printing surface, nozzle size, temperature, pressure and speed of each print head was selected through the bioprinter's screen. The selected parameters for each print head are presented below (Table 7).

**Table 7:** Selected parameters for each material, used during bioprinting.

	Material	Nozzle size	Temperature	Pressure	Speed
<b>Print head 1</b>	Hydrogel (deep zone)	0.2 mm	RT	14 kPa	12 mm/sec
<b>Print head 2</b>	Hydrogel (superficial, middle zones)	0.2 mm	RT	14 kPa	12 mm/sec
<b>Print head 3</b>	PCL	0.2 mm	210 °C	200 kPa	4 mm/sec (base) 0.4 mm/sec (struts)

Next, the three print heads were manually calibrated to be as close to the surface as possible, without touching it and then the printing could start. The printer waited until the thermoplastic print head reached the desired temperature (210 °C) and then the printing started automatically. The scaffolds were printed on 16 mm coverslips which had been glued radially into a larger plastic petri-dish 10 cm. The reason for printing on cover slips is that the scaffolds could easily be detached for the printing surface and the reason they were placed on a petri-dish and not on a well plate is that the petri-dish provided better visibility between the nozzle tip and the printing surface during the calibration phase. Since the cartridges used for bioprinting were five (the 3 hydrogel mixtures with different cell densities, the support and the PCL) and the printer only had three printing heads, it was decided that the PCL and the support would be constantly assigned to the 2<sup>nd</sup> and 3<sup>rd</sup> print heads at all times, while the hydrogel cartridges were rotated in the 1<sup>st</sup> printing head, because only one of them was used at any specific moment during bioprinting. Therefore, after the deep zone was printed (first 5 layers) using the lowest cell density, the cartridge was switched to the one containing the medium cell density for the printing of the middle zone (the next 7 layers), which was in turn switched for the use of the highest cell density for the top zone (top 3 layers).

### Culturing the Scaffolds

After the cell-embedded scaffolds were bioprinted, the culture medium was changed from chondrocyte growth medium to chondrocyte differentiation basal medium (Clonetics™ CDM™ BulletKit™, Lonza) containing 1:20 FBS (CDMTM SingleQuots™ Kit, Lonza), 1:500 Insulin (CDMTM SingleQuots™ Kit, Lonza), 1:500 R3-IGF-1 (CDMTM SingleQuots™ Kit, Lonza), 1:1000 Gentamicin/Amphotericin-B (CDMTM SingleQuots™ Kit, Lonza), 1:200 Transforming Growth Factor-β1 (TGF-β1) (CDMTM SingleQuots™ Kit, Lonza) and 1:500 Transferrin (CDMTM SingleQuots™ Kit, Lonza). The differentiation medium was further enriched with 1:2000 lyophilized Transforming Growth Factor-β3 of 20 µg/ml stock solution (TGF-β3 - E. coli human, Sigma), and 1:1000 of 70mM Ascorbic Acid (Sigma) prior to adding it to the scaffolds. The 20µg/ml TGF-β3 stock solution was prepared by adding 2 µl of 2N Hydrochloric Acid, 13 µl of 7.5% Bovine Albumin Fraction and 85 µl of cell culture water to the vial containing 2 µg of lyophilized TGF-β3. The stock solution was

divided into 4  $\mu\text{l}$  aliquots and stored at  $-80\text{ }^{\circ}\text{C}$  in order to be added fresh to the differentiation medium, every time this was changed. The effects of the differentiation medium on expanded chondrocytes were investigated in a pilot experiment. It was observed that the medium helps the fibroblastic chondrocytes differentiate back to their spherical natural phenotype after approximately 9 days of culture. The differentiation medium was changed three times a week, using 2ml of medium per well (each well contained one scaffold), in a 24-well plate.

## 2.1.5 Mechanical Characterization of the Scaffolds

### Unconfined Compression Testing

Based on previous studies (Chen et al. 2018, Daly et al. 2016, Levato et al. 2017, Markstedt et al. 2015, Jeon et al. 2013), in the current project, the scaffolds were characterized utilizing a *compression test*, due to the fact that the major loading conditions cartilage receives are compressive loads. During the unconfined compression test, uniaxial stress was applied to compress the scaffold and the outcome is a relationship between the applied stress and the resulting strain of the material. This relationship can be used to calculate the elastic modulus (stiffness) of the construct.

The scaffolds were tested mechanically using the LLOYD Instruments LR5k compression machine (AMETEK test & calibration instruments), in order to measure their compressive stiffness. Both the PCL framework as well as the full scaffolds (PCL & hydrogel) have been tested separately using a 100 N load cell with a 0.1 N preload, a 1 mm deflection, and a strain rate of  $0.002\text{ sec}^{-1}$  (i.e. speed equal to 0.36 mm/min ). From the Load – Deflection curve generated by the machine on Nexygen software, 200 data points were exported per test, for further analysis. Each of the data points included information of time (s), load (N), extension (mm), and deflection from preload (mm)), which were used for the generation of the stress-strain curves and the calculation of the scaffolds' compressive stiffness. Stiffness calculations were performed based on a moving regression algorithm generated using R-code. The R-code is divided in three parts: the first part reads the .txt files of the 200 data points as extracted from the machine's software and calculates the stress and strain value for each point. The calculation of the stress is performed by dividing the "*load*" values with the base area (A) of the scaffold ( $\sigma=F(N)/A(\text{m}^2)$ ), and the calculation of the strain is performed by dividing the "*deflection from preload*" values with the height ( $L_0$ ) of the scaffolds ( $\epsilon=\Delta L/L_0$ ). The second part of the code plots the stress-strain curve for each of the scaffolds, based on the calculations of the first step. The third step calculates the linear line with the steepest slope, that fits to the linear part of the previously generated stress-strain curve, using a moving regression algorithm. Next, the slope of the linear curve is assigned to the stiffness variable and this yields the calculation of the compressive stiffness of the scaffolds ( $E=\sigma/\epsilon$ ). Figure 12 illustrates (a) the general process of an unconfined compression test and (b) the machine configuration used during the experiments.

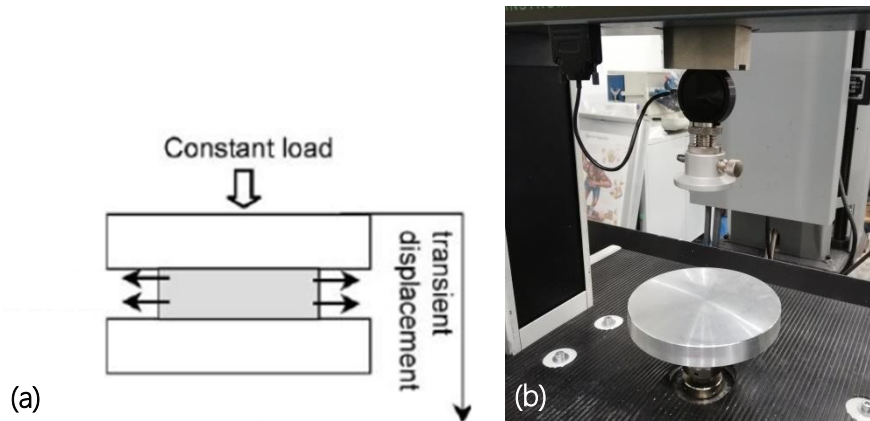


**Figure 12:** (a) Illustration of an unconfined compression test (Boschetti et al. 2004). (b) Configuration of the LLOYD LR5k machine used for the mechanical characterization of the scaffolds.

### 2.1.6 Immunohistochemical Evaluation of Cells and Scaffolds

#### Live-Dead Staining

For this staining, the Invitrogen Live/Dead™ Viability/Cytotoxicity Kit was used. The kit contains two reagents: Calcein, AM which gives the green color, indicating the live cells, and Ethidium homodimer-1 (EthD-1) which gives the red color, indicating the dead cells. The non-fluorescent calcein AM, once absorbed by living cells, is converted to the green-fluorescent calcein, after reacting with the intracellular esterases. Ethidium homodimer-1 is a high-affinity nucleic acid stain that is weakly fluorescent, until bound to DNA when it emits strong red fluorescence. Figure 13 depicts the principle of a live-dead fluorescent staining.

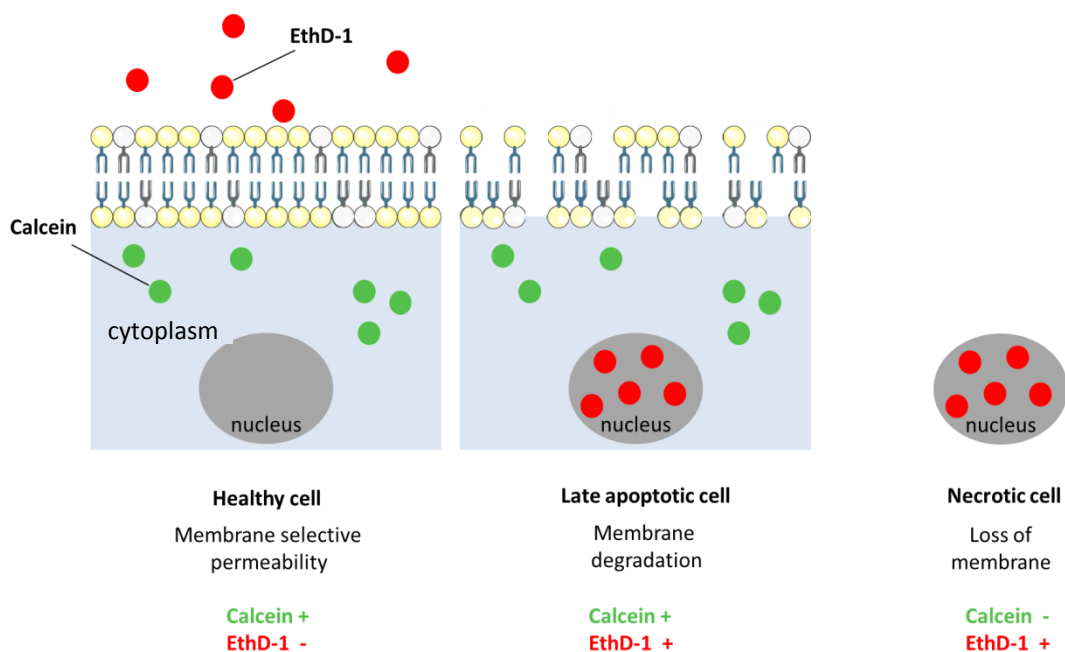


**Figure 13:** In viable cells, the selective permeability of the membrane allows for calcein entry, but prevents EthD-1 from entering the cells (calcein+/EthD-1-). As a consequence, live cells appear green. During late apoptosis, membrane degradation creates pores in the plasma membrane allowing EthD-1 to enter the cells (calcein+/EthD-1+). Finally, the necrosis stage is characterized by membrane loss, so these last cells appear only red (calcein-/PI+) (Basmaciyar et al. 2017).

The protocol for the live-dead staining starts with the removal of the medium from the wells. The scaffolds are then cut in half in the sagittal plane using a scalpel, as illustrated in Figure 14. Each sample (cells or cell-embedded hydrogels) is washed with DPBS\* two times under the cell hood. Then, the plates are transferred under the chemical hood where the DPBS is removed. An appropriate volume of solution containing 0.05% of Calcein, AM and 0.15% of Ethidium Homodimer, diluted in 1× DPBS is added to each sample. The samples are then incubated with the solution for 30' at room temperature. After this time, the reagents' solution is discarded. Samples are washed with 1× DPBS one time (5' per wash). Finally, the samples are mounted on glass slides (Menzel-Glaser Superfrost, ThermoScientific) using Prolong Gold antifade reagent (with or without DAPI) to image them under the fluorescent microscope (ZOE fluorescent cell imager, Biorad). To image full thickness scaffolds (3 mm height), after cutting them in half, the flat cross section is placed facing down towards the bottom of the well plate where it is kept hydrated during imaging with the fluorescent microscope (ZOE fluorescent cell imager, Biorad). It is important to note that, in 3D constructs there may be cells with "blurry" appearance because they are out of the focal plane.

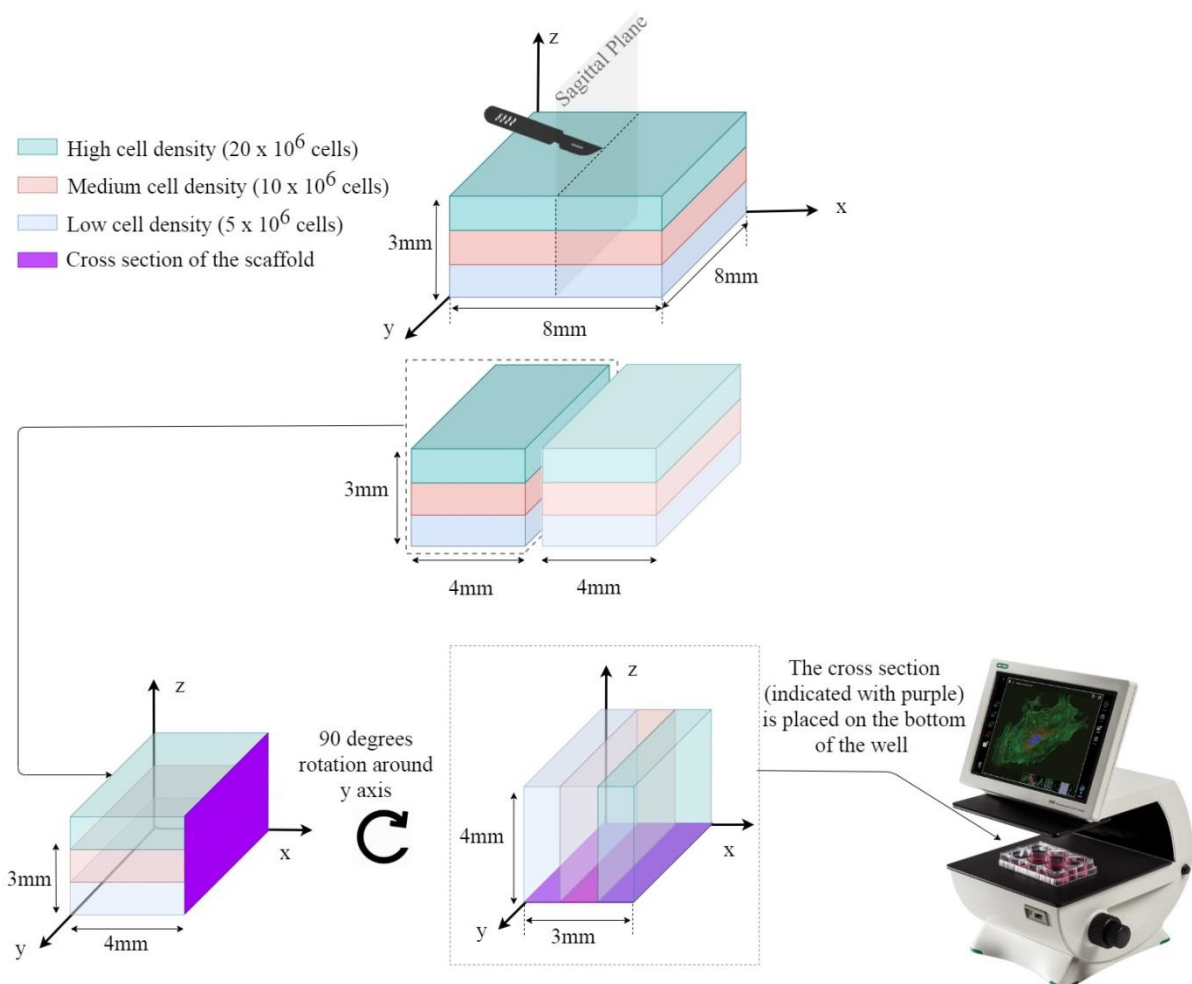


**Figure 14:** The procedure of cutting the scaffold in half, before Live-Dead staining, and imaging the cross section under the ZOE fluorescent microscope. The thicknesses of the three scaffold zones are not illustrated in their actual scale.

\* Note: Phenol-free media may be a more indicated solution than PBS when performing the live/dead assay for alginate-based hydrogels, which may de-crosslink and accumulate calcium phosphate crystallizations in the presence of PBS solutions.

### Indirect Immunofluorescent Staining (for Collagen II or Aggrecan) of monolayer cells or cell-embedded droplet hydrogels

First, the medium is removed from the wells and each sample (cells or cell-embedded hydrogels) is washed with 1 x DPBS two times under the cell hood. The plates are then transferred under the chemical hood and the DPBS is removed. In case the samples are alginate-based hydrogels, an appropriate volume of crosslinking agent (Cellink) is added after washing so that they will not dissolve in the paraformaldehyde solution during the next step. After 2 minutes the crosslinking agent is removed and an appropriate volume of 4% paraformaldehyde (4% PFA) solution is added to the samples until they are fully covered. Samples are incubated for 20' at room temperature and then the formaldehyde solution is discarded into the correct chemical bin. Next, each sample is washed with 1x DPBS two times (5' per wash). Then 0.5% of Triton solution (diluted in DPBS) is added to the samples which are incubated for 5' at 4°C (fridge) until the cells are permeabilized. Triton is then discarded. 1% BSA solution (diluted in DPBS) is added to the samples and they are incubated for 5' at 37°C to block the receptors. Next, the primary antibody<sup>1,3</sup> is added (1:100 dilution in 1% BSA) and the samples are incubated at 37°C for 1h. The antibody solution is removed and the samples are washed with 0.5% Tween three times at room temperature (5' per wash). Then the secondary antibody<sup>2,4</sup> is added (1:500 dilution in 1% BSA) and the samples are incubated at room temperature for 1h. The secondary antibody solution is removed and the samples are washed with 0.5% Tween three times at room temperature (5' per wash). After Tween the samples are washed with 1x DPBS one time at room temperature (5' per wash). Finally, the samples are mounted on glass slides (Menzel-Glaser Superfrost, ThermoScientific) using a reagent (Prolong™ Gold antifade reagent, Invitrogen), with or without DAPI, to image them under the fluorescent microscope.

### Direct Immunofluorescent Staining (for Actin)

First, the medium is removed from the wells and each sample (cells or cell-embedded hydrogels) is washed with 10x DPBS two times under the cell hood. The plates are then transferred under the chemical hood and the DPBS is removed. In case the samples are hydrogels, an appropriate volume of crosslinking agent (Cellink) is added after washing so that they will not dissolve in the paraformaldehyde solution during the next step. After ~2 minutes the crosslinking agent is removed and an appropriate volume of 4% paraformaldehyde (4% PFA) solution is added to the samples until they are fully covered. Samples are incubated for 20' at room temperature and then the formaldehyde solution is discarded into the correct chemical bin. Next, each sample is washed with 1x DPBS two times (5' per wash). Then 0.5% of Triton solution (diluted in DPBS) is added to the samples which are incubated for 5' at 4°C (fridge) until the cells are permeabilized. Triton is then discarded. 1% BSA solution (diluted in DPBS) is added to the samples and they are incubated for 5' at 37°C to block the receptors. Then, the primary antibody<sup>5</sup> is added (for Actin: Rhodamine phalloidin 415 (red), Invitrogen) in a 1:2000 dilution in 1% BSA, and the samples are incubated at 37°C for 1h. After the incubation the antibody solution is removed and the samples are washed with 0.5% Tween three times at room temperature (5' per wash). After washing with Tween, the samples are washed with 1x DPBS one time at room temperature (5' per wash). Finally, the samples are mounted on glass slides (Menzel-Glaser Superfrost, ThermoScientific) using the

Prolong Gold antifade reagent, with or without DAPI, to image them under the fluorescent microscope. Table 8 contains the primary and secondary antibodies used in immunofluorescent staining and Figure 15 presents a scheme of the direct and indirect immunofluorescent processes.

**Table 8:** Primary and secondary antibodies used during direct (Actin) and indirect (Collagen II, Aggrecan) immunofluorescent staining.

---

Antibodies used for immunofluorescence staining:

---

**Collagen II**

1. Primary antibody: IgG ab34712 rabbit pAb to Collagen II (Abcam)
2. Secondary antibodies: IgG A-21206 Alexa Fluor TM 488 donkey anti-rabbit IgG H&L (green), IgG A-21207 Alexa Fluor TM 594 donkey anti-rabbit IgG H&L (red) (Invitrogen by Thermo Fisher Scientific)

**Aggrecan**

3. Primary antibody: IgG1 ab3778 mouse mAb to Aggrecan [6-B-4] (Abcam)
4. Secondary antibody: IgG ab205719 goat anti-mouse IgG H&L (HRP) (Abcam)

**Actin**

5. Primary antibody: R415 Rhodamine phalloidin 415 (red) (Invitrogen)
- 

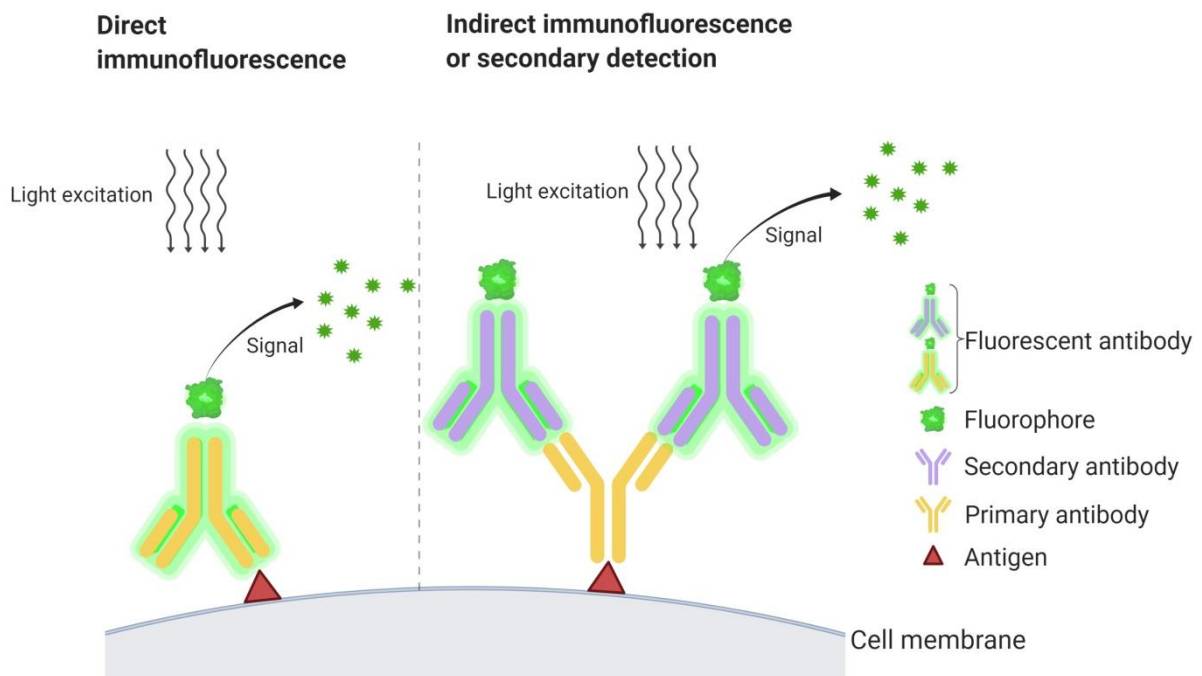


**Figure 15:** The principle of direct and indirect immunofluorescence processes with the corresponding antibodies.

### 2.1.7 Histochemical Evaluation of the Scaffolds

Histological evaluation was performed to reveal the presence or absence of specific molecules, and the distribution and morphology of the cells embedded in the scaffold. The histological procedure included the following steps: fixation of the sample, dehydration of the sample, embedding of the sample in paraffin, sectioning of the sample into thin slices using a microtome, staining of the sample's slices and imaging the stained slices. An illustration of a complete, general histological process is presented in Figure 16.



**Figure 16:** Workflow of the tissue (or scaffold) processing steps during a general histological evaluation process.

#### Fixation of Samples

Fixation is performed to preserve the structure of the tissue in a state (both chemically and structurally) as close to living tissue as possible. Preservation of a tissue's or scaffold's structure requires a chemical fixative that can stabilize the proteins, nucleic acids and muco-substances of the tissue by making them insoluble. For this reason, the bioprinted cartilage scaffolds were fixated using 4% paraformaldehyde (pfa) overnight in the fridge, with a volume ratio of tissue : fixative of 1 : 5. For new materials fixation time may need to be optimized, as longer fixation times can cause artifacts apparent at high levels of magnification. Moreover, pfa should always be buffered, since non-buffered pfa is acidic and would degrade the specimens. The next day after the overnight incubation, the scaffolds were washed twice with PBS, placed in a 1 : 1 solution of 100% EtOH : Cellink crosslinking agent ( $\text{CaCl}_2$ ), and stored in the fridge until further transferred to the Orthopedics department of Erasmus MC for histological analysis. Adding the crosslinking agent in the solution is important for the scaffolds, since Alginate may dissolve over time.

#### Dehydration & Embedding of Scaffolds

Before fixation, all 8 mm × 8 mm × 3 mm cartilage scaffolds had been cut through the middle into two parts of 4 mm × 8 mm × 3 mm parts as seen in Figure 14. These parts were numbered and put in labeled cassettes for the dehydration process, which took place, according to the Erasmus MC protocol, on the day prior to the embedding. The dehydration is performed by first using graded ethanol solutions (70% ETOH, 80% ETOH, 96% ETOH, 2x 100% ETOH), then 2x xylene, and finally 4x liquid paraffin. Each of the dehydration steps lasted 1h, and they were all performed under vacuum. The reason for using graded dehydrating solutions is that they gradually expose the sample to changes in hydrophobicity, minimizing damage to cells and ensuring a

homogeneous diffusion of wax throughout the sample. On the day of the embedding (the day following the dehydration), the process started with a small amount of melted paraffin (60°C) being poured in the mold, dispensing from the paraffin reservoir. The scaffolds, in which the PCL part had been melted away by the xylenes during dehydration, were placed inside the metal molds using warm forceps. They were positioned standing on their side, with their cross section facing the bottom of the mold. The mold was then quickly transferred to a cold plate, for the paraffin to solidify in a thin layer that would hold the sample in position. When the tissue was fixed in the desired orientation, the bottom of the cassette corresponding to this specific sample was added on top of the mold as a backing. Then, more melted paraffin was added on top of the sample from the paraffin dispenser, up to the point where the face of the cassette was fully covered in wax. The importance of placing the plastic cassette on top of the sample and binding them together with paraffin was, first, to keep track of the sample by having the correct label on it, second, to be able to detach the paraffin-embedded sample from the mold, and third, to be able to place the sample in the microtome (since the opening for the sample on the microtome is of the size and shape of the cassette). The “mold-sample-cassette” sandwich was allowed to solidify at room temperature forming a block that can be held in a microtome, for approximately 2 hours. The paraffin-embedded samples were detached from the metallic molds and were collected in a bucket in order to be transferred to the microtome for slicing (Figure 17).

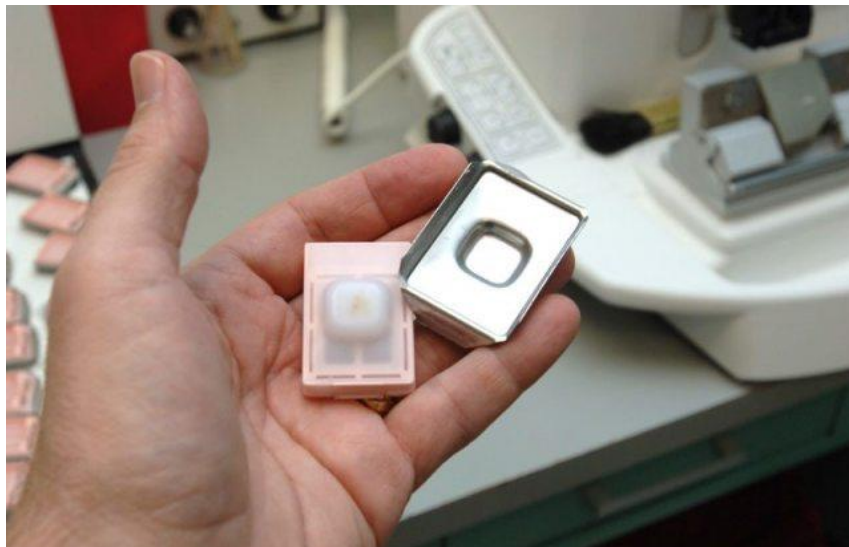


**Figure 17:** Tissue embedded in paraffin (tissue block) with the cassette attached to it and the metallic mold in which it had been casted (adapted from <https://www.protocolsonline.com/histology/sample-preparation/paraffin-processing-of-tissue/>).

### Sectioning of Paraffin-Embedded Samples

Once the paraffin-embedded samples had solidified, they were ready for sectioning in the microtome. Samples were placed in a Leica RM2135 microtome, with a slice thickness set at 6 $\mu$ m and a sectioning angle of 5 degrees. Usually 30-40 slices needed to be cut before the whole sample was exposed to the blade, however sections were numbered starting with the first section containing a full piece of the sample, which was labeled as section n<sup>o</sup> 1. After a few sections

containing the whole sample were cut, they were gently picked up from the machine using a scalpel and placed in a bowl of warm water (50-60°C, below the melting point of wax) in order to relax. Relaxation of the slices allows for the wax to stretch and regain its original shape when placed in warm water, eliminating grooves and waves formed on the sections during cutting. After relaxation, the slices were picked up on a glass slide (Menzel-Glaser Superfrost, ThermoScientific) from the water and allowed to dry overnight in an oven at 37°C. The drying step is very important for the sample to stick on the coated glass slide and remain attached during the histological staining process.

## Histology Staining

After the overnight incubation in the oven the sections were ready for the histological staining process. During this step, the sections obtained from the microtome, were first stripped from paraffin and then were stained with specific dyes targeting nucleic acids (e.g. the DNA in the cells nuclei) or ECM components (e.g. sGAGs and Collagens). The following protocols describe the processes of the three histological staining (H&E, PSR, and Alcian Blue) performed on the samples' sections.

### a. Haematoxylin and Eosin (H&E) Staining

The H&E staining is the quickest and most commonly used staining to check cell and tissue morphology. Eosin is an acidic dye, which due to its negative charge, stains basic (or acidophilic) structures pink. For example, the cytoplasm of the cells is stained pink by H&E staining. Haematoxylin, the other component of the HE staining, can be considered as a basic dye. It is used to stain acidic (or basophilic) structures with a purplish blue color. This color shift (towards purple) only happens when the red staining is passed on to a neutral or alkaline solution such as hard tap water. For example, the nucleus of the cells is stained purple by H&E staining, while the cytoplasm stains up a pinkish color in its RNA-free areas.

The protocol for the H&E staining, for paraffin embedded sections, starts with the deparaffinization of the sections. For that, the sections are submerged two times in Xylene (Sigma #X1040), two times in 100% EtOH, one time in 96% EtOH and one time in 70% EtOH. Each step lasts 5'. Next, sections are rinsed in distilled water twice, with each rinse lasting 3'. Then, samples are submerged in hematoxylin (Haematoxylin Gill's, ready-to-use, Sigma #GHS232) for 5'. Haematoxylin should always be filtered before use. Then, samples were put under running tap water for 5', to convert red staining into blue. Then, they were given a quick dip in distilled water. After that, samples were submerged in Eosin (Eosin Y (Merck, 1.15935), 2% in 50% EtOH, then add 0.5ml glacial acetic acid per 100 ml staining solution) for 45". Next, samples were submerged in 70% EtOH for 10". Finally, samples were dehydrated by being submerged in 96% EtOH, 100% EtOH, and two times Xylene. Each step lasted 1'. Sections were mounted using Depex (Merck #1.07961.0500), while slides were still wet from xylene. Slides were allowed to dry in the recirculation cabinet for at least 60'.

### b. Picrosirius Red (PRS) Staining

The PRS stain is intended for use in the histological visualization of collagen. This stain can be imaged using standard light microscopy or polarized light to distinguish the different types of collagen fibers based on their thickness and maturity. In this thesis, images were taken only under a bright-field microscope, where collagen (all types) appears red on a pale yellow background.

The protocol for the PRS staining, for paraffin embedded sections, starts with the deparaffinization of the sections. For that, the sections are submerged two times in Xylene (Sigma #X1040), two times in 100% EtOH, one time in 96% EtOH and one time in 70% EtOH. Each step lasts 5'. Next, sections are rinsed in distilled water twice, with each rinse lasting 3'. Then, samples are submerged in Picro-sirius Red solution (0.1g PSR (Direct Red 80, Sigma, # 365548) in 100 ml Picric acid solution 1.3% in H<sub>2</sub>O (saturated) (P6744 Sigma)) for 60'. After that, samples were washed in 0.1% acetic acid two times, with each wash lasting 10". Next, sections were submerged in 100% ethanol three times, with each time lasting 1'. Finally the sections were submerged in Xylene twice, for 1' each time. Sections were then mounted using Depex (Merck #1.07961.0500), while slides were still wet from xylene. Slides were allowed to dry in the recirculation cabinet for at least 60'.

### c. Alcian Blue Staining

Cartilage is composed to a large extent of GAGs, which are the dominant part of the proteoglycan Aggrecan and are located primarily on the surface of cells or in the extracellular matrix. Alcian blue is a tetravalent cation (cationic dye) with a hydrophobic core. Using these four charges, the dye binds strongly to negatively charged polymers such as GAGs. Alcian blue is most often used to selectively stain acidic mucosubstances. At pH 1.0, Alcian blue stains only sulphated GAGs and glycoproteins. At pH 2.5, on the other hand, this dye can also stain hyaluronic acid and glycoproteins that owe their acidity to sialic acids. GAGs are colored more intensely at PH 2.5 than at pH 1.0 because their ionized uronic acid carboxy groups add to the negative charges of the half-sulfate esters. In the current study, the focus lies on sGAGs deposition and hence, a dye with pH=1 was selected.

The protocol for the Alcian Blue staining, for paraffin embedded sections, starts with the deparaffinization of the sections. For that, the sections are submerged two times in Xylene (Sigma #X1040), two times in 100% EtOH, one time in 96% EtOH and one time in 70% EtOH. Each step lasts 5'. Next, sections are rinsed in distilled water twice, with each rinse lasting 3'. Then, samples are submerged in Alcian Blue pH 1 (Sigma, # A3157), 1% in 0.1M Hydrochloric Acid (Sigma, #84422. Dilute in distilled water) for 10'. The dye can be reused many times, but the pH must be checked before every use. Next, samples are rinsed with distilled water three times, with each wash lasting 1'. Then, the sections are counterstained in nuclear fast red solution (Nuclear fast Red (Merck, #1.00121.0500) ready-to-use.) for 1'. Then, samples were rinsed in distilled water for 1'. Finally, samples were dehydrated by being submerged in 70%, 96%, 100% EtOH and Xylene (2x). Each step lasted 1'. Sections were then mounted using Depex (Merck #1.07961.0500), while slides were still wet from xylene. Slides were allowed to dry in the recirculation cabinet for at least 60'. The resulting colors are: GAGs/mucins stained in bright blue and cell nuclei stained in red/pink.

## Histology Imaging

The stained histological slices were imaged under a DM500 optical Leica microscope. An image acquisition protocol was established to ensure consistent data generation. All relevant parameters, such as exposure time, white balance, light intensity, and plate dimensions, were fixed for all image acquisitions. All images were captured using the microscope camera under the following conditions set on the Leica Application Suite (LAS software):

Brightness	Exposure	Gain	Gamma	Saturation
60%	2ms for 4× magnification	1	0.7	100
	13ms for 10× magnification			
	144ms for 40×40 magnification			

H&E stained slices with 4× magnification were used for the determination of the cell density gradient. Alcian Blue and Picosirius Red stained slices were used to define the presence of sGAGs and Collagen, respectively, in the scaffolds.

## 2.2 Data Analysis

### 2.2.1 Image Analysis

Histology images were analysed based on the cell density in each of the scaffold's zones, the neo-tissue formation (sGAG and Collagen deposition) and the morphology of the chondrocytes' nuclei within the hydrogel, between the three zones. The analysis of the data was performed using the Image J v2.0.0 software. Before analysis all images were spatially calibrated using their integrated scale bar so that the area values were calculated in mm. For the *analysis of the H&E staining*, the microscope images were first split into the three colour channels (red, green, blue) for the different colours to be separated and enable focusing on different objects and areas. Depending on the focus of the analysis (e.g. nuclei stained with H&E), the desired channel was selected based on how clear and distinct the desired objects look on it. For H&E the best channel for nuclei separation was the green channel. Then, for the selected channel the threshold was adjusted in order to make the depicted objects even more distinguishable from the background. Using the "Analyse particles" plugin and by setting the correct size and circularity range for the particles, the software detects and counts the desired objects present in the image. The minimum size was set between 5 and 35 pixels, depending on the image, and the maximum size was set at 300. The circularity range was set as 0.45-1.00 for all images. This analysis on the H&E images was performed using the ROI (Region of Interest) manager. This tool allows working with multiple selections on a single image. Based on this principle, each image was divided into three regions of interest, corresponding to the three zones of different cell densities, and each of these regions was analysed separately from the others using a different threshold and size spectrum depending on the data of the region. This process, which customizes the threshold and object size parameters for each zone, yields better results in terms of detection and counting of the cells located in different zones. It is, therefore, ideal for assessing the cell density gradient between the different zones of the scaffolds. The H&E analysis was performed for both scaffold cultures (with and without ascorbic acid) and the analysis stages are presented in detail in Figure 19.

For the *analysis of the Alcian Blue and Picrosirius Red staining*, was performed with the use of the Trainable Weka Segmentation plugin (Arganda-Carreras et al. 2017). This plugin utilized a segmentation algorithm which combines a collection of machine learning algorithms with a set of selected image features, to produce pixel-based segmentations. Three classes used for the training of the algorithm and the classification of the results: (a) a class for the negative background staining of the Alginate, (b) a class for the stained cell nuclei and (c) a class for the positively staining areas (areas with darker blue or red colour for Alcian Blue and Picrosirius Red, respectively). The training of the algorithm was performed by manually selecting multiple areas belonging to each of the classes (using Image J's selection tool) and categorize them according to their corresponding class. After that, the features of the input image were extracted and converted to a set of vectors of float values, which is the format the Weka classifiers are expecting. Finally, the plugin creates and displays the resulting image. This image is equivalent to the current overlay (8-bit colour, with each colour corresponding to a specific class) (Figure 18). The training features used for the training of the algorithm, were the Gaussian blur, the Sobel filter, the Hessian matrix, and the difference of Gaussians.

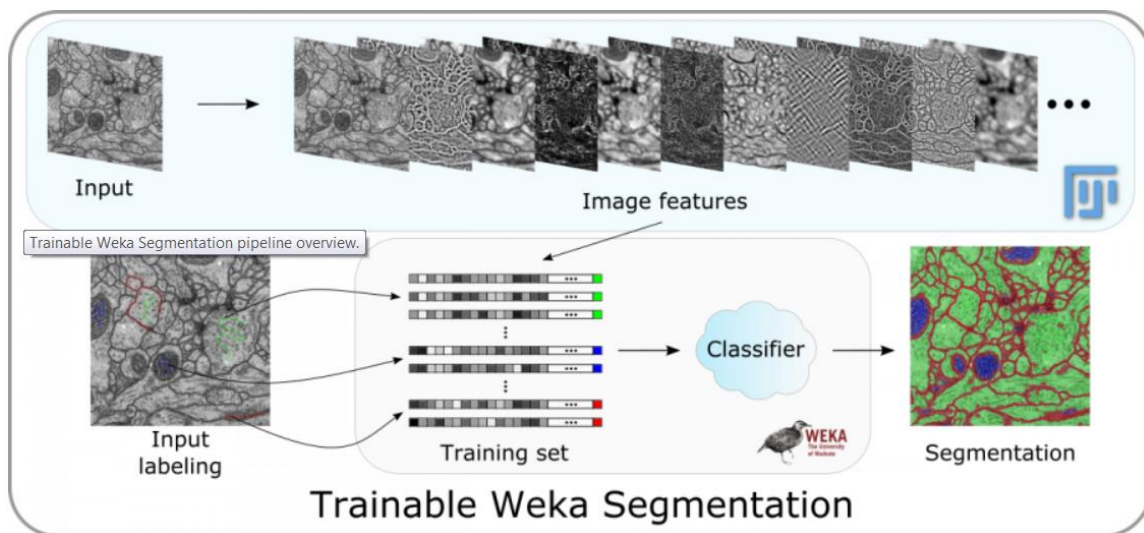


**Figure 18:** TWS pipeline for pixel classification. First, image features are extracted from an input image using Fiji-native methods. Next, a set of pixel samples is defined and represented as feature vectors, and a WEKA learning scheme is trained on those samples and finally applied to classify the remaining image data. The user can then interactively provide feedback by correcting or adding labels (Arganda-Carreras et al. 2017).

After training, the same classifier was applied to all the images of the same staining. The plugin performed the image segmentation based on the current classifier and the selected features, and created a stack of images; each one highlighting one of the selected features. By selecting the desired 8-bit color image from the stack and setting an appropriate threshold, we performed the area and intensity measurements on the image's objects, to evaluate the sGAG and Collagen content between the zones, at different time points. The semi-quantitative analysis for sGAGs and Collagen was performed only on the samples of the second experiment, which were cultures in differentiation medium with ascorbic acid. The stages of the analysis are presented in detail in Figure 20.

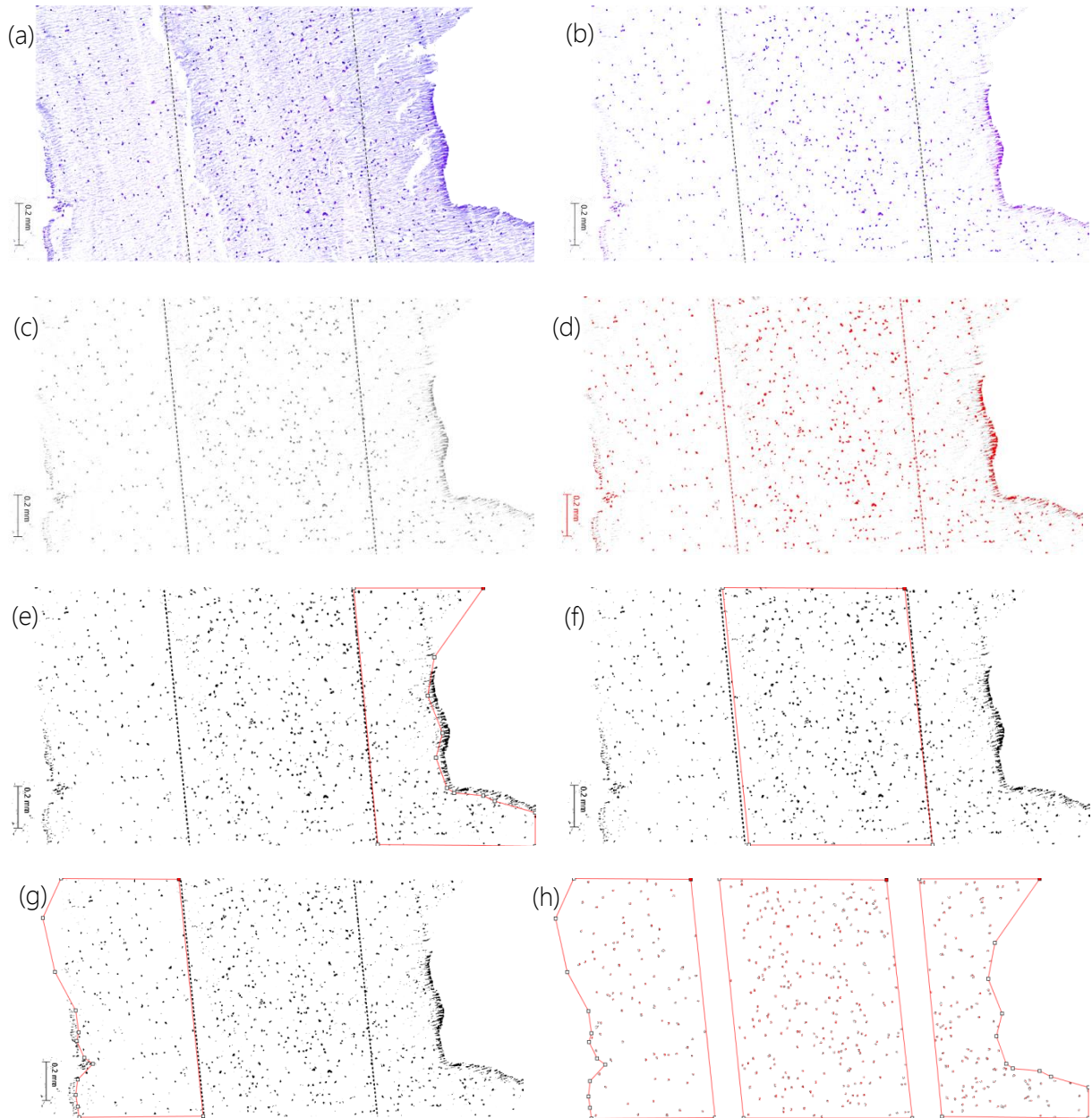


**Figure 19:** (a) H&E image ( $\times 10$  magnification) of is opend in Image J. (b) The brightness and the contrast of the image are each increased by 40%, to get a clearer distinction of the cell nuclei. (c) The image is transformed into an 8-bit (greyscale) image by splitting it into the three color channels (red, green, blue). The best channel which allows for better distinction of the nuclei from the background, is selected for further analysis (green channel). (d) The threshold is being adjusted in order to achieve optimal object separation from the background. (e), (f), (g) The threshold color is shifted to black & white and the regions of interest corresponding to the three scaffold zones are set. (h) The three zones are analyzed separately for their cell number and the results of these images are evaluated by comparing them with the initial image, using the outlines of the distinct particles. The zones are defined from left to right starting from the bottom layer. The scale bars represent 0.2 mm.

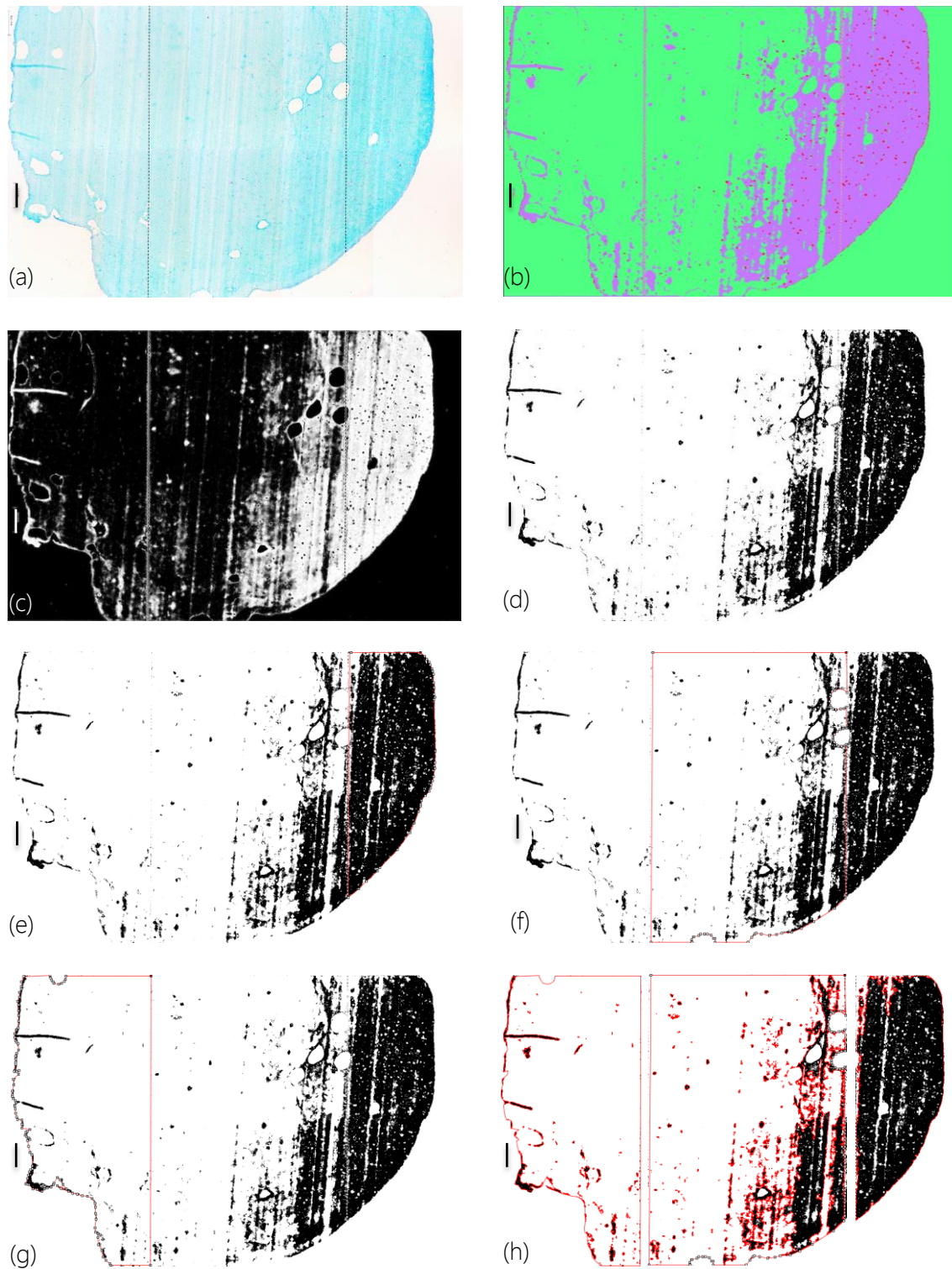


**Figure 20:** (a) Alcian Blue image ( $\times 10$  magnification) is opened in Image J. (b) The Weka segmentation plugin is employed to classify the areas corresponding to cells, sGAGs and background stain. (c) The segmented image is transformed into an greyscale image by splitting it into the three channels according to the defined classes. The channel which allows for better distinction of the sGAGs from the background, is selected for further analysis. (d) The threshold is being adjusted in order to achieve optimal object separation from the background. (e), (f), (g) The regions of interest corresponding to the three scaffold zones (bottom, middle, top) are set. (h) The three zones are analyzed separately for their sGAGs content and the results of these images are evaluated by comparing them with the initial image, using the outlines of the distinct areas corresponding to sGAGs. Scale bars = 0.2 mm.

## 2.2.2 Statistical Analysis

All quantitative results are presented as mean  $\pm$  standard deviation. Statistical analysis was performed using the GraphPad Prism 8 software (GraphPad Software, USA, Version 8.0.2). For the analysis of the cell density and sGAG and Collagen content, experimental groups were analysed for significant differences using a two-way Analysis of Variance (ANOVA) and the results were corrected for multiple comparisons, using Bonferroni's post hoc test. P-values  $<0.05$  were considered significant and the significance levels were subdivided into \*(p value  $\leq 0.05$ ), \*\* (p value  $\leq 0.01$ ), \*\*\* (p value  $\leq 0.001$ ), and \*\*\*\* (p value  $\leq 0.0001$ ). For the comparison of the PCL vs the PCL+hydrogel stiffness, as well as for the difference in cell viability between the two different scaffold designs, an unpaired t-test was performed ( $p < 0.05$ ). Finally, for the comparison of the 3D experimental vs theoretical cell density of the homogeneous scaffolds (due to the fact that the theoretical values do not follow a Gaussian distribution) a non-parametric paired Wilcoxon test was performed with a significance level of  $p < 0.05$ .

# 3. Results

## 3.1 Design, Fabrication and Mechanical Characterization of the Scaffolds

The optimal design and printing conditions of the bioprinted scaffolds were determined based on some preliminary experiments presented in Appendices B and D. Based on these results, the effect of bioprinting on the stability, mechanical properties and cell viability of the constructs was investigated (Figure 21).

The PCL and the alginate-based hydrogel were combined into a final design to fabricate the full scaffold (Figure 21a). A 10% infill density and a rectilinear infill pattern were selected for the hydrogel part, which resulted in 5 fibers being printed per layer of the scaffold. For higher infill densities the bilateral over-extrusion of the hydrogel fibers, following the extrusion, resulted in a merging of the distinct fibers together, which was not desirable. Figure 21b depicts a 3D representation of the resulting scaffold and its parts after setting the desired infill pattern, angle and density in the slicing software.

Combining the designed scaffold with the results of the optimization study, the bioprinting of the cartilage scaffolds took place. Figure 21c (left) shows the resulting scaffolds after bioprinting. The bioprinted scaffolds were evaluated based on their mechanical properties and cell viability. The results showed that the constructs were characterised by enhanced compressive stiffness with the PCL framework reaching a mean stiffness of  $8.02 \pm 0.69$  MPa, and the full scaffold (PCL framework + hydrogel) a mean stiffness of  $8.35 \pm 0.35$  MPa. The addition of the hydrogel to the PCL framework caused an increase of the compressive stiffness of around 300 kPa, but this difference was not marked as significant. A live-dead staining was performed on the full scaffolds ( $n=2$ ) and the images were obtained from both sides of the scaffolds (top and bottom) with a fluorescent microscope (Figure 21d). The viability of the selected design was ~98% right after bioprinting.

The rest of the results regarding the gradient generation and the evaluation of neo-tissue formation are structured as follows, in the next paragraphs: section 3.2 includes the cell viability data after bioprinting for day 0, 14 and 28, and the assessment of the fabrication and maintenance of the cell density gradient which was performed based on the analysis of the H&E images of the scaffolds cultured in differentiation medium without ascorbic acid. Following that section is section 3.3 which includes the evaluation of the ECM deposition in the bioprinted scaffolds. This evaluation was performed based on the analysis of Alcian Blue and Picrosirius Red images for scaffolds cultured in differentiation medium with ascorbic acid, for enhanced ECM synthesis. Due to this addition in the culture medium, an evaluation of the fabrication and maintenance of the cell density gradient was again performed, for this batch of scaffolds, and is presented in the beginning of section 3.3, before the results of the ECM biosynthesis.

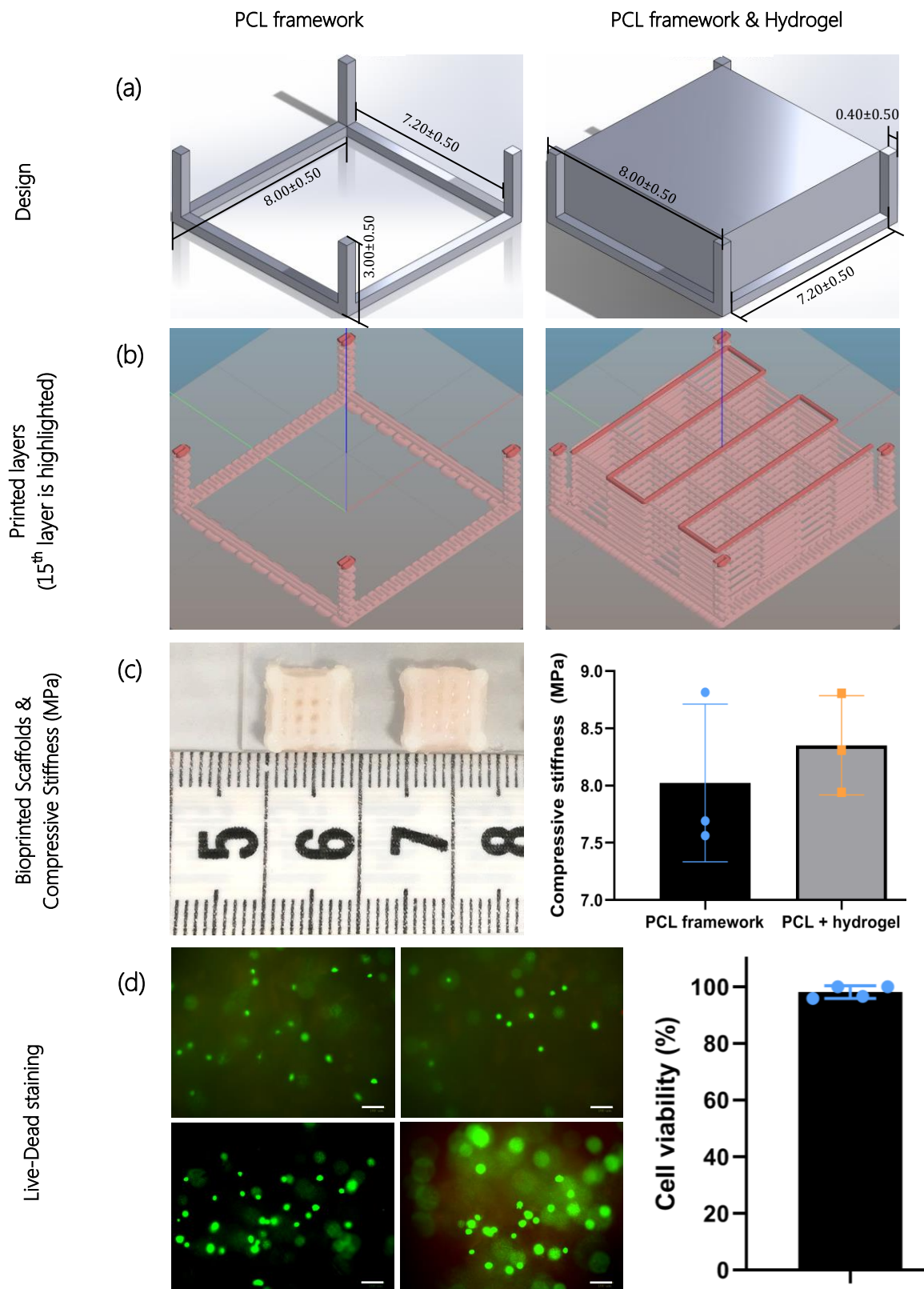
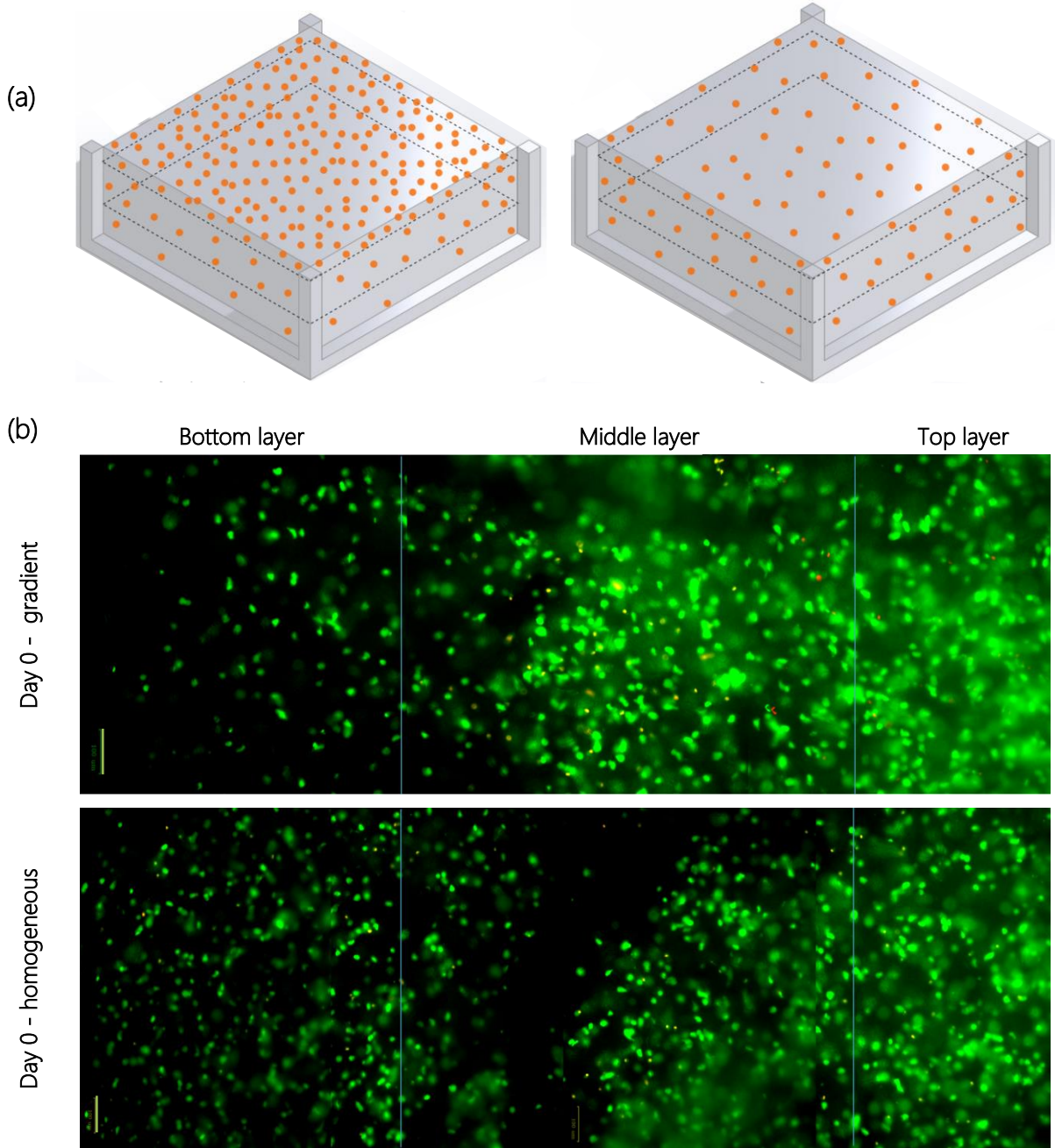


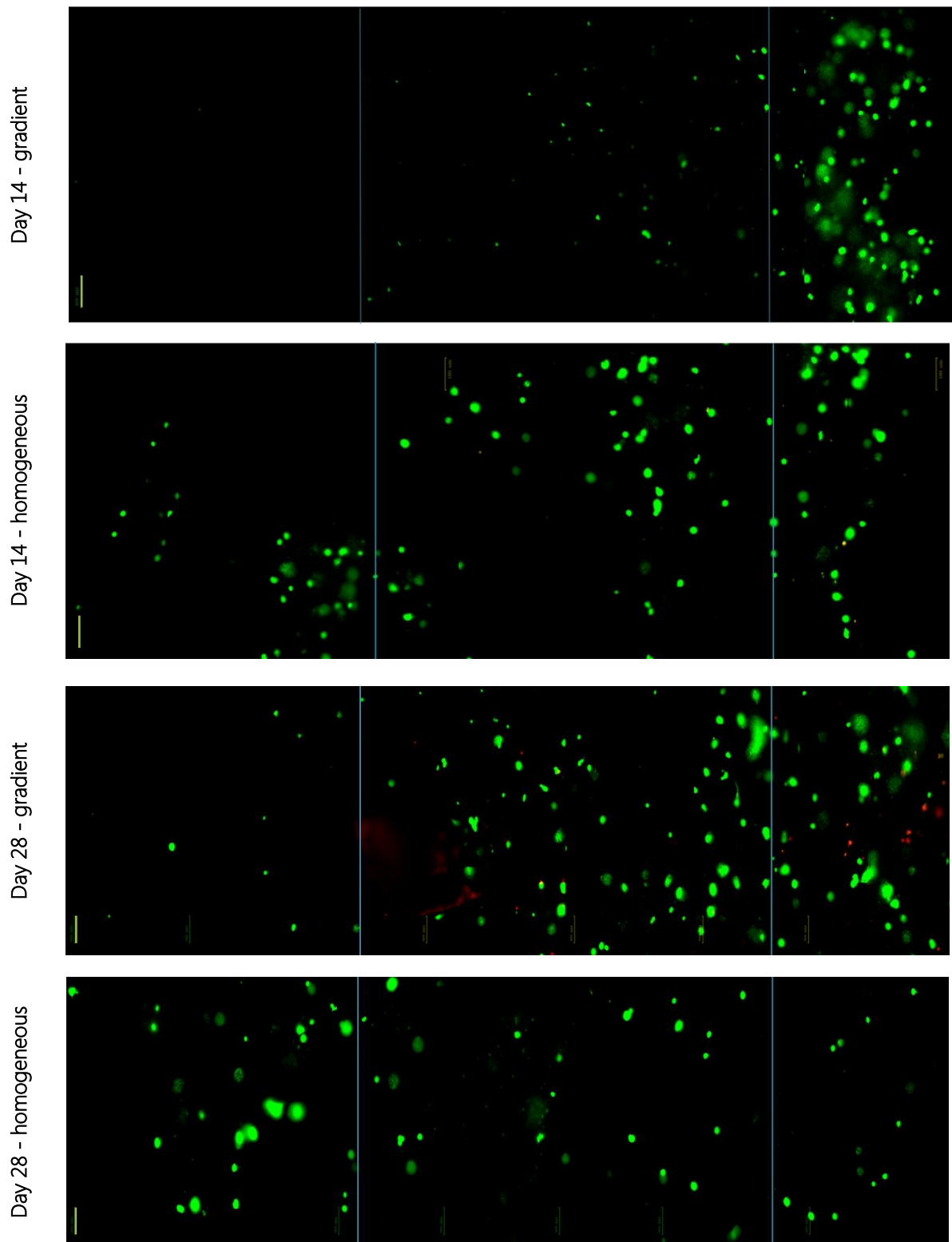
**Figure 21:** (a) Design of the PCL framework (left) and the full scaffold (PCL + hydrogel) (right) with their respective dimensions in mm. (b) Schematic representation of the PCL and the PCL + hydrogel parts with a  $0^\circ$ - $90^\circ$  infill pattern and a 10% infill density. The image illustrates the distinct layers of the scaffolds' parts with a highlight on the final printed zone (15<sup>th</sup> zone). (c) Compressive stiffness of the PCL and the PCL + hydrogel parts, respectively. (d) Viability data for the selected design, after bioprinting, at day 0. The images were obtained from the bottom and top planes of the printed scaffolds (N=2). The scale bars in the live/dead staining represent 100  $\mu$ m.

### 3.2 Bioprinting of the scaffolds with different cell densities

#### Live-Dead Staining

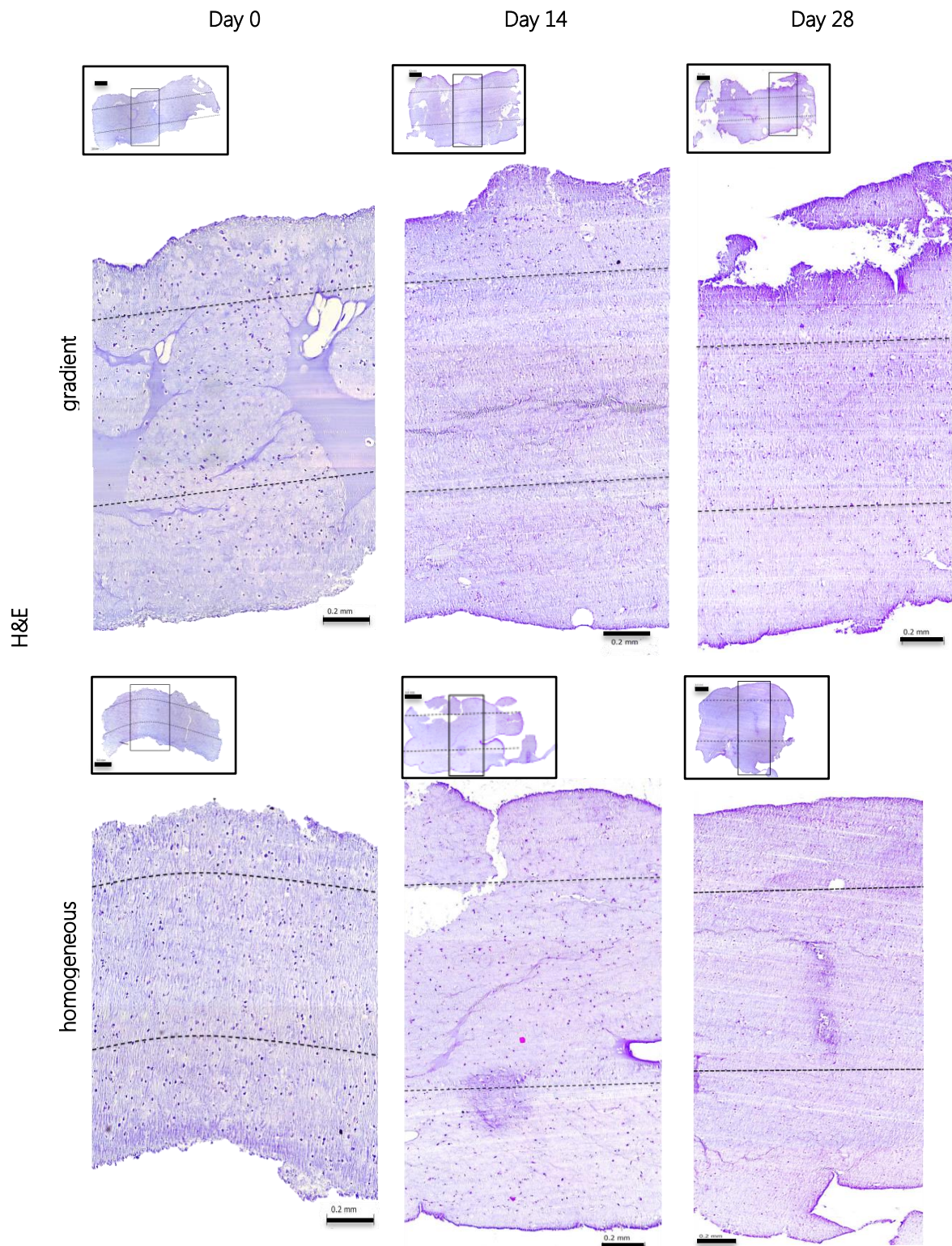
To assess the viability of the embedded chondrocytes over time, as well as the generation of a gradient cell distribution between the scaffolds' zones, live-dead staining was performed to the scaffolds, at days 0, 14, and 25. The results demonstrated a high cell viability right after bioprinting, which was maintained during the course of the experiment, for all scaffolds' zones, despite a small decrease at day 25 (Figure 22). At the same time, the gradient distribution pattern appeared visually different from the homogeneous pattern, for all time points, and the images of two distribution patterns agreed with their corresponding schematic (theoretical) representations for the full duration of the experiment, which indicates maintenance of the patterns.



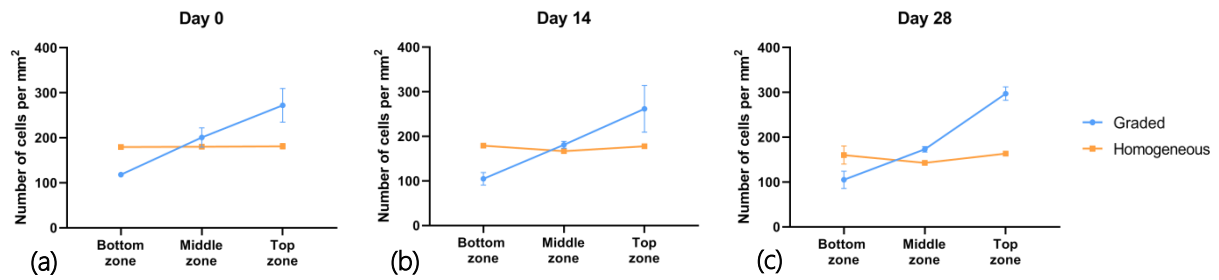


**Figure 22:** (a) Illustrations of the expected cell distribution patterns, graded (left) and homogeneous (right), throughout the zones of the designed scaffolds. (b) Live-dead images of a cross section of the scaffolds at days 0, 14 and 25. For the graded scaffolds the cross section is expected to yield an increasing amount of green fluorescent, when moving from the bottom to the top layers (when moving from left to right in the images), indicative of the increasing cell density. On the other hand, the cross section of a homogeneous scaffold is not expected to display any significant difference in the amount of green fluorescent between the scaffolds zones. The zones are divided from each other with a vertical blue line on the images and the scale bar represents 100  $\mu\text{m}$ .

## Histological Evaluation - Cell density gradient is maintained across the different zones

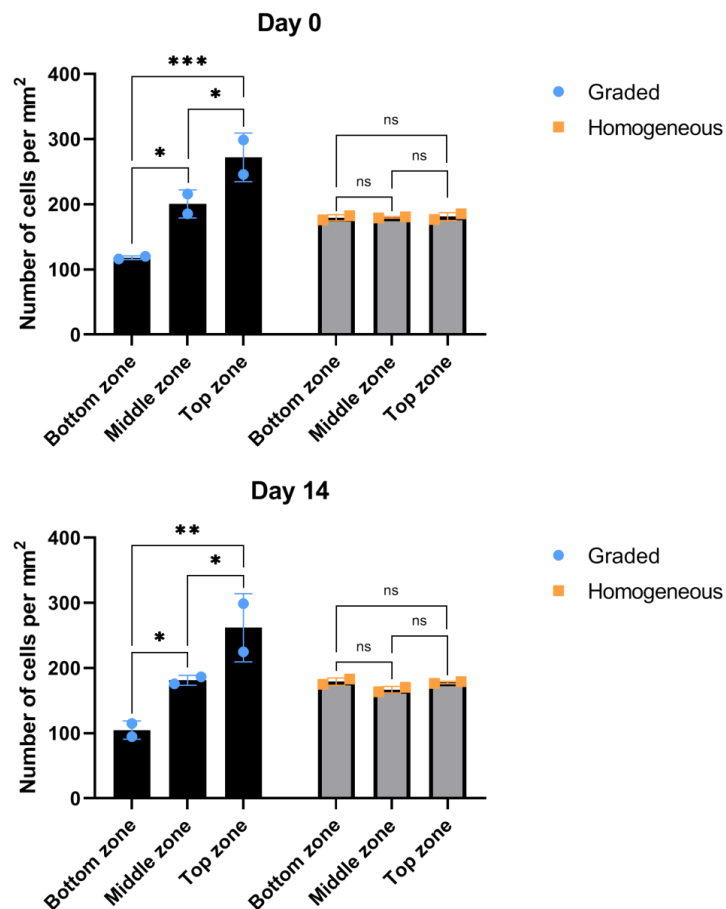


**Figure 23:** H&E images of the bioprinted scaffolds cultured in medium without ascorbic acid after 0, 14 and 28 days showing the localization of the cell nuclei. The images shown in the box on the top left, illustrate a full stained slice of the scaffold (scale bar = 0.5 mm), while the higher magnification images on the bottom illustrate a specific region of interest of the slice, indicated by a rectangle on the top left image (scale bar = 0.2 mm). The dashed lines represent the borders of each of the scaffolds' three zones (bottom, middle, top). All images were acquired using a DM500 Leica optical microscope.



**Figure 24:** Graphs a, b, and c depict the mean and standard deviation of the 2D cell density (number of cells/mm<sup>2</sup>) as calculated for the two scaffold groups (graded and homogeneous), for the different scaffold zones (bottom, middle, top) and for days 0, 14 and 28, respectively. Each scaffold group was composed of N=2 samples, and the cell density calculation was obtained by image analysis of the H&E stained histological sections. The error bars show the standard deviation.

H&E staining was used to count the cell number per area in each sample. It was observed that the mean density for the graded scaffolds at day 0 increases from the bottom to the top zone, while the density of the homogeneous scaffolds remains constant between the zones (Figure 24). This result validates the live/dead analysis on the scaffolds, showing that the bioprinting of scaffolds with a cell density gradient into three different zones was possible. Moreover, the cell density gradient appears to be maintained for the whole duration of the experiment, after 28 days. Now, more specifically, taking a look at the graded and homogeneous graphs only, we can focus on some details.



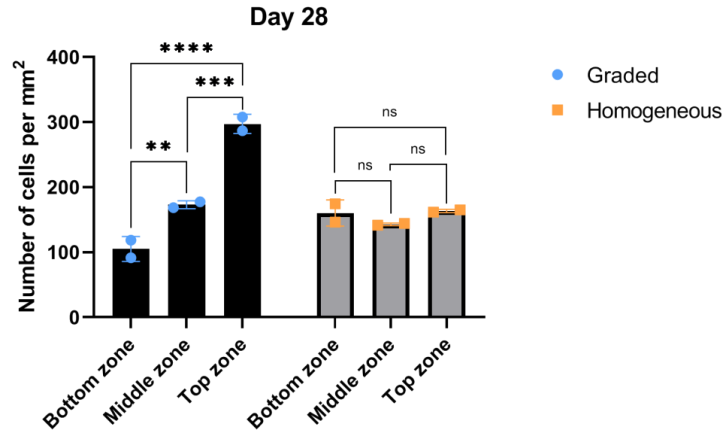


Figure 25: Between-zones comparison of the cell density (cells/mm<sup>2</sup>) within the constructs with a cell density gradient and within the constructs with homogeneous cell distribution, for days 0, 14 and 28. The \*, \*\*, \*\*\*, and \*\*\*\* indicate significance of  $p < 0.05$ ,  $p < 0.01$ ,  $p < 0.001$  and  $p < 0.0001$ , respectively, while the "ns" indicates a non-significant difference. The error bars show the standard deviation ( $n=2$ ).

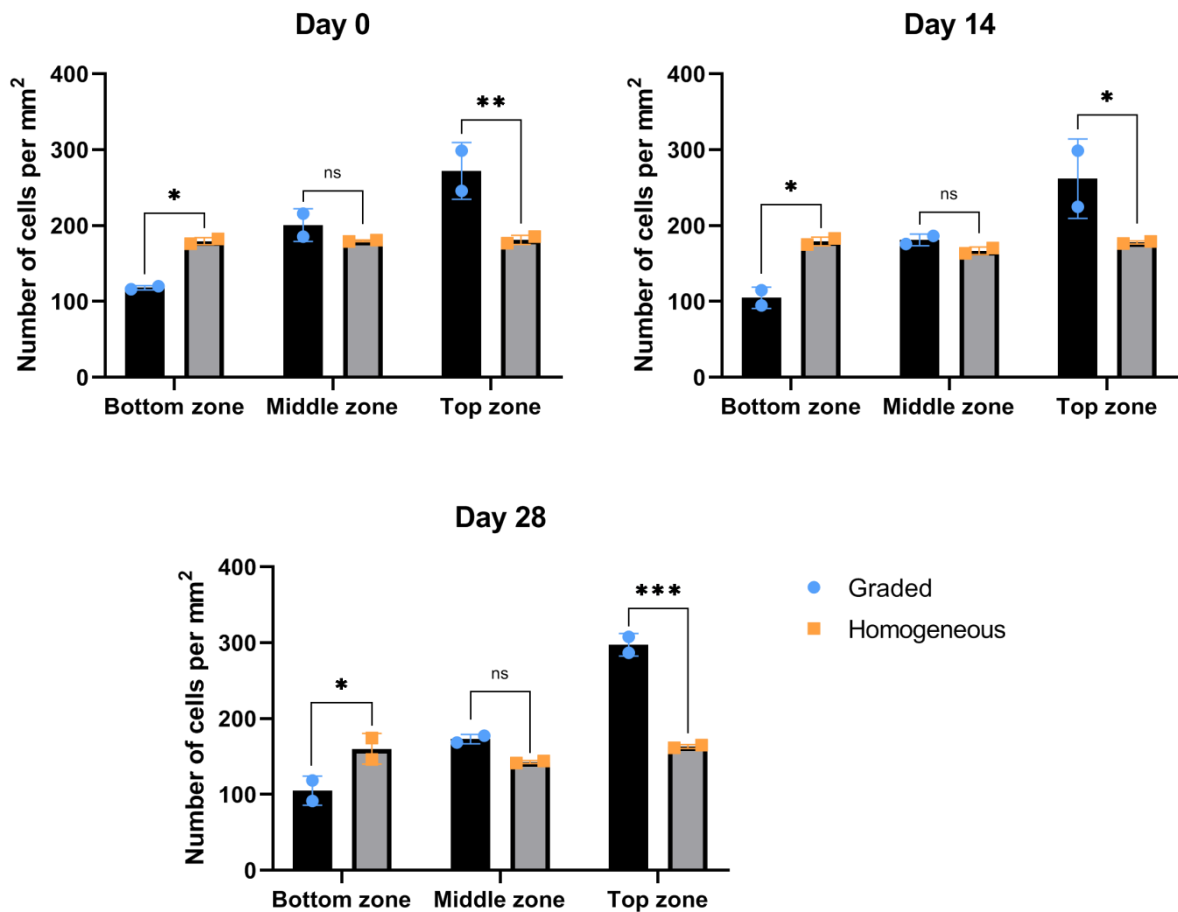


Figure 26: Zone-by-zone comparison of the cell density (cells/mm<sup>2</sup>) between constructs with a cell density gradient and constructs with homogeneous cell distribution, for days 0, 14 and 28. The \*, \*\*, and \*\*\* indicate increasing significance levels (with  $p < 0.05$ ,  $p < 0.01$ , and  $p < 0.001$ , respectively), and the "ns" indicates a non-significant difference. The error bars show the standard deviation ( $n=2$ ).

The comparison of the cell density between the zones of a scaffold allows the investigation of the desired density gradient. Figure 25 illustrates the difference in cell density between (a) the bottom and middle zones, (b) the middle and top zones, and (c) the bottom and top zones, for the graded and homogeneous scaffolds, respectively, at 0, 2, and 4 weeks of the experiment. It can be observed that there was a significant difference between each of the different zones of the graded scaffolds for each time point, with the bottom zone having the lowest and the top zone having the highest cell density, in all cases. The most significant difference in cell density was found between bottom and top zones at day 28. At the same time, the cell density between the zones of the homogeneous scaffolds was almost constant for all time points and therefore exhibits no significant difference under statistical testing.

Besides, however, the within-sample comparisons, a comparison of the cell density of the graded scaffolds versus the cell density of the homogeneous scaffolds, in their respective zones, can provide additional insight on the generation of the cell density gradient. The printing cell density of the homogeneous scaffolds was  $10 \times 10^6$  cells/ml, which equals the cell density of the middle zone of the graded scaffolds. The bottom and top zones of the graded scaffolds were printed with half and double cell densities than that of the homogeneous scaffolds, accordingly. The cell density of the bottom zones and the top zones in the graded scaffolds remained significantly lower and higher, respectively, than that of the homogeneous scaffolds, for all time points. On the other hand, the middle zones of the graded and homogeneous scaffolds showed no significant difference in terms in cell density during the 4 weeks of the experiment. Hence, it can be safely assumed that there was a clear difference in the manner the two scaffold types were fabricated and this difference was maintained for the full duration of the experiment.

### Cell Density Estimation in 3D

After calculating the 2D cell density of the H&E sections of the scaffolds, an estimation of the 3D cell density (experimental) was performed. The experimental cell density values were compared to the known initial cell density of the cells mixed with the hydrogel, before bioprinting (theoretical), to validate the cell numbers seen in the semi-quantitative histological analysis (Table 9).

**Table 9:** 3D cell density calculated from the 2D cell density of the H&E slices.

		Number of cells/mm <sup>2</sup>			N <sup>o</sup> of cells/ml (experimental density)			N <sup>o</sup> of cells/ml (theoretical density)		
		Bottom	Middle	Top	Bottom	Middle	Top	Bottom	Middle	Top
Day 0	G.	116.09	215.99	298.68	$7.28 \times 10^6$	$12.40 \times 10^6$	$16.72 \times 10^6$	$5 \times 10^6$	$10 \times 10^6$	$20 \times 10^6$
	H.	182.66	180.77	176.9	$11.06 \times 10^6$	$11.12 \times 10^6$	$11.12 \times 10^6$	$10 \times 10^6$	$10 \times 10^6$	$10 \times 10^6$
Day 14	G.	94.89	186.53	298.8	$6.46 \times 10^6$	$11.19 \times 10^6$	$16.08 \times 10^6$	-	-	-
	H.	183.33	163.37	179.25	$11.06 \times 10^6$	$10.32 \times 10^6$	$10.93 \times 10^6$	-	-	-
Day 28	G.	118.62	168.63	307.84	$6.48 \times 10^6$	$10.69 \times 10^6$	$18.26 \times 10^6$	-	-	-
	H.	146.06	141.56	161.55	$9.89 \times 10^6$	$8.83 \times 10^6$	$10.03 \times 10^6$	-	-	-

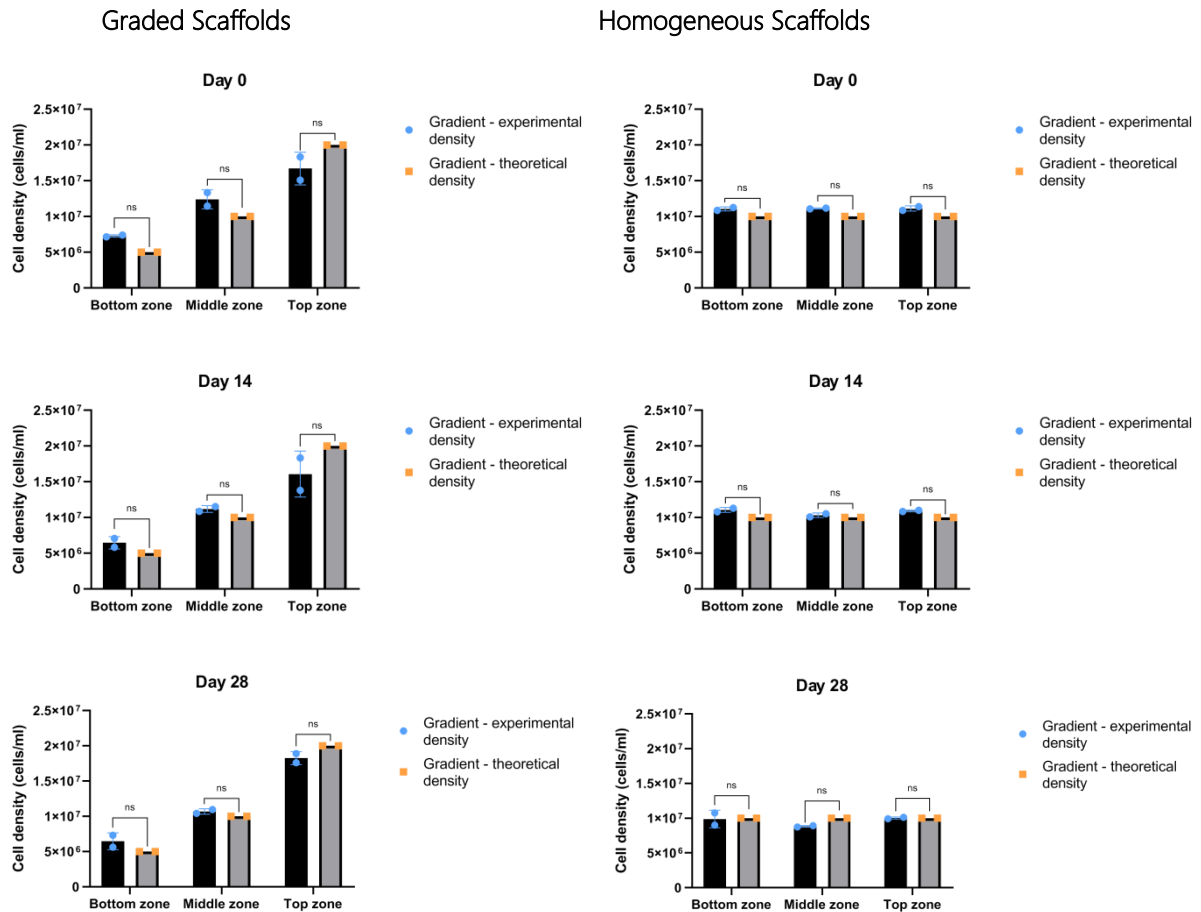
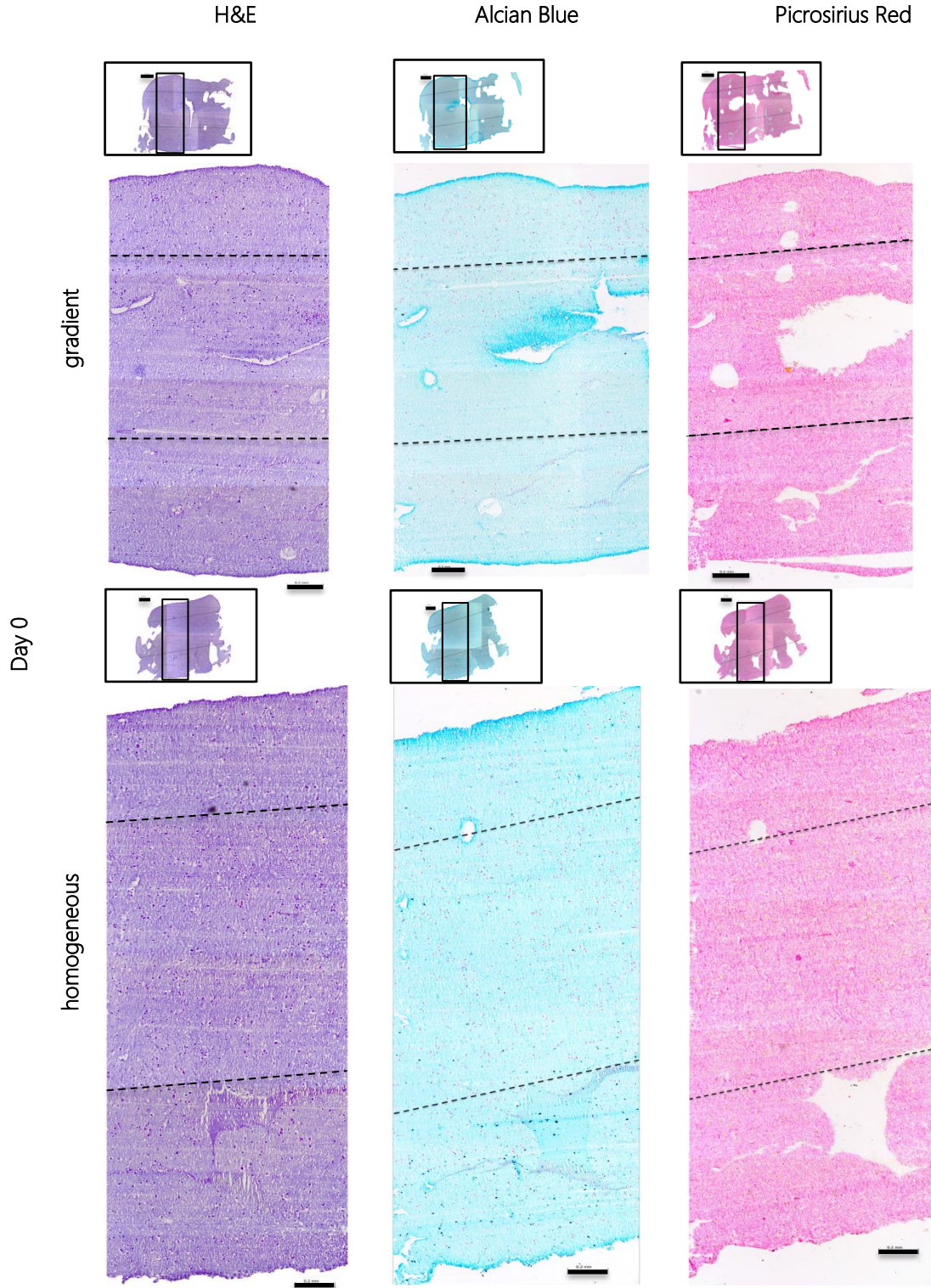


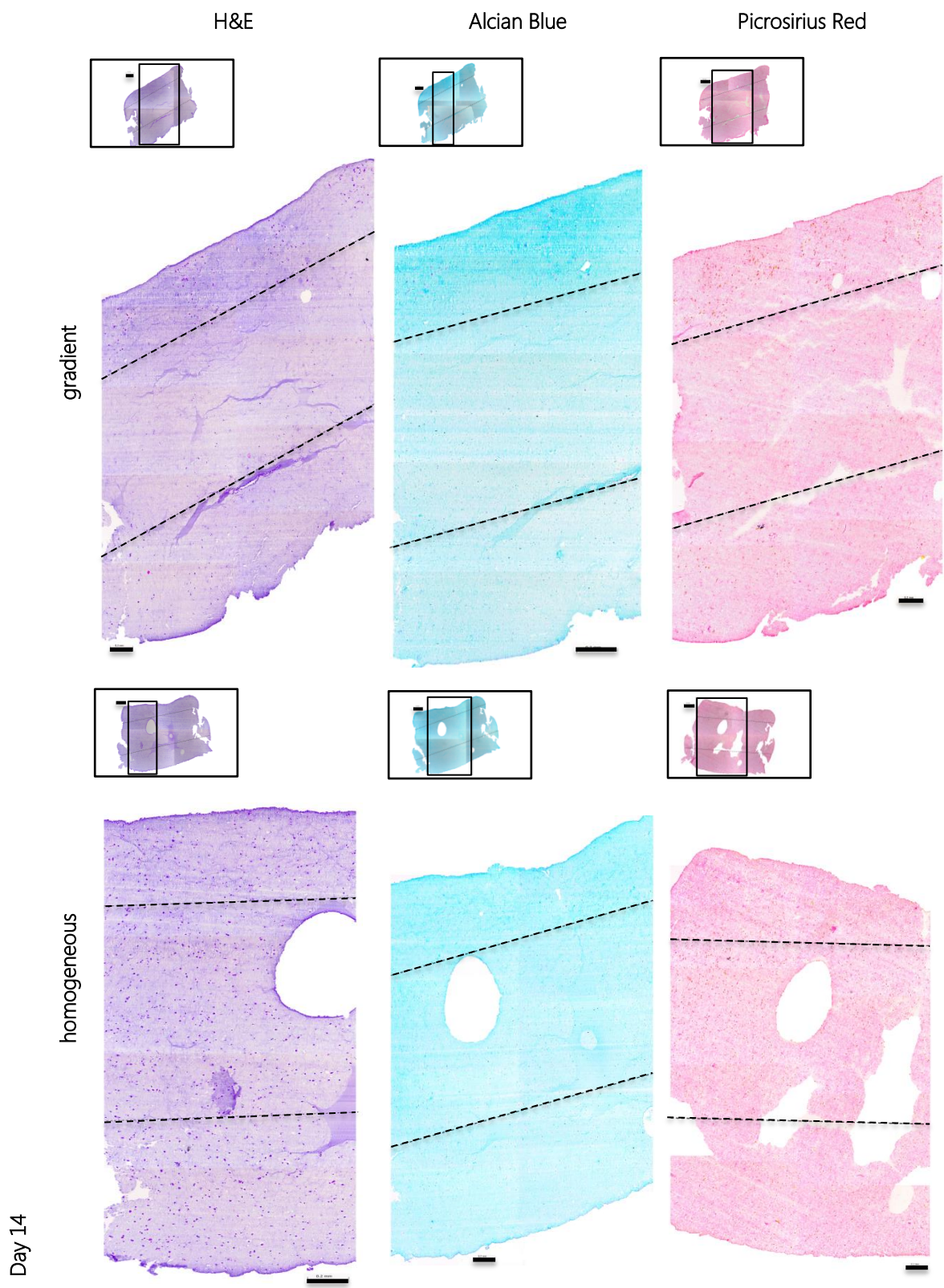
**Figure 27:** Comparison of the initial cell density with which the cells were embedded in the hydrogel, before printing (theoretical cell density), and the cell density measured from the H&E histological images of the scaffolds at 0, 14 and 28 days after bioprinting (experimental cell density). The ns indicates no significant difference ( $p > 0.05$ ) between two values.

The theoretical and the experimental values for the 3D cell density are of the same order of magnitude for all scaffold zones and for all time points, and, the statistical analysis (two-way ANOVA with Bonferroni's test to correct for multiple comparisons for graded scaffolds, and Wilcoxon paired test for homogeneous scaffolds) showed no significant difference between them for any of the comparisons.

### 3.3 ECM deposited by the cells embedded in the zonal scaffolds

For the evaluation of neo-tissue formation, scaffolds were cultured in chondrogenic medium with ascorbic acid for 25 days. Scaffolds were sectioned and stained for sGAGs and Collagen to evaluate the ECM deposition at different time points (days 0, 14, and 25). A visual inspection of the images showed an increase in sGAG deposition, in the top zone of the graded scaffolds, after day 14, which led to a gradient distribution of sGAGs within the scaffolds at day 14 and 25 (Figure 28).





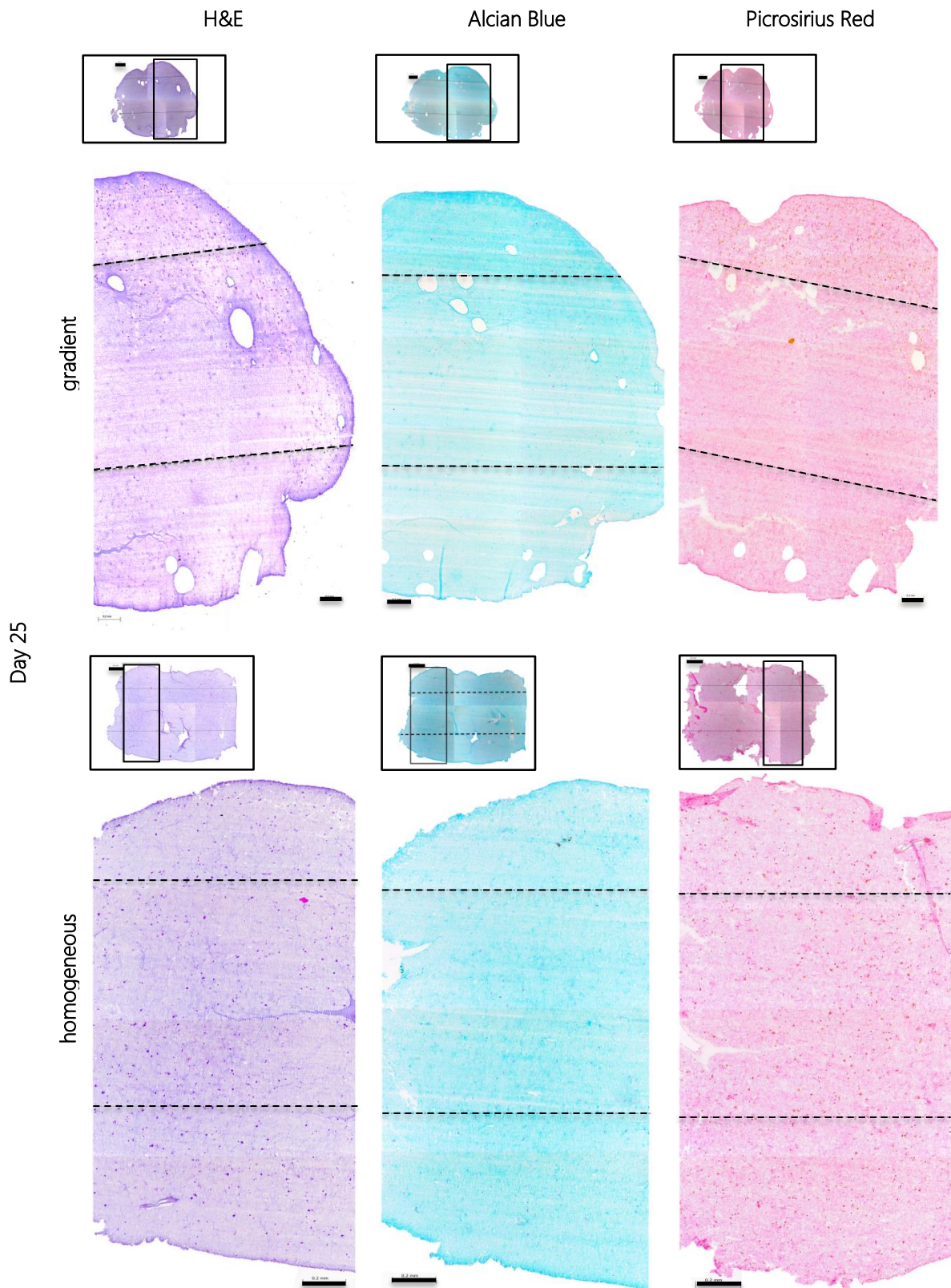


**Figure 28:** Histological images of the bioprinted scaffolds cultured after 0, 14 and 25 days and stained for localization of the cell nuclei (Hematoxylin & Eosin), sGAGs (Alcian Blue) and Collagen (Picrosirius Red). The images shown in the box on the top left, illustrate a full stained slice of the scaffold (scale bar = 0.5 mm), while the higher magnification images on the bottom illustrate a specific region of interest of the slice, indicated by a rectangle on the top left image (scale bar = 0.2 mm). The dashed lines represent the borders of each of the scaffolds' three zones (bottom, middle, top). All images were acquired using a DM500 Leica optical microscope.

## Cell Density Gradient

To check the reproducibility of the results on the generation of the cell density gradient, the bioprinting and H&E staining were repeated, this time with an N=3 samples per condition. These samples were cultured in differentiation medium with ascorbic acid, to enhance the production of neo-cartilage by the chondrocytes. The analysis of the nuclei localization using the H&E is presented in Figures 29 and 30. The results of the cell densities shown in the graphs represent the mean of 3 samples for each zone (bottom, middle, top) and each type of scaffold (graded, homogeneous).

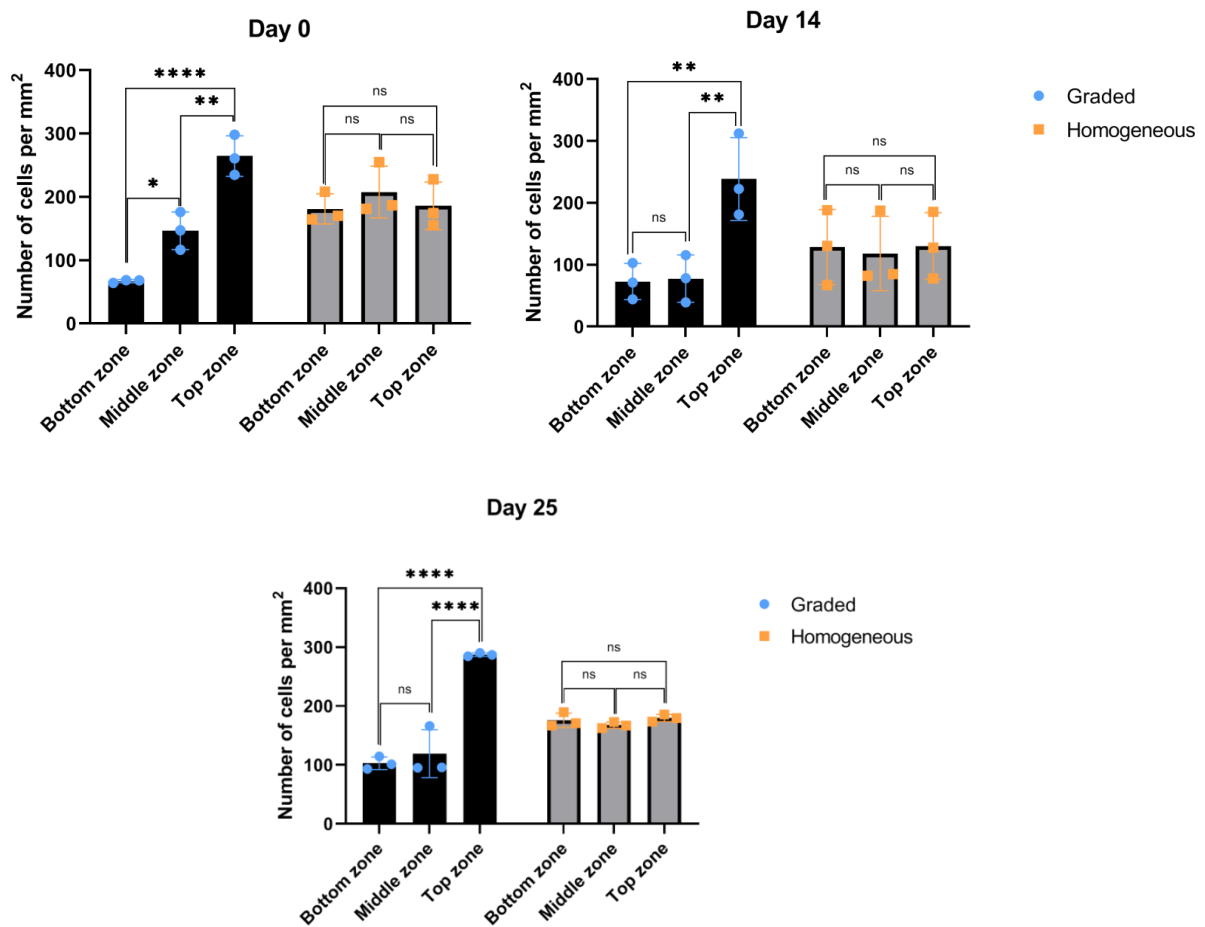


**Figure 29:** Between-zone comparison of the cell density (cells/mm<sup>2</sup>) within the constructs with a cell density gradient and within the constructs with homogeneous cell distribution, for days 0, 14 and 25. The \*, \*\*, \*\*\*, and \*\*\*\* indicate significance of  $p < 0.05$ ,  $p < 0.01$ ,  $p < 0.001$  and  $p < 0.0001$ , respectively, while the "ns" indicates a non-significant difference. The error bars show the standard deviation (n=3).

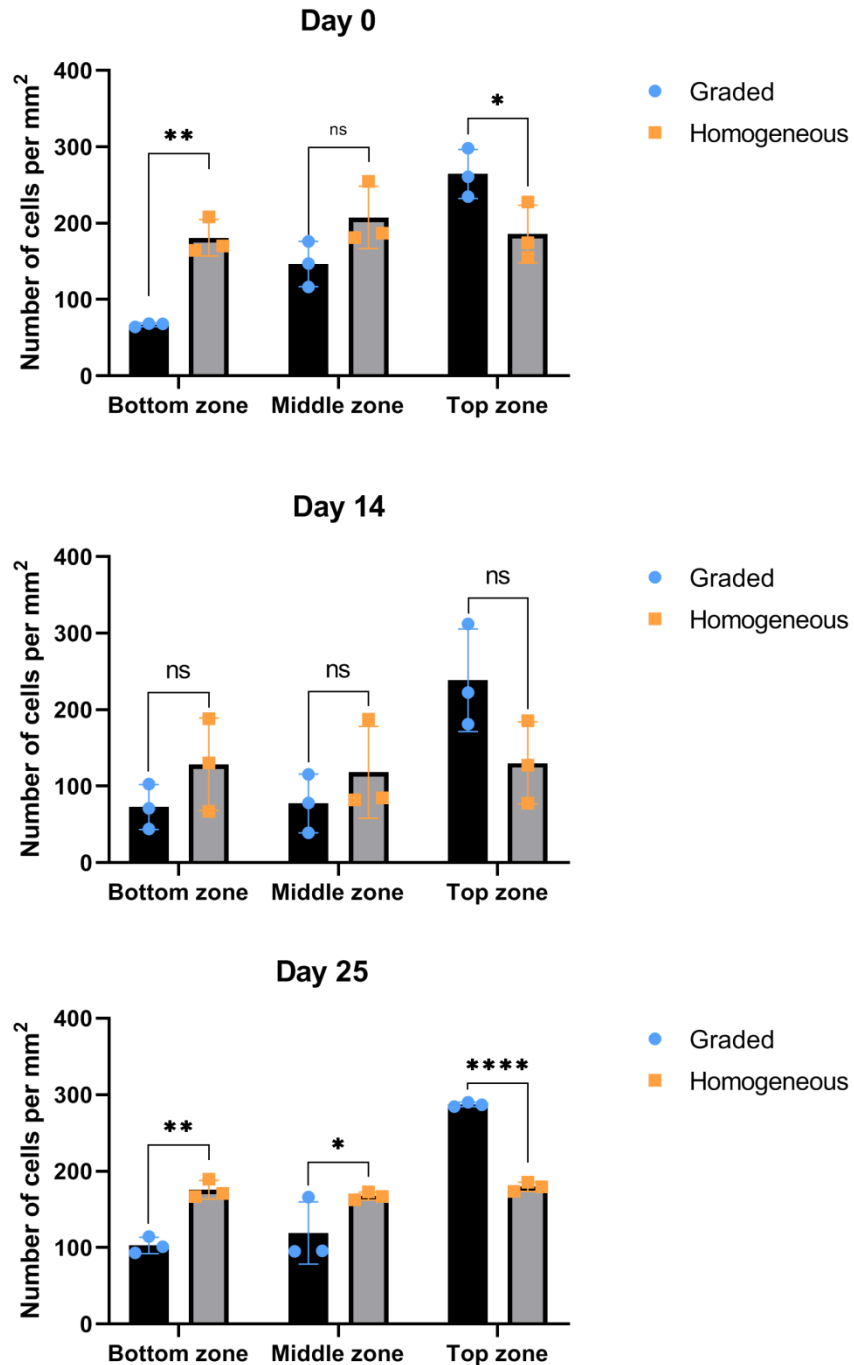


**Figure 30:** Zone-by-zone comparison of the cell density (cells/mm<sup>2</sup>) between constructs with a cell density gradient and constructs with homogeneous cell distribution, for days 0, 14 and 28. The \*, \*\*, and \*\*\* indicate increasing significance levels (with  $p < 0.05$ ,  $p < 0.01$ ,  $p < 0.001$  and  $p < 0.0001$ , respectively, while the “ns” indicates a non-significant difference. The error bars show the standard deviation ( $n=3$ ).

In Figure 30, a comparison of the cell density between the layers of the scaffolds is performed. It was observed that, right after bioprinting the scaffolds (day 0) the difference between the bottom-middle, middle-top and bottom-top zones of the graded scaffolds is significant, while there is no significant difference between the cell densities of the zones of the homogeneous scaffolds. These results are in agreement with the results of the previous experiment ( $N=2$ ), and showcase that the

generation of a scaffold with a cell density gradient is indeed possible using the selected bioprinting method. However, at day 14, a decrease of the cell density of the middle zone was observed, which rendered the density difference between the middle and the bottom zone as not significant. Aside from the non-significant difference in cell density between the bottom and middle zones, the bottom-top and middle-top zones of the gradient scaffolds show a significant difference, while the cell density of the homogeneous scaffolds remains almost constant throughout the scaffolds' thickness. For Day 25, the difference observed between the bottom-top and middle-top zones of the graded scaffolds was increased to extremely significant ( $p < 0.0001$ ), but the difference between the bottom and middle zones remained non-significant. On the other hand, the homogeneous scaffolds at day 25 show no significant difference between the cell densities of their zones.

Also, it would be interesting to check the differences between the individual samples, before concluding that the three-zone cell density gradient could not be maintained throughout the second experiment, as was the case for the first experiment. It was observed that from the 3 graded samples of day 0, all 3 samples were printed with the desired cell density gradient (three different cell densities), just like in the previous experiment (Figure 31a). For day 14, one out of the three samples maintained the three-zone gradient (sample 3), while the other two samples showed either a very small increase or a decrease from the bottom to the middle zone density (Figure 31b). In the first experiment all samples ( $N=2$ ) had maintained their gradient at two weeks post printing. Finally, at day 25, one sample (sample 1) managed to maintain the density gradient in all three zones, while the other two demonstrated almost constant densities between the bottom and middle zone, and a significant increase between these zones and the top zone (gradient with two distinct cell densities) (Figure 31c). The corresponding scaffolds of the first experiment had maintained the three-zone density structure for the full 28 days of the experiment.

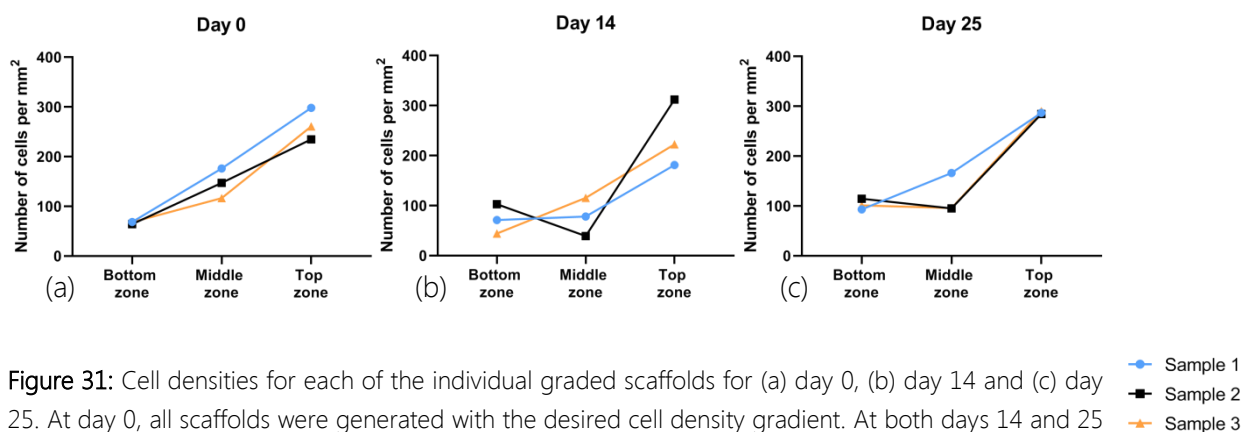


**Figure 31:** Cell densities for each of the individual graded scaffolds for (a) day 0, (b) day 14 and (c) day 25. At day 0, all scaffolds were generated with the desired cell density gradient. At both days 14 and 25 there is one out of the three samples that maintains the cell density gradient (consisted of three different densities), throughout the scaffold's zones.

A calculation of the 3D cell density based on the 2D data was performed and the calculations are presented at Table 10 and Figure 32. The results showed no significant difference between theoretical and experimental values for any of the zones and scaffold types.

## Cell Density Estimation in 3D

**Table 10:** 3D cell density calculated from the 2D cell density of the H&E slices for the 2<sup>nd</sup> experiment.

		Number of cells/mm <sup>2</sup>			N <sup>o</sup> of cells/ml (experimental density)			N <sup>o</sup> of cells/ml (theoretical density)		
		Bottom	Middle	Top	Bottom	Middle	Top	Bottom	Middle	Top
Day 0	G.	66.92	146.55	267.60	$4.13 \times 10^6$	$9.06 \times 10^6$	$16.25 \times 10^6$	$5 \times 10^6$	$10 \times 10^6$	$20 \times 10^6$
	H.	180.95	207.66	185.89	$11.16 \times 10^6$	$12.83 \times 10^6$	$12.09 \times 10^6$	$10 \times 10^6$	$10 \times 10^6$	$10 \times 10^6$
Day 14	G.	72.77	77.54	238.51	$4.48 \times 10^6$	$4.79 \times 10^6$	$14.71 \times 10^6$	-	-	-
	H.	183.33	163.37	179.25	$8.55 \times 10^6$	$7.30 \times 10^6$	$8.00 \times 10^6$	-	-	-
Day 28	G.	72.71	77.56	307.84	$6.35 \times 10^6$	$7.36 \times 10^6$	$17.64 \times 10^6$	-	-	-
	H.	128.60	118.21	130.31	$10.84 \times 10^6$	$10.35 \times 10^6$	$11.02 \times 10^6$	-	-	-

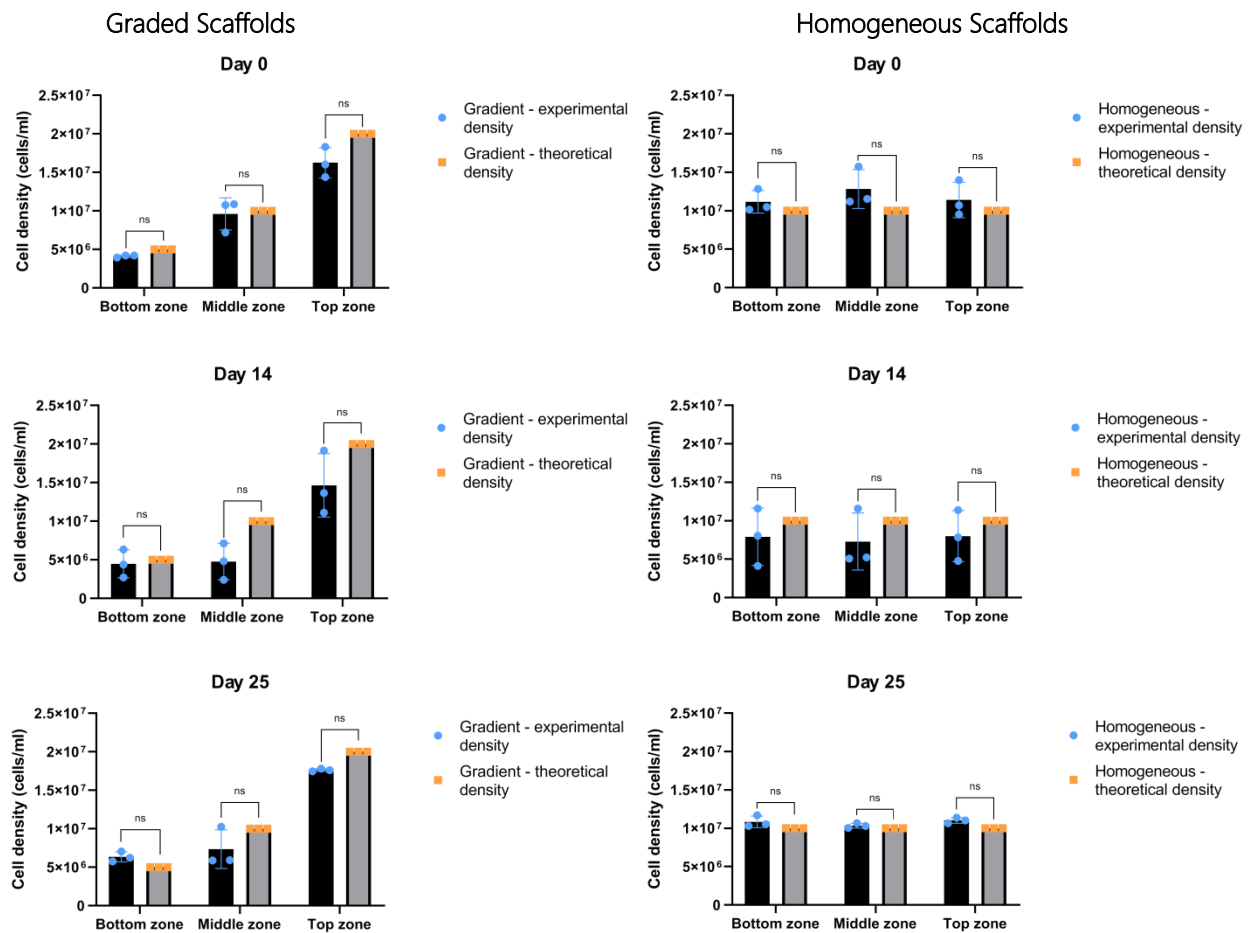
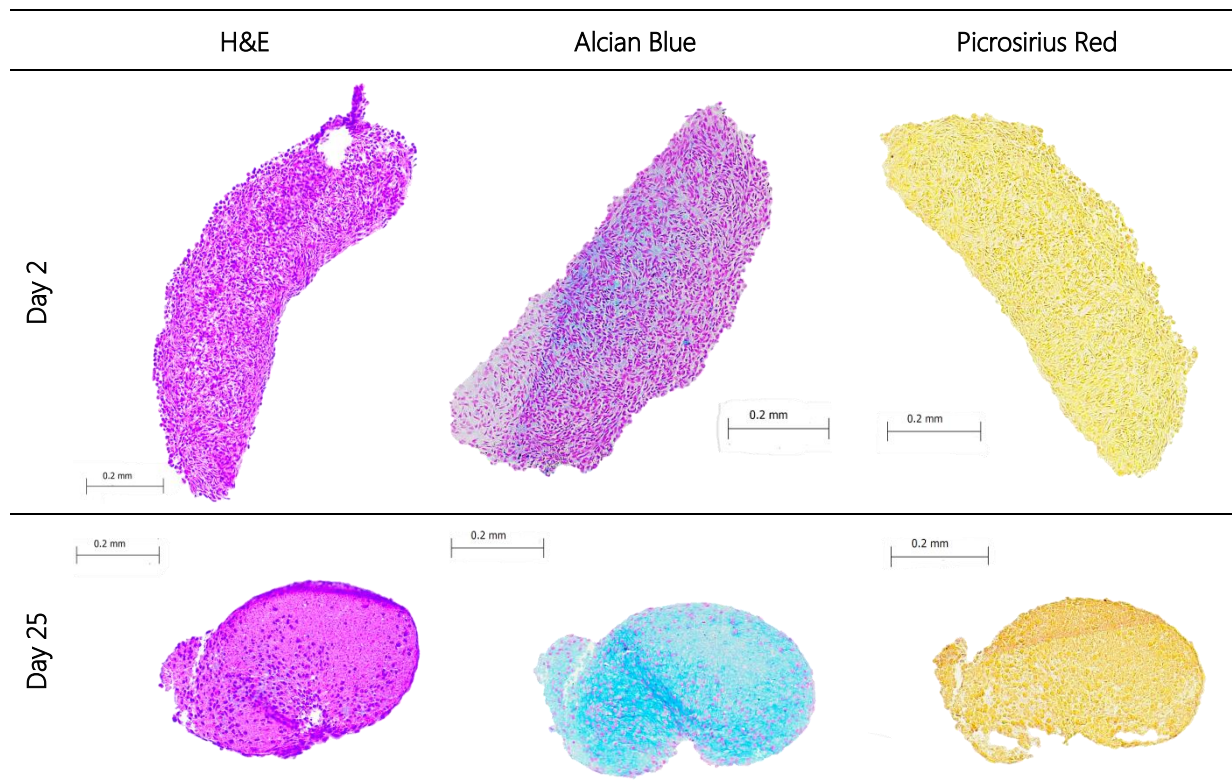


**Figure 32:** Comparison of the initial cell density with which the cells were embedded in the hydrogel, before printing (theoretical cell density), and the cell density measured from the H&E histological images of the scaffolds at 0, 14 and 28 days after bioprinting (experimental cell density). The ns indicates no significant difference ( $p > 0.05$ ) between two values.

### Histological Analysis demonstrated different deposition in the different zones of the graded scaffold

Alcian Blue and Picosirius Red staining were performed to analyze the sGAG and collagen deposition in the scaffolds. Pellets made with 250,000 chondrocytes were used as controls and provided information regarding the ability of the cells to produce sGAGs and Collagens (which indicate the formation of tissue) in a three-dimensional environment. The pellets were cultured in the same differentiation medium for 2 and 25 days, respectively, before staining. The staining results revealed that the production of sGAGs started as early as day 2 and continued until day 25, at which point the characteristic blue color of the aggregated sGAGs became very profound. Collagens, on the other hand, would appear pinkish-red with the Picosirius Red dye, but are not present in the 3D pellet environment, for any of the tested samples (N=3 for each time point) (Table 11).

**Table 11:** Histological analysis of chondrocytes cultured in pellets, in differentiation medium, for 2 and 25 days, respectively. Pellets were stained for nuclei localization, sGAGs and Collagens.



Next, the quantification of the sGAGs on the scaffolds slices was performed. Figure 33 illustrates the amount of sGAGs detected on the Alcian Blue-stained scaffold slices, as the percentage of the fraction: *total GAGs area/area of the stained slice*.

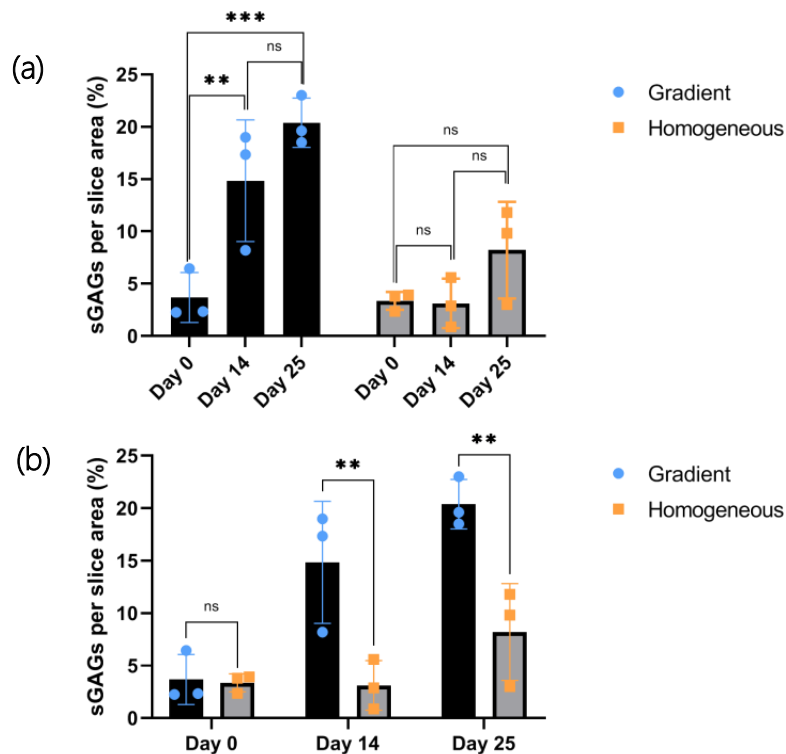


**Figure 33:** (a) Percentage of the total amount of sGAGs (total sGAGs area in a slice/slice area) within the constructs with a cell density gradient and within the constructs with homogeneous cell distribution, for days 0, 14 and 25. (b) Percentage of the total amount of sGAGs (total sGAGs area in a slice/slice area) between the graded and homogeneous scaffolds, for days 0, 14 and 25. The \*, \*\*, \*\*\*, and \*\*\*\* indicate significance of  $p < 0.05$ ,  $p < 0.01$ ,  $p < 0.001$  and  $p < 0.0001$ , respectively, while the "ns" indicates a non-significant difference. The error bars show the standard deviation ( $n=3$ ).

At day 0, sGAGs amount is expected to be zero, however, it can be observed that both the graded and homogeneous samples contain a very small amount of positively stained area (~ 4%) with no significant difference between the groups' values. Despite using Alcian Blue with a  $pH \sim 1$ , to minimize background staining of the alginate, it is known that alginate can be positively stained with Alcian blue due to its similarities to glycosaminoglycans (Shomura 2011). Therefore, this initial amount can be considered negligible. At day 14 a significant difference ( $p < 0.01$ ) between the amount of sGAGs in graded and the amount of sGAGs in homogeneous scaffolds is detected. Finally, at day 25, the percentage of sGAGs on the slice area has increased slightly since day 14, for both the graded and the homogeneous scaffolds, - possibly due to the effect of time - but this increase is not considered significant. Still, there is a significant difference between the graded and homogeneous sGAGs percentages, at day 25, with the graded scaffolds exhibiting a significantly higher sGAG deposition. Overall, the total sGAG amount produced during the course of the experiment (from day 0 to day 25) was significant for the graded scaffolds, even though the production between days 14 - 25 took place at a slower rate than that between day 0 and day 14. On the other hand, the total amount of sGAGs from day 0 to day 25 was not significant for the homogeneous scaffolds, despite a small increase in sGAGs production between days 14-25.

A more in depth analysis of the partial sGAGs production within the different scaffolds' zones is illustrated in Figure 34.

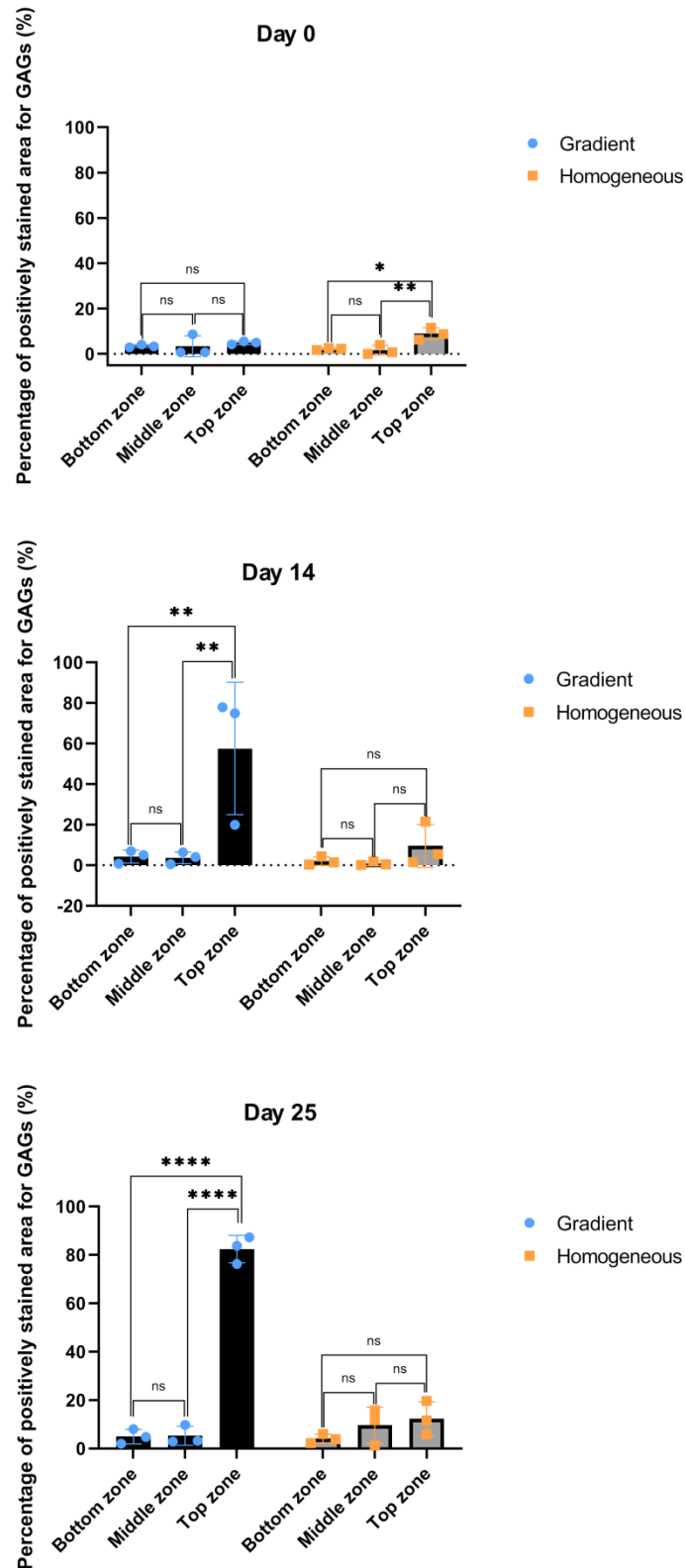


**Figure 34:** Between-zone comparison of the sGAGs percentage (sGAGs area in a zone/zone area) within the constructs with a cell density gradient and within the constructs with homogeneous cell distribution, for days 0, 14 and 25. The \*, \*\*, \*\*\*, and \*\*\*\* indicate significance of  $p < 0.05$ ,  $p < 0.01$ ,  $p < 0.001$  and  $p < 0.0001$ , respectively, while the "ns" indicates a non-significant difference. The error bars show the standard deviation (n=3).

As previously mentioned, sGAGs production is not expected at day 0. At day 14, the bottom and middle zones of the graded scaffolds show no signs of sGAG deposition, since the sGAGs percentages are very low and almost constant for both zones. This result is in line with the overall observations of the H&E analysis in which, after day 14, the cells of the middle zone had migrated to the adjacent zones and the cell density difference between the bottom and the middle zone was non-existent. However, the difference between the cell density of the top zone and the other two zones appears to have a significant effect on the deposited sGAGs, since the top zone, having practically 3 times higher cell density than the other zones, produced 27 times more sGAGs than them. On the other hand, the homogeneous scaffolds do not appear to have produced a significant amount of sGAGs until day 14. Finally, at day 25, the sGAG formation in a gradient manner is established, since there is a significant difference in the amount of sGAGs between the bottom-top and middle top zones.

Next, the Collagen analysis was performed and the results are presented in Figures 35 and 36.

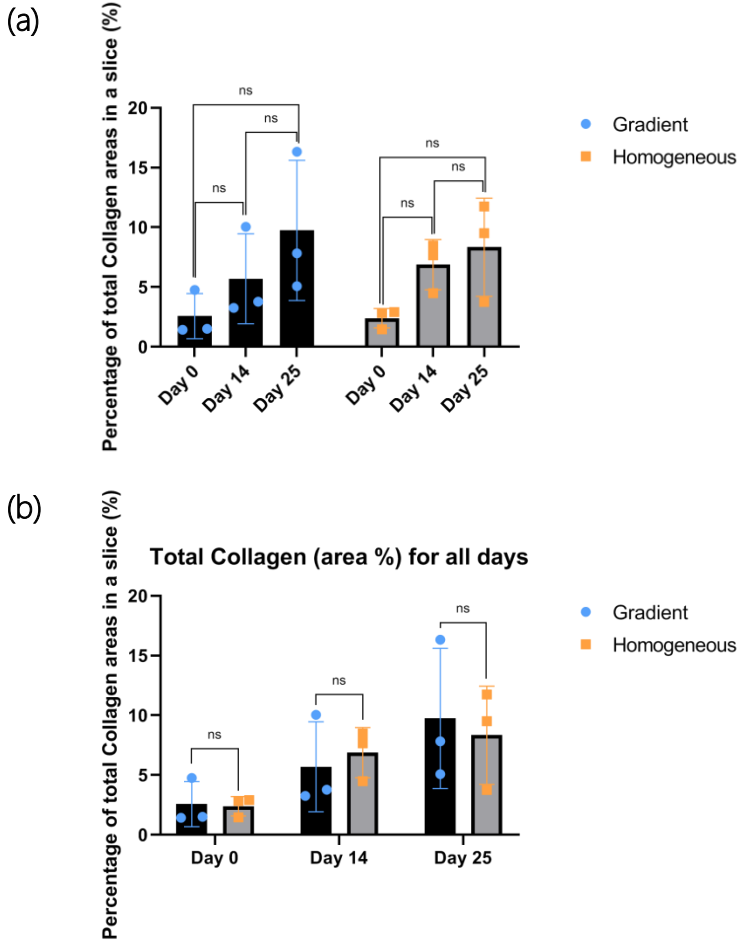


**Figure 35:** (a) Percentage of the total amount of Collagen (total Collagen area in a slice/slice area) within the constructs with a cell density gradient and within the constructs with homogeneous cell distribution, for days 0, 14 and 25. (b) Percentage of the total amount of Collagen (total Collagen area in a slice/slice area) between the graded and the homogeneous scaffolds, for days 0, 14 and 25. The \*, \*\*, \*\*\*, and \*\*\*\* indicate significance of  $p < 0.05$ ,  $p < 0.01$ ,  $p < 0.001$  and  $p < 0.0001$ , respectively, while the “ns” indicates a non-significant difference. The error bars show the standard deviation ( $n=3$ ).

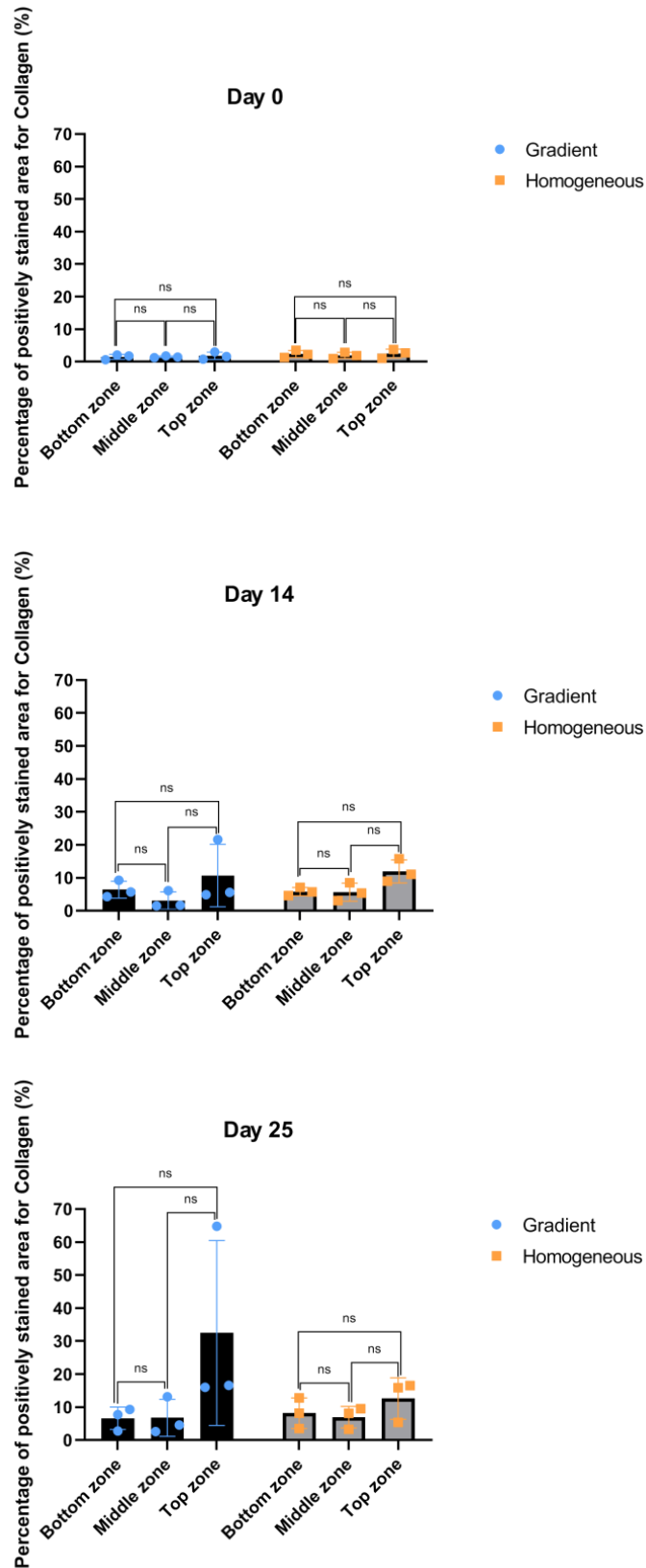


**Figure 36:** Between-zone comparison of the Collagen percentage (Collagen area in a zone/zone area) within the constructs with a cell density gradient and within the constructs with homogeneous cell distribution, for days 0, 14 and 25. The \*, \*\*, \*\*\*, and \*\*\*\* indicate significance of  $p < 0.05$ ,  $p < 0.01$ ,  $p < 0.001$  and  $p < 0.0001$ , respectively, while the "ns" indicates a non-significant difference. The error bars show the standard deviation (n=3).

The statistical analysis of the samples stained with Picrosirius Red showed that no significant amount of Collagens was produced by the chondrocytes of neither by the graded, nor the homogeneous scaffolds during the course of the 25 days of the experiment. An increase in the amount of Collagen was observed for the top zone of the graded scaffolds at day 25, but this can solely be attributed to the contribution of a single sample on the sample mean. This sample presented a gradient production of Collagen between its three layers, with the larger amount detected within the top zone. However, this difference was not marked as significant by the statistical test. This result was somewhat expected, since the histological analysis of the pellets revealed no Collagen production in the 3D environment. The discrepancy between the deposition of sGAGs and Collagen by the scaffolds' chondrocytes can also be observed by a closer look at the molecules' localization in the samples (Table 12).

**Table 12:** Histological images for sGAGs and Collagen at days 0, 14 & 25, for graded (top zone) and homogeneous scaffolds. The 40x magnification allows for a visual assessment of these two ECM components as produced by the chondrocytes. The images were captured with the Leica DM500 optical microscope. Scale bar = 0.05 mm.

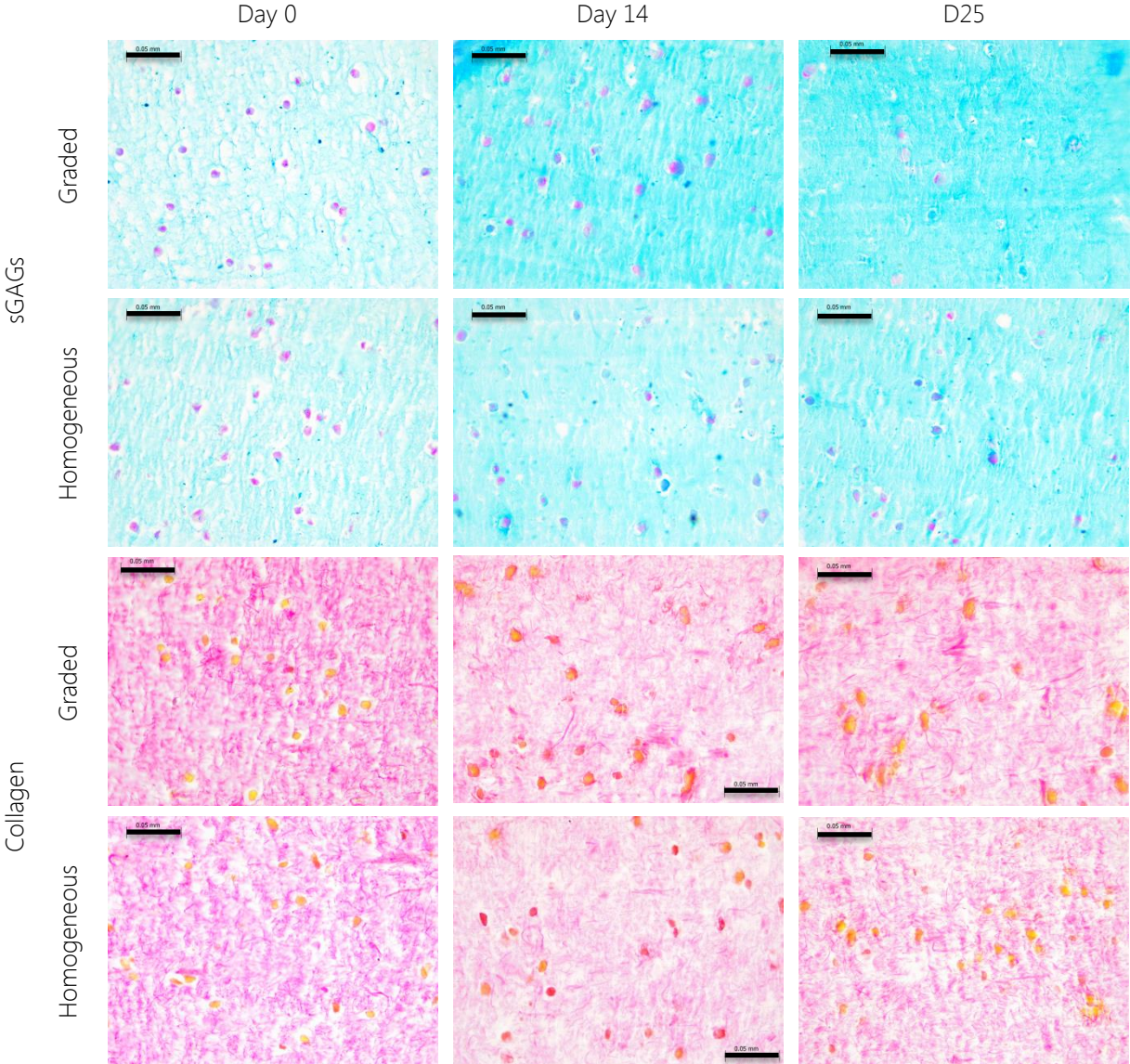


Table 12 illustrates a close-up observation of the hydrogel-embedded chondrocytes, highlighting the differences their surrounding space undergoes at different time-points of the scaffold culture. Both graded and homogeneous scaffolds show a clear image of their cells at day 0, in which case the nuclei staining (purple for Alcian Blue and yellow for Picrosirius Red) produces clearly visible cells, easily distinguishable from the background, which are located within small lacunae created in the hydrogel. At day 14, at which point sGAGs have been produced and have started to concentrate around the pericellular area, we can see that the lacunae of day 0 have almost been completely covered in blue (sGAGs) and some of the cells are also partially covered by a blue membrane, which indicates sGAGs secretion. A difference can be detected between the graded and homogeneous scaffolds, even though some cells of the homogenous scaffold are also secreting sGAGs. The difference is on the color of the background (deeper blue for the graded scaffolds), which demonstrates that a larger amount of sGAGs is accumulated on the top zone of the graded scaffolds, than in the homogeneous scaffolds. On the other hand, Picrosirius Red at day 14 revealed that some cells are indeed producing Collagen, as some of the cells are partially or fully covered with a red membrane which covers the initial yellow stain of the nuclei. However, the Collagen produced is in very low amounts because it did not cover up the lacunae nor was it concentrated on the surrounding hydrogel so as to cause a significant difference in the background color. Also, there appears to be no difference in the secreted amount of Collagen between the graded and the homogeneous scaffolds. Finally, at day 25, a significant amount of sGAGs has accumulated on the top zones of the graded scaffolds and has started occupying larger areas in the in-between space of the chondrocytes. The sGAGs accumulation has reached the extent that the purple dye of the cells nuclei is barely visible at day 25. The homogeneous scaffolds appear to produce significantly less sGAGs, almost similar to the amount of day 14. As for the Collagen, chondrocytes do not appear to have produced any significant until at day 25 and only secrete small amounts that partially surround or cover the cells. These observations are in line with the statistical analysis of the histological staining of the scaffolds.

# 4. Discussion

## 4.1 Design, Fabrication, and Mechanical Characterization of the Scaffolds

In the current project, the goal was to generate a cartilage scaffold of clinically relevant size, which would approximate the mechanical properties of the native cartilage of the human femoral condyle, and would mimic the gradient distribution of cells which is observed between the three distinct zones of the biological tissue. Upon successful generation of this cell density gradient, a second objective was to report the effects of this biomimetic gradient on tissue biosynthesis and more specifically on the deposition of sGAGs and Collagen after 25 days of culturing the scaffolds. The first step towards the bioprinting of a cartilage scaffold was the selection of the ideal materials which would allow for the generation of a robust structure with increased mechanical properties and would ensure the viability, growth and phenotypic stability of the embedded cells, leading to the formation of neo-cartilaginous tissue. Taking into consideration the project's requirements, a PCL-reinforced Alginate/NFC hydrogel was selected for bioprinting, as described in the "*Introduction*" section.

### 4.1.1 Cell Type Selection – Cell Culture

Making the right choice for the biomaterials, however, is only half of the work for the generation of a cartilage scaffold. The living part of the scaffolds plays an equally significant (if not more significant) role in the success of the construct. Most of the recent bioprinting studies have chosen articular chondrocytes usually isolated from animal or human knee for their scaffolds ([Chen et al. 2018](#), [Betsch et al. 2018](#), [Müller et al. 2017](#), [Ren et al. 2016](#)).

In the present study, human articular chondrocytes isolated from the full thickness of the donor's knee cartilage were used for the scaffold bioprinting. A slightly different option proposed by the literature is the use of zonal articular chondrocytes isolated from the different cartilage zones. These cells differ in terms of growth kinetics and gene expression and contribute to the generation of a heterogeneous matrix that mimics natural cartilage ([Klein et al. 2009](#), [Klein et al. 2003](#), [Kim et al. 2003](#)). However, the problem with this approach is that isolated zonal chondrocytes are not always pure and they tend to fuse and mix when printed in neighboring hydrogel fibers. Thus, the maintenance of chondrocytes' phenotype, the high-resolution bioprinters, and effective crosslinking between the different cartilage zones is required to bring this concept to real applications. The use of zonal chondrocytes – if optimized – could be combined with the cell density gradient and it would be very interesting to see the results of this endeavor. An interesting alternative to the use of articular chondrocytes could be the use of chondrocytes isolated from the nasal septum since these cells have been proven to increase the formation of functional tissue ([Apelgren et al. 2017](#), [Markstedt et al. 2016](#)).

However, even though chondrocytes are the most obvious choice for cartilage scaffolds since they are the only cell type present in healthy cartilage, their use holds many disadvantages. The limited

cell source, the second wound site in case of autologous chondrocyte implantation, or the risk of disease transmission or rejection in case of allogeneic chondrocytes, and the ease with which these cells lose their phenotype during culture introduce difficulties for the translation of their use into the clinic (Nukavarapu et al. 2013). In our study, passage 3 chondrocytes cultured in 2D, in differentiation medium can produce Collagen II after 7 and 10 days of culture. However, they appear to lose their capacity of producing Collagen when cultured in the 3D cartilage scaffolds and this could be associated with a change in the cells' phenotype. The extent of de-differentiation of chondrocytes passaged until passage four has been quantified by Fröhlich et al. 2007. The results showed a 480 fold decrease in the type II collagen expression after the first passage and approximately a 29,000 fold decrease after passage four. In addition, with every passage the cells appear larger and more elongated than before. This observation regarding the morphology of chondrocytes was confirmed in the current study by a visual inspection of passage 2 chondrocytes and passage 3 re-differentiated chondrocytes after 17 days of culture (Figure 29). Even though the differentiation of the passage 3 chondrocytes had been successful, it appears that these cells could never reach the normal phenotype of freshly isolated chondrocytes or even passage 2 chondrocytes, in practice.

Another factor which could affect the gene expression in human chondrocytes is the donor's age. The primary chondrocytes used during the course of the experiment were purchased by Lonza B.V. and hence there was no control over the donor's characteristics. Moreover, the chondrocytes used for the 2D culture were probably originated from different donors than the ones used for scaffold bioprinting, since they were bought in different batches. Studies have shown that the differences between donors in the proliferation rate and post-expansion chondrogenic capacity (GAG and Col.II expression) decrease with age (Barbero et al. 2004). This observation is related to the fact that only some of the donors respond to the induced differentiation over the age of 40, and to presence of high levels of senescence-associated enzymes as donor age increases. Moreover, GAG and Collagen II content have presented a high variability between similar-aged donors over the age of 40 (Barbero et al. 2004). Therefore, the absence of Collagen expression in 3D in the present study could be associated with the donor's age or other characteristics for which there was no control over. A future development could be the direct isolation of primary chondrocytes in the lab, from a selected donor.

To overcome the chondrocytes disadvantages, mesenchymal stem cells (Daly et al. 2016, Shim et al. 2016) as well as chondroprogenitor cells (ACPCs) (Mouser et al. 2020) and induced pluripotent stem cells derived from chondrocytes (Nguyen et al. 2017), have already been investigated by researchers to explore their ability to generate functional cartilage tissue. MSCs have successfully been used in multilayered scaffolds (atelocollagen/HA) for the reconstruction of osteochondral tissue and managed to express layer-specific markers (Col. II for the cartilage part, Col. X for the interface between cartilage and bone) corresponding to the different materials of the layers (Shim et al. 2016). Also, MSCs have displayed higher values of GAGs and Col. II than chondrocytes and multipotent chondrocyte progenitor cells (Levato et al. 2017). Articular cartilage progenitor cells (ACPCs), on the other hand, which are mainly located in the superficial zone of articular cartilage, allow expansion in monolayer culture without losing their chondrogenic phenotype (Jiang et al.

2015). In a recent study, ACPCs outperformed chondrocytes in GAGs and Collagen II production, when cultured in gelMA/gellan gum filaments with the incorporation of HAMA. Finally, induced pluripotent stem cells, were tested in a Nanocellulose/Alginate Bioink, similar to the one used in this study (Nguyen et al. 2017). They managed to maintain pluripotency and produce hyaline-like cartilaginous tissue with an increased expression of Col. II and a lack of tumorigenic Oct4 expression (Nguyen et al. 2017). Besides single cell types, also co-cultures of different cell types have been utilized in cartilage engineering. The co-culture of MSCs and chondrocytes, which has been selected by a few studies, has been observed to enhance cell proliferation and chondrogenesis in vitro, to reduce the mineralization of the cartilage phase in vivo compared to the use of only one cell type in a construct (Mesallati et al. 2015) and has assisted the generation constructs with a layered distribution of Collagen and GAGs (Levato et al. 2017). This means that the generation of zonal tissue formation could, besides the cell density gradient approach of our study, be potentially achieved using a cell type gradient.

#### 4.1.2 Scaffold Design

Early on in the course of the study it was determined that an alginate hydrogel could not have the desired shape fidelity and biomimetic compressive stiffness, and its mechanical properties should thus be enhanced with the addition of PCL (Castilho et al. 2018, Daly et al. 2016, Lee et al. 2014). Therefore, the question of how much PCL should be used in the scaffold needed to be answered. According to a recent study, the maximum PCL percentage used in a cartilage scaffold with biomimetic compressive stiffness, generated with the melt-electrospinning writing (MEW) technique, was between 3% and 7% (Castilho et al. 2018). For this reason, the upper threshold of the PCL volume included in the scaffold was set at 7%. Moreover, in most studies using PCL to enhance the properties of their hydrogel, this is done in the form of a mesh where a PCL fiber is printed in between every two hydrogel fibers and the fiber orientation is alternating orthogonally after every layer (Castilho 2018, Kang 2016, Daly 2017, Shim 2016). However, in our case it was determined that a passing of the hot thermoplastic nozzle right next to or on top of the cell-embedded hydrogel fibers would negatively affect cell viability. Therefore, two alternative designs were considered in which the PCL would act as an outer skeleton for the hydrogel, concentrating the cell-embedded volume of the hydrogel in the centre and maintaining its shape throughout its thickness. To achieve a relative PCL density in the range mentioned above (3% - 7%) with our extrusion system, the smallest thermoplastic nozzle (0.2 mm) needed to be used, and the print of at least two adjacent PCL fibers (two nozzle passes, one next to each other) was necessary in order for the scaffold to be more rigid and avoid breaking during its detachment from the printing surface. Taking into consideration these requirements, the final designs yielded a PCL percentage of 5.8% (with the top base) and 3.5% (without the top base).

Two more parameters – besides the relative density of PCL – that are crucial in every scaffold design due to their effect on cell attachment, cell proliferation and mechanical properties, are the porosity and the lay-down (infill) pattern, with the porosity having a more pronounced effect than the lay-down pattern regarding the stress-strain behaviour (Guo et al. 2017). In our case, the primary goal of the project was the generation of the scaffold with a three-zone cell density

gradient. Therefore, a high and prolonged viability of the cells was the primary concern and a larger pore size would support this goal by allowing for better oxygen and nutrition transfer, as well as, waste exchange between the cells and their environment (O' Connell et al. 2017). Additionally the growth factors of the medium, the tissue inducing factors and the re-differentiation factors could be distributed to all the cells easier with a larger network of pores (O' Connell et al. 2017). Scaffold pores of 90µm-120 µm diameter have been proven to favour chondrogenesis because they induce the generation of more dense tissue (Monzon et al. 2018), while a pore size larger than 300 µm has been proven to provide space for bone formation (Chen et al. 2018). However, pore sizes even higher than 400 µm are have been used in cartilage engineering studies involving larger scaffolds to overcome cell death due to malnutrition (Gao et al. 2018, Castilho et al. 2018, Kang et al. 2016). For our study, given the BIO-X extrusion bioprinter and the selected Alginate-based hydrogel, we selected the minimum infill density (10%) in order to have visible pores on each of the scaffolds' layers. A full porosity analysis was not performed after printing, but individual pore measurements performed with the Leica DM500 optical microscope revealed a mean pore size of 0.230 mm<sup>2</sup>, which corresponds to square pores of 480 µm x 480 µm. The creation of square pores in the hydrogel was selected because it has exhibited a significantly higher cell adhesion and proliferation rate compared to other pore shapes, due to the higher curvature of the square pores, which is related to higher force concentrations at these regions (Aliabouzar et al. 2017, Zhou, et al. 2016). In order to achieve the square pores, the 0°-90° lay-down pattern was selected, which is the most common pattern in cartilage bioprinting, probably because of the high cell proliferation rate it exhibits, even in less porous scaffolds (Zhou et al. 2016). Besides proliferation, the lay-down pattern, also, affects the type of ECM production (Daly et al. 2017), since it has been demonstrated that different lay-down patterns (parallel pattern, 0°-45° pattern, and random pattern) have an effect on the morphology and orientation of the seeded MSCs (Guo et al. 2018).

After the specifications of the two proposed designs were set (relative density of PCL, infill density, infill pattern), the choice between them was made based on the cell viability after bioprinting. The reason for this assessment was because the thermoplastic head, which was used for printing the PCL at a high temperature (210°), could have a negative thermal effect on the surrounding material and the cells embedded in it. The difference between the post-printing cell viability was, as expected, quite significant with the viability of the scaffold without the top PCL base being 1.8 times higher than that of the other design (Figure 25). Therefore, the design without the top base was selected. Before printing, an outer wall of support was added to the final design, surrounding the scaffold all around. The support was used to counterbalance the tension between the fibers of the PCL, which was created by the movement of the printing head and tended to pull the four struts at the corners of the square base inwards, risking the structural integrity of the scaffold and jeopardizing its mechanical properties.

### 4.1.3 Bioprinting

An earlier study on the generation of a cell density gradient in engineered scaffolds tested three groups of cell densities and demonstrated that the biomimetic cell density group achieved higher

sGAG production per single cell (Ren et al. 2016). Based on this assumption, a biomimetic cell density for each of the three distinct cartilage zones was applied in our study, with  $5 \times 10^6$  cells/ml in the bottom zone,  $10 \times 10^6$  cells/ml in the middle zone, and  $20 \times 10^6$  cells/ml in the top zone.

When cell-embedded hydrogels are extruded using a bioprinter, they are exposed to shear stress, which can cause damage to the cells and affect cell morphology and metabolic activity (Murphy et al. 2014). The main factors affecting the shear stress applied to the cells include the printing pressure, the nozzle diameter and shape and the viscosity of the mixture of hydrogel and the chondrocytes, which depends on the cell density (Panwar et al. 2016). Therefore, with constant printing parameters, the top zone of the constructs, which has the highest cell density, has a higher risk of increased cell death. In our study, a 27-gauge (200  $\mu$ m) nozzle was selected because high printing resolution (small strand diameter) was desirable, while the dispensing pressure for the hydrogel was set 12 kPa - 14 kPa. The effect of the pressure is more substantial than the effect of nozzle diameter on cell viability and thus, even though the nozzle diameter was the smallest possible, the low pressure during bioprinting enabled a high viability of the chondrocytes after printing at day 0, for all three scaffold zones, as seen from the live/dead staining (Figure 34).

Besides the inflicted shear stress which affects cell viability, the extrusion bioprinting also affects the dimensions of the designed scaffolds. In our case, the bioprinted scaffolds had an increase of 0.5 mm on the x and y directions of the square base, which led to a higher amount of PCL being deposited in the scaffold, that what was designed. The hydrogel part also had an increase in its dimensions, but this increase had been compensated by a 400 $\mu$ m decrease on both the x and y directions from the design. This compensation inhibited the over-extrusion of the hydrogel outside of the PCL framework.

#### 4.1.4 Mechanical Characterization

The fact that most cartilage bioprinting studies (Chen et al. 2018, Levato et al. 2017, Daly et al. 2016, Markstedt et al. 2015, Jeon et al. 2013) are using compression testing to characterize their scaffolds can be explained from the fact that cartilage, and osteochondral tissue in general, are mostly loaded under compressive loads. On the other hand, the employment of tensile or shear tests by a few studies is justified by the nature of the specific applications investigated in them. For example, a study combined a freeze-drying method with a 3D printing to generate an osteochondral scaffold with graded porosity in each layer (Li et al. 2018). For this application, a tensile and a shear test is vital, since the non-monolithic design of the scaffold holds a risk of separation, after implantation and the only loads that can cause separation are tensile and shear loads. Another example is the bioprinting of the cartilage part of a human ear for which a tensile test would be more useful than a compression test (Lee et al. 2014). Since the main scope of the current project was the generation of the gradient scaffolds and not a complete study on the mechanical characterization of the scaffolds, only a quasi-static uniaxial compression test was performed for the mechanical characterization of the scaffolds. The limitations of performing such a test include the simplification of the time-dependent behavior (viscoelasticity) of the scaffolds, and, the lack of information about viscous and/or elastic responses that occur under dynamic

loads (such as the loads resembling physiological deformations of the cartilage tissue) (Guimarães et al. 2020).

In general, the compressive modulus of articular cartilage increases from 79 kPa in the superficial zone to 2.10 MPa in the deep zone (Datta et al. 2017). In the present study, we tried to achieve scaffolds with stiffness close to the mean stiffness of the native cartilage (~1 MPa). However, the results for the compressive stiffness of the PCL framework were around 8 MPa and for the PCL framework with the hydrogel around 8.35 MPa, which make them almost 8 times higher than the desired value. One of the reasons for this discrepancy is the over-extrusion of the nozzle, due to the high temperature and pressure used to print the PCL, which created a variation between the designed and the experimental relative density of the PCL framework (i.e. the extruded PCL had a larger volume than designed). This caused the vertical struts to be thicker (with larger cross-section area), thus withstanding higher compressive load. Nonetheless, the achieved framework had the lowest PCL percentage that could be achieved, with the given extrusion system, since the smallest nozzle and the minimum possible number of adjacent fibers were used. This limitation in the resolution of the extrusion systems can be tackled with the use of different techniques for the enhancement of the hydrogel properties, which would be able to achieve thinner polymer fibers. Melt electrospinning writing is an example of such a technique, which can be used for the formation of fibers with thicknesses between 800 nm and 150  $\mu\text{m}$ . A recent study utilized this method to generate PCL-enhanced GelMA scaffolds with a low PCL relative density and, hence, a biomimetic compressive stiffness of (Castilho et al. 2018).

The second - and most important - reason for the high stiffness of our scaffolds is related to the scaffold design. It is known that stiffness is a general structural property that depends not only on the material itself but also on its amount and distribution (shape) (Guimarães et al. 2020) and in our case, the PCL framework was printed with a square base parallel to the printing surface and four vertical struts, at the corners of the square base, running up its full thickness. This means that the stiffness of the PCL framework is governed mainly by the struts, which resist compression. In the case of the complete scaffolds (PCL framework and hydrogel), besides the struts there is a second mechanism that contributes to the stiffness, at a smaller degree. This mechanism is the resistance of the hydrogel which tends to avoid the buckling of the struts inwards, hence slightly reinforcing the stiffness of the scaffold. The contribution of the hydrogel to the scaffolds' stiffness was found to be around 350 kPa which lies in the same order of magnitude with previously reported stiffness values of 250 kPa for 0.75% Alginate with nanocellulose (Markstedt et al. 2015), and 150 kPa for 2% Alginate with RGD (Jeon et al. 2013).

It is well known that matrix stiffness affects most cellular events such as adhesion and differentiation. Thus, an important question, at this point, is whether the high stiffness of the bioprinted scaffolds is affecting the chondrocytes in such a way so as to alter their gene expression and biosynthetic ability after bioprinting. Due to the fact that the PCL struts – which are mainly responsible for the increased stiffness – are located at the corners of the scaffolds and there is an absence of PCL fibers at any point inside the volume of the scaffold, it is hypothesized that the cells encapsulated in the hydrogel do not sense the stiffness of the scaffold, as calculated from the

stress-strain curve, but rather the stiffness of the hydrogel matrix that surrounds them. Therefore the chondrocytes' expression of neo-cartilage markers is not expected to be inhibited due to the framework's stiffness.

The mechanical characterization described above, was performed to scaffolds that contained no cells (the hydrogel used for printing the scaffolds did not contain any cells). For that reason, an interesting future advancement of this experiment would be to test the stiffness of the cell-embedded scaffolds, after 25 days of culture. That way we could determine whether there is any difference in the stiffness that could be attributed to the tissue synthesis by the chondrocytes and whether this stiffness follows the distribution of the cell density gradient in the scaffold.

## 4.2 Evaluation of the Cell Density Gradient's Generation

The data from the H&E slices showed an increase of the mean cell density (2D) for the graded scaffolds from the bottom to the top zone, after bioprinting, while the density of the homogeneous scaffolds remained almost constant between the zones. These trends were maintained for 28 days, for both scaffold types. This result validates the qualitative assumptions made from the live/dead images of the cells, that the generation of scaffolds with a cell density gradient was achieved, using the bioprinting method. Moreover, the cell density gradient appears to be maintained for the whole duration of the experiment, after 28 days.

The significant difference of cell density between the bottom-middle, middle-top and bottom-top zones of the graded scaffolds and the non-significant difference between the same zones of the homogeneous scaffolds, for each time point, show that two different types of scaffolds have successfully been generated. The first, a construct with a varying cell-density depending on the scaffold's distinct, depth-dependent zones, and the second, a construct with homogeneously distributed cell density throughout the volume of the construct.

An alternative comparison between the cell density of the graded scaffolds and the cell density of the homogeneous scaffolds, at their respective zones, was performed to provide more insight on the generation of the gradient. The printing cell density of the homogeneous scaffolds was  $10 \times 10^6$  cells/ml, which equals the cell density of the middle zone of the graded scaffolds. The bottom and top zones of the graded scaffolds were printed with half and double cell densities than that of the homogeneous scaffolds, accordingly. Thus, the comparison of the same zones between graded and homogeneous scaffolds – if indeed the gradient was generated and maintained throughout the experiment – would yield a significant difference between the densities of the bottom and top zones, and a non-significant difference between the densities of the middle zones. As indicated by the graphs in Figure 25, the cell density of the bottom layers in the graded scaffolds remained significantly lower than that of the bottom layers of the homogeneous scaffolds, for all time points, the middle zones of the graded and homogeneous scaffolds show no significant difference in terms of cell density during the 4 weeks of the experiment, and finally, the density of the top zones of the graded scaffolds remained significantly higher than that of the top zones of the homogeneous scaffolds for all time points. Based on these observations, it can be safely assumed that there is a clear difference in the manner with which the two scaffold types (graded and

homogeneous) were fabricated. This difference in the distribution of cell density was maintained for the full duration of the experiment.

Finally, a comparison between the 3D cell density derived from these 2D measurements (experimental) and the initial cell density with which the cells were mixed with the hydrogel, before bioprinting (theoretical), was performed. The results showed some discrepancies between the theoretical and experimental cell density of the samples, but no difference was marked as significant. The detected discrepancies between theoretical and experimental values could be attributed partly to the merging of a few layers at the interface of the zones, and partly to the errors introduced during the calculation of the experimental 3D cell density. The fact that all experimental densities of the top zones are lower than the corresponding theoretical ones, while the experimental densities of the middle and bottom zones are always higher than the respective theoretical ones, adds to the previous explanation, since the top zone only borders with lower density zones, while middle and bottom both border with higher density zones. This merging of the layers yields minimal results to the homogeneous scaffolds, because there is no significant difference in cell density between the scaffolds' zones.

It is important to keep in mind that the aim of the experimental 3D density was to act as a rough estimation of the initial cell density and not as an exact calculation. Therefore, errors were introduced in the calculation of the experimental cell density, as a consequence of the many assumptions made during this estimation. The chondrocyte diameter (width) was considered 15  $\mu\text{m}$ , the scaffolds' experimental dimensions were considered 8.5 mm  $\times$  8.5 mm  $\times$  3 mm and the zones' thicknesses were set equal to their theoretical (designed) values. The fact that the separation of the zones was done based on their theoretical thickness, might not always be correct for histological images, because in some cases parts of the scaffold slice could be torn and slide away from the glass slide, hence not being depicted in the image. Also, the experimental 3D cell densities were calculated based on the 2D data of only one section per scaffold. However, the selection of a very small number of specific sections does not provide an equal opportunity for analysis throughout the sample. Hence, in order to avoid selection bias, sections from all regions of the scaffolds ought to be included to the analysis (Jensen et al. 2013). Nonetheless, even with the introduced errors, the vast majority of the 3D experimental density estimations show a good approximation of the theoretical (initial) cell density.

## 4.3 Tissue Formation in the Cell-Embedded Scaffolds

### 4.3.1 Cell Density Gradient

The assessment of the ECM deposition on the bioprinted scaffolds was performed in scaffolds cultured in CDM medium with an addition of ascorbic acid (AA), since the later has been proven to enhance the formation of Collagen by chondrocytes (Farquharson et al. 1998). To check the reproducibility of the results, regarding the generation of the cell density gradient, on the scaffolds cultured with AA, an H&E analysis was repeated, this time with an N=3 samples per condition. The results of the new analysis for day 0 were in agreement with the previous results showcasing that the generation of a relative-sized scaffold with a cell density gradient is possible using the selected

bioprinting method. However, the three-zone gradient was not maintained, in the replication experiment, for the majority of the scaffolds between days 14 and 25, and it rather became a two-zone gradient defined by a low cell density (bottom and middle zones) and a high cell density (top zone). More specifically, at day 14 a decrease of the cell density of the middle zone was observed, which rendered the density difference between the middle and the bottom zone as non-significant. The cell density between the bottom-top and middle-top zones of the gradient scaffolds maintained a significant difference, while the cell density of the homogeneous scaffolds remained almost constant throughout the scaffolds' thickness. One reason for the drop in cell density of the middle zone could have been the increased number of dead cells at this zone, but after evaluation of the live-dead staining at day 14, there was no indication of excessive cell death for any of the zones. An alternative explanation would be that the cells migrated from the middle zone to the adjacent scaffold zones, thus enhancing the density difference between the middle and top zones and lowered the difference between the bottom and top zones. This migration could be due to the increase in the amount of ECM being synthesized by the chondrocytes of the top zones at day 14, an outcome which was probably facilitated with the addition of ascorbic acid in the culture medium. It is known that in cell-embedded hydrogels the chondrocytes interact with the produced ECM. The accumulation of that matrix is especially high in Alginate-based hydrogels due to their significant resistance to large molecules diffusion (Mouw et al. 2005). This results in a more concentrated, pericellular deposition of the secreted ECM, and hence in an increased interaction between the ECM and the cells (Mouw et al. 2005). Moreover, the addition of ascorbic acid (AA) promotes Collagen synthesis and enables subsequent tissue specific gene expression, through the establishment of cell-matrix interactions (Farquharson et al. 1998). The significant increase in the deposition of sGAGs observed at day 14, strengthens the above hypothesis, that ECM might have provided biochemical cues to the chondrocytes, that signaled their migration towards areas of higher cell concentration (or higher sGAG concentration).

The results for day 25 are similar to the ones of day 14 for the graded and the homogeneous scaffolds. The significant difference ( $p < 0.0001$ ) observed between the cell density of the bottom-top and middle-top zones at this time point matches the results of the previous experiment, and could be attributed to either the increased cell proliferation in the areas of high cell density, or to the continuous migration of chondrocytes from the middle to the top zone. However, findings of previous studies using chondrocytes in Atelocollagen and Alginate gels, respectively, have reported that chondrocyte proliferation is inversely correlated with cell density (Iwasa et al. 2003), (Gagne et al. 2005) and thus, the cause of increased cell density in the top zones of the scaffolds after 25 days of culture is probably due to cell migration. A proliferation assay during the different time points of the experiment would have been a good idea in order to clarify the conditions for the expansion of the cell density in the top zones.

As stated before, the three-zone cell density gradient is not maintained for the majority of the scaffolds between days 14 and 25 and transforms into a two-zone gradient defined between the combined bottom-middle zones and the top zone. To further explain this claim, we need to take a closer look at the gradients of the individual samples for days 14 and 25. At both time points, 33% of the scaffolds (one out of three samples) maintained the three-zone gradient, while 67% of the

scaffolds (two out of three samples) demonstrated a two-zone cell density gradient, defined by constant cell densities between the bottom and middle zones, and a significant increase of the cell density between these zones and the top zone (gradient with two distinct cell densities). This observation could be attributed to individual differences of the scaffolds generated during bioprinting.

The estimation of the 3D cell density based on the 2D data for the replication experiment showed no significant differences between theoretical and experimental values for any of the zones and scaffold types and this indicates that the cell counting in 2D is reliable. Cell apoptosis might account for the slight decrease.

#### 4.3.2 ECM Deposition

##### Histological Evaluation of the Pellets

The staining results of the pellets revealed a constant production of sGAGs from day 2 until day 25, but no production of Collagen, in any of the samples. This observation comes in contrast with the immunofluorescent results of the 2D culture, where re-differentiated chondrocytes were producing Collagen II even after 17 days of culture. This change of behavior in the 3D culture might be an indication of phenotypic instability of the cells which could have led to the inhibition of the synthesis of proteins which are characteristic of a healthy cartilaginous tissue (Hall et al. 2019). A morphological analysis of the samples' chondrocytes would be an interesting idea which could shed some light to the lack of Collagen production and explore potential changes in the cell shape, cytoskeletal structure and metabolism which could have altered the chondrocytes behavior. However, since the pellets were cultured in differentiation medium, which should induce the normal chondrocyte phenotype, another possible explanation could be the lack of external stimuli. It is known that the presence of mechanical loading enhances the matrix biosynthesis by the chondrocytes and thus, a static 3D culture might not provide the cells with the necessary cues for the production of all the cartilage components (O'Conor et al. 2013).

##### Evaluation of the sGAGs deposition

A very small amount of sGAGs (around 4%) was detected at day 0 in both the graded and the homogeneous scaffolds with no significant difference between the groups' values. This falsely positive measurement can be attributed the background staining of the Alginate hydrogel due to its structural similarity with the GAGs (Shomura 2011) and to detection errors of the extraction algorithm, and the image thresholding. At day 14, a significant difference ( $p < 0.01$ ) between the amount of sGAGs in the graded and the amount of sGAGs in the homogeneous scaffolds was detected. This observation leads to the conclusion that the chondrocytes, which are embedded in the scaffolds with biomimetic cell density (graded scaffolds), have started to actively produce sGAGs within the first two weeks after bioprinting, and the produced amount of sGAGs is significantly larger compared to the amount of the homogeneous group. Finally, at day 25, the percentage of sGAGs on the slice area increased slightly since day 14, for both the graded and the homogeneous scaffolds, - possibly due to the effect of time - but this increase was not considered

significant. A significant difference was, however, detected between the graded and homogeneous sGAGs percentages, with the graded scaffolds exhibiting a significantly higher deposition of sGAGs. Overall, the total sGAG amount produced during the course of the experiment (from day 0 to day 25) was significant for the graded scaffolds, even though the production between days 14 - 25 took place at a slower rate than that between day 0 and day 14. On the other hand, the total amount of sGAGs from day 0 to day 25 was not significant for the homogeneous scaffolds, despite a small increase in sGAGs deposition between days 14-25.

Regarding the specific sGAG deposition between the zones of the scaffolds, a negligible amount of sGAGs was detected in every zone of both the graded and the homogeneous scaffolds at day 0 (these amounts can be attributed to background staining as mentioned above). At day 14, the bottom and middle zones of the graded scaffolds showed no signs of sGAGs deposition, since the sGAGs percentages remained very low and almost constant for both zones. This result is in line with the overall observations of the H&E analysis in which, after day 14, the cells of the middle zone had migrated to the adjacent zones and the cell density difference between the bottom and the middle zone was non-existent. However, the sGAGs deposition in the top zone exhibited a significant difference compared to the amount of sGAGs of the other zones and this difference is proportional to the difference in cell density between the top zone and the other two zones. It can, therefore, be concluded that cell density appears to have a significant effect on sGAGs deposition by chondrocytes, since the top zone, which had practically 3 times higher cell density than the other zones, produced 27 times more sGAGs than them. On the other hand, the homogeneous scaffolds did not appear to have deposited a significant amount of sGAGs until day 14. Finally, at day 25, there is a significant difference in the amount of sGAGs between the bottom-top and middle-top zones of the graded scaffolds, indicating that sGAGs were deposited in a graded manner.

Unfortunately, the gradient did not follow a three-zone distribution pattern, due to the fact that the average cell density of the middle zone decreased significantly during the course of the second experiment, and that, in turn, caused a decrease of the sGAGs deposition in this zone. Based on the above, it is clear that the sGAGs deposition is directly proportional to the cell density. This conclusion comes in agreement with the results of a previous study according to which culture of Collagen II scaffolds with a cell density gradient distribution, resulted in a gradient distribution of ECM in the constructs (Ren et al. 2016). The researchers observed that tissue formation (i.e. sGAG, Collagen II, and PRG4) was enhanced in the superficial zone, where the cell density was higher, and decreased with depth (Ren et al. 2016). Regarding the tissue formation of the homogeneous scaffolds, they do not appear to have produced significant amounts of sGAGs and a reason for that is the lower cell density of the constructs. According to previous findings, high cell density stabilizes the chondrocyte phenotype to a greater extent than low seeding density, in which enhanced de-differentiation is observed, due to cell spreading (Webb et al. 2017). In addition to that, the low sGAGs deposition of the homogeneous scaffolds could also be attributed to the micro-environment of the scaffolds, which is not biomimetic, as it is for the graded scaffolds. The missing biological cues due to the uniform cell density may have caused

cells to “sense” that they are not located within cartilage tissue, and thus, to alter their biological functions of ECM production.

### Evaluation of the Collagen Deposition

Moving on to the Collagen deposition, the statistical analysis of the samples showed no significant amount of Collagens produced in either by the graded, or the homogeneous scaffolds during the course of the 25 days of the experiment. This result was somewhat expected, since the histological analysis of the pellets revealed no Collagen production by the chondrocytes in the 3D environment. This could be attributed to a lack of mechanical stimuli, or change in the morphology of the cells, due to reasons mentioned in the “Cell type selection – Cell culture” paragraph. However, most of the studies which have reported neo-cartilage formation on their scaffolds, have observed simultaneous production of sGAGs and Collagen, concentrated in the zone with the highest cell density and decreasing with depth (Ren et al. 2016), which comes in contrast with our findings. The sGAG deposition pattern seems to be followed by Collagen, after day 14, without however any of the Collagens amount to be significant in the scaffolds. Even though the addition of ascorbic acid in the differentiation medium has been widely utilized to increase Collagen synthesis by chondrocytes, in our study it did not have the expected results.

The difference between previous studies reporting a gradient ECM distribution formed by a cell density gradient distribution, and our study, lies in the fact that this is the first study, to our knowledge, to generate a cell density gradient using cell distribution patterns with human chondrocytes, and thus, it is possible that some cellular mechanisms (related to donor characteristics or cell-cell communication) have inhibited the Collagen deposition and have caused an absence of Collagen despite the abundance sGAGs (Asnaghi et al. 2018).

Summarizing the results of our study, the three-zone cell density gradient was achieved in 3 mm thick scaffolds using extrusion bioprinting. Moreover, this three-zone gradient was maintained for 28 days, for all samples (N=2), when they were cultured in the absence of ascorbic acid, but was not maintained in the majority of the scaffolds after day 14, when they were cultured in differentiation medium with ascorbic acid. Instead, in this case, the gradient was transformed into a two-zone gradient regarding both the cell density, and the sGAGs deposition. This observation comes in contrast with previously reported results demonstrating the maintenance of the three-zone gradient in Collagen II hydrogels for 28 days (Ren et al. 2016). However, the same study used 6 mm thick scaffolds and 0.4 mm thick printing layers in order to generate and maintain the gradient, because their previous attempts with 3 mm thick scaffolds had failed due to the fusion of the zones during bioprinting (Ren et al. 2016).

## 4.4 Limitations of the Study – Future Recommendations

Cartilage engineering has been widely investigated, with different scaffold generation techniques being combined with different biomaterials, and multiple cell types, to achieve optimal results. However, there are still questions to be answered and approaches to be explored, before complete cartilage regeneration is achieved.

The bioprinting of a relative-sized cartilage scaffold with a cell density gradient is a project that could be the first step in providing more insight about the way cells communicate and produce matrix while in a biomimetic environment. The completion of this project entailed important limitations and required making several compromises regarding the factors affecting the generation and functionality of the constructs. A deeper understanding of these limitations can allow for a just discussion of the results and a clearer path towards future advancements.

First, the use of chondrocytes may not be translational in clinical use due to their scarcity and phenotypic instability. Other cell types, such as MSCs, might be a more viable choice. Second, the use of an alginate/nanocellulose hydrogel may not be the best option for bioprinted cartilage scaffolds, due to the absence of important components of the ECM cartilage, such as Collagen and Hyaluronic Acid, which provide structural and chemical cues to the cells for increased tissue synthesis. Decellularized ECM could be another very promising biomimetic biomaterial, since it maintains the micro-architecture of the native tissue and alleviates the risk of infections or rejection from the patient. Moreover, the static conditions under which the scaffolds were cultured are not representative of the physiological environment of the native cartilage. The lack of mechanical and/or chemical stimulation down-regulates gene expression of the markers which signal the production of cartilage. An important future advancement on this study would be the use of a bioreactor for the dynamic culture of the bioprinted scaffolds. Bioreactors allow for optimized incubation conditions that mimic the actual physiological conditions of the human body, for a faster and better quality ECM production. In addition, further investigation of the mechanical behavior of the constructs under shear stress, as well as under cycling loading would provide information about the behavior of the constructs under more relative/relevant conditions. Another limitation of the current study is the fact that during generation of the scaffolds only one gradient was applied to them. In the case of a fully functional cartilage scaffold, which could be implanted into the patients' bodies, a more biomimetic approach should be followed and that includes the generation of multiple gradients within the scaffolds, at the same time. A biomimetic distribution of zonal marker proteins and growth factors, for example, could assist this endeavor. An additional advancement, for similar future studies, would be the morphological analysis of the chondrocytes while in the 3D printed scaffold. The use of transfected fluorescent chondrocytes could make their detection and imaging within the scaffolds easier and would enable their phenotypic analysis. Finally, instead of the low resolution extrusion-based system that was used in this study, and affected the dimensions of the printed objects, new methods (such as MEW) should be tested to reinforce the hydrogels and tune the scaffolds' mechanical properties to those of the native cartilage. An interesting trend is the incorporation of a fourth dimension (time) in bioprinting to fabricate dynamic 3D architectures that can change their shapes under various stimuli by employing stimuli-responsive materials ([Wan et al. 2020](#)).

# 5. Conclusion

3D bioprinting of scaffolds has been receiving increasing attention recently, due to its exciting potential for engineered tissue development. Despite the fact that many studies have achieved gradient properties between the scaffold's zones the generation of a cell density gradient has not been investigated in depth. In the present study, we have demonstrated the generation of a biomimetic cell density gradient in relative-thickness scaffolds, with the use of extrusion-based bioprinting. The study aimed to match the mechanical properties of the generated scaffolds to those of the native cartilage and to investigate the biological effects of the cell density gradient on matrix biosynthesis. In order to do that, a PCL-enhanced Alginate/nanocellulose hydrogel was mixed with human articular chondrocytes to achieve three different final concentrations of cells. The different concentrations were used to bioprint two types of constructs: one with a cell density gradient (bottom zone:  $5 \times 10^6$  cells/ml, middle zone:  $10 \times 10^6$  cells/ml, top zone:  $20 \times 10^6$  cells/ml), and a second with a homogeneous cell distribution ( $10 \times 10^6$  cells/ml) for the comparison of the biological effects of the gradient. The results of the study showed that a distinct three-zone cell distribution was established in the 3 mm thick scaffolds, after bioprinting, but was transformed into a two-zone gradient during the course of 25 days due to cell migration. This gradient distribution of cell density resulted in a gradient ECM distribution, in which the total ECM production was positively correlated with the cell density. These findings can shed some light on the effects of zonal gradients in cell-cell signaling and behavior, regarding neo-cartilage synthesis, and assist in addressing the remaining obstacles, in order to accelerate the translation of cartilage bioengineering into clinical practice.

# Bibliography

- [1] Ahern B. J., Parvizi J., Boston R., Schaer T. P. Preclinical animal models in single site cartilage defect testing: A systematic review, *Osteoarthritis and Cartilage* 17(6), (2009), 705–713.
- [2] Aliabouzar M., Lee S., Zhou X., Zhang G. L., Sarkar K. Effects of scaffold microstructure and low intensity pulsed ultrasound on chondrogenic differentiation of human mesenchymal stem cells. *Biotechnology and Bioengineering*, 115(2), (2017), 495-506.
- [3] Ansari S., Khorshidi S., Karkhaneh A., Engineering of gradient osteochondral tissue: From nature to lab, *Acta Biomaterialia* 87, (2019), 41-54.
- [4] Antich C., de Vicente J., Jiménez G., Chocarro C., Carrillo E., Montañez E., Gálvez-Martín P., Marchal J. A. Bio-inspired hydrogel composed of hyaluronic acid and alginate as a potential bioink for 3D bioprinting of articular cartilage engineering constructs, *Acta Biomaterialia*, 106, (2020), 114-123.
- [5] Apelgren P., Amoroso M, Lindahl A, Brantsing C, Rotter N, Gatenholm P., Kölby L. Chondrocytes and stem cells in 3D-bioprinted structures create human cartilage in vivo. *PLOS ONE* 12(12), (2017), e0189428.
- [6] Arganda-Carreras I., Kaynig V., Rueden C., Eliceiri K. W., Schindelin J., Cardona A., Seung H.S., Trainable Weka Segmentation: a machine learning tool for microscopy pixel classification. *Bioinformatics*, 33 (15), (2017), 2424–2426.
- [7] Asnaghi M. A., Duhr R., Quasnichka H., Hollander A. P., Kafienah W., Martin I., Wendt D. Chondrogenic differentiation of human chondrocytes cultured in the absence of ascorbic acid. *Journal of Tissue Engineering and Regenerative Medicine* 12(6), (2018), 1402-1411.
- [8] Ávila H. M., Schwarz S., Rotter N., Gatenholm P. 3D bioprinting of human chondrocyte-laden nanocellulose hydrogels for patient-specific auricular cartilage regeneration, *Bioprinting* 1–2, (2016), 22-35.
- [9] Awad H.A., W. M. Chondrogenic differentiation of adipose-derived adult stem cells in agarose, alginate, and gelatin scaffolds. *Biomaterials*, 25(16), (2014), 3211-3222.
- [10] Axpe E., M. O. Applications of Alginate-Based Bioinks in 3D Bioprinting. *International journal of molecular sciences*, 17(12), (2016). E1976.
- [11] Barbero A., Grogan S., Schäfer D., Heberer M., Mainil-Varlet P., Martin I. Age related changes in human articular chondrocyte yield, proliferation and post-expansion chondrogenic capacity. *Osteoarthritis and Cartilage*, 12(6), (2004), 476-484.
- [12] Basmacıyan L., Azas N., Casanova M. Calcein+/PI- as an early apoptotic feature in Leishmania. *PLoS ONE* 12(11), (2017), e0187756.
- [13] Beck E. C., Detamore M. S., Nanomaterials for hard–soft tissue interfaces, in, *Nanomater. Tissue Eng.* (2013) 363–386.

- [14] Bentley G., Biant L.C., Vijayan S., Macmull S., Skinner J.A., Carrington R.W. Minimum ten-year results of a prospective randomised study of autologous chondrocyte implantation versus mosaicplasty for symptomatic articular cartilage lesions of the knee. *J Bone Jt Surg Br.* 94, (2012), 504–509.
- [15] Betsch M., Cristian C., Lin Y. Y., Blaeser A., Schöneberg J., Vogt M., Buhl E. M., Fischer H., Duarte-Campos D. F. Incorporating 4D into Bioprinting: Real-Time Magnetically Directed Collagen Fiber Alignment for Generating Complex Multilayered Tissues. *Advanced Healthcare Materials.*7(21), (2018), e1800894.
- [16] Bittner S. M., Guo J. L., Melchiorri A., Mikos A. G. Three-dimensional printing of multilayered tissue engineering scaffolds. *Materials today,* 21(8), (2017), 861-874.
- [17] Boschetti F., Pennati G., Gervaso F., Peretti G. M., Dubini G., Biomechanical properties of human articular cartilage under compressive loads, *Biorheology* 41, (2004), 159-66.
- [18] Bracaglia L. G., Smith B. T., Watson E., Arumugasaamy N., Mikos A. G. 3D printing for the design and fabrication of polymer-based gradient scaffolds. *Acta Biomaterialia,* 56, (2017), 3-13.
- [19] Brittberg M., Lindahl A., Nilsson A., Ohlsson C., Isaksson O., Peterson L., Treatment of deep cartilage defects in the knee with autologous chondrocyte transplantation, *N Engl J Med,* 331(14), (1994), 889-895.
- [20] Castilho M., Hochleitner G, Wilson W, Van Rietbergen B., Dalton P. D., Groll J., Malda J., Ito K. Mechanical behavior of a soft hydrogel reinforced with three-dimensional printed microfiber scaffolds. *Scientific Reports* 8(1), (2018), 1245.
- [21] Chang R., Nam J., Sun W. Effects of dispensing pressure and nozzle diameter on cell survival from solid freeform fabrication-based direct cell writing. *Tissue Engineering, part A,* 14(1), (2008), 41-48.
- [22] Chen D. X. B. Extrusion Bioprinting of Scaffolds for Tissue Engineering Applications, Chapter 3: Biomaterials for Bioprinting, *Springer Nature Switzerland AG* 2019.
- [23] Chen L., Deng C., Li J., Yao Q., Chang J., Wang L., Wu C. 3D printing of a lithium-calcium-silicate crystal bioscaffold with dual bioactivities for osteochondral interface reconstruction. *Biomaterials,* 196, (2018), 138-150.
- [24] Chu C. R., Szczodry M., Bruno S. Animal Models for Cartilage Regeneration and Repair. *Tissue Engineering Part B Reviews* 16(1), (2010), 105-15.
- [25] Daly A. C., Freeman F. E., Gonzalez-Fernandez T., Critchley S. E., Nulty J., Kelly D. J. 3D Bioprinting for Cartilage and Osteochondral Tissue Engineering. *Advanced Healthcare Materials.* 6(22), (2017), 10.1002/adhm.201700298.
- [26] Daly A. C., Critchley S. E., Rencsok E. M., Kelly D. J. A comparison of different bioinks for 3D bioprinting of fibrocartilage and hyaline cartilage. *Biofabrication.* 8(4), (2016), 045002.
- [27] Datta, P., Dhawan, A., Yu, Y., Hayes, D., Gudapati, H., & Ozbolat, I. T. Bioprinting of osteochondral tissues: A perspective on current gaps and future trends. *International Journal of Bioprinting,* 3(2), (2017), 109-120.
- [28] De Caro F, Bisicchia S, Amendola A, Ding L. Large fresh osteochondral allografts of the knee: a systematic clinical and basic science review of the literature. *Arthroscopy* 31, (2015), 757-765.

- [29] Desimone E., Schacht K., Jungst T., Groll J., Scheibel T., Biofabrication of 3D constructs: fabrication technologies and spider silk proteins as bioinks. *Pure and Applied Chemistry*. 87(8), (2015).
- [30] Disease GBD, Injury I, Prevalence C. Global, regional, and national incidence, prevalence, and years lived with disability for 354 diseases and injuries for 195 countries and territories, 1990-2017: a systematic analysis for the Global Burden of Disease Study 2017. *Lancet* 392(10159), (2018), 1789-1858.
- [31] Du M., Chen B., Meng Q., Liu S., Zheng X., Zhang C., Wang H., Li H., Wang N., Dai J. 3D bioprinting of BMSC-laden methacrylamide gelatin scaffolds with CBD-BMP2-collagen microfibers. *Biofabrication*, 7(4), (2015), 044104.
- [32] Du Y., Liu H., Yang Q., Wang S., Wang J., Ma J., Noh I., Mikos A. G., Zhang S. Selective laser sintering scaffold with hierarchical architecture and gradient composition for osteochondral repair in rabbits. *Biomaterials*, 137, (2017), 37-48.
- [33] Ducheyne P., Healy K., Hutmacher D.W., Grainger D.W., Kirkpatrick J. Cartilage Tissue Engineering, *Compr. Biomater.* 1, (2008), 201.
- [34] Fang M., Noiseux N., Linson E., Cram P. The Effect of Advancing Age on Total Joint Replacement Outcomes, *Geriatr Orthop Surg Rehabil.* 6(3), (2015), 173–179.
- [35] Farquharson C., Berry J. L., Mawer E. B., Seawright E., Whitehead C. C. Ascorbic acid-induced chondrocyte terminal differentiation: the role of the extracellular matrix and 1,25-dihydroxyvitamin D. *European Journal of Cell Biology* 76, (1998), 110-118.
- [36] Fox A. J. S., Bedi A., Rodeo S. A., The basic science of articular cartilage: structure, composition, and function, *Sports Health.* 1, (2009), 461–468.
- [37] Foyt D. A., Norman M. D. A., Yu T., Gentleman E. Exploiting Advanced Hydrogel Technologies to Address Key Challenges in Regenerative Medicine, *Advanced Healthcare Materials* 7(8), (2018).
- [38] Fröhlich M., Malicev E., Gorenssek M., Knezevic M., Velikonja N. K. Evaluation of rabbit auricular chondrocyte isolation and growth parameters in cell culture. *Cell Biology International* ,31(6), (2007), 620-625.
- [39] Gao F., Xu Z., Liang Q., Liu B., Li H., Wu Y., Zhang Y., Lin Z., Wu M., Ruan C., Liu W. Direct 3D Printing of High Strength Biohybrid Gradient Hydrogel Scaffolds for Efficient Repair of Osteochondral Defect. *Advanced Functional Materials*, 28(13), (2018).
- [40] Gagne, T.A., Chappell, Afonso, K., Johnson, J.L., McPherson, J.M., Oldham, C.A., Tubo, R.A., Vaccaro, C. and Vasios, G.W. Enhanced proliferation and differentiation of human articular chondrocytes when seeded at low cell densities in alginate In Vitro . *J. Orthop. Res.*, 18 (2000), 882-890.
- [41] Getgood A., Bhullar T. P. S., Rushton N. Current concepts in articular cartilage repair, *Orthopaedics and Trauma*, 23(3), (2009), 189-200.
- [42] Gillogly S. D., Voight M., Blackburn T., Treatment of articular cartilage defects of the knee with autologous chondrocyte implantation, *J Orthop Sports Phys Ther*, 28 (4), (1998), 241-251.
- [43] Gopinathan J., Noh I. Recent trends in bioinks for 3D printing. *Biomaterials research*, 22(11), (2018).

- [44] Guimarães C. F., Gasperini L., Marques A. P., Reis R. L. The stiffness of living tissues and its implications for tissue engineering. *Nat Rev Mater* 5(1), (2020), 351-370.
- [45] Guo T., Lembong J., Zhang L. G., Fisher J. P. Three-Dimensional Printing Articular Cartilage: Recapitulating the Complexity of Native Tissue. *Tissue Engineering: Part B*, 23(3), (2017).
- [46] Guo T., Ringel J. P., Lim C. G., Bracaglia L. G., Noshin M., Baker H. B., Powell D. a., Fisher J. P. Three dimensional extrusion printing induces polymer molecule alignment and cell organization within engineered cartilage. *Journal of biomedical materials research, Part A*, 106(8), (2018), 2190-2199.
- [47] Hall, A.C. The Role of Chondrocyte Morphology and Volume in Controlling Phenotype—Implications for Osteoarthritis, Cartilage Repair, and Cartilage Engineering. *Curr Rheumatol Rep* 21(38), (2019).
- [48] Haene R., Qamirani E., Story R. A., Pinsker E., Daniels T. R. Intermediate outcomes of fresh talar osteochondral allografts for treatment of large osteochondral lesions of the talus. *The Journal of bone and joint surgery*, 94(12), (2012), 1105-1110.
- [49] Huang C.Y., Reuben P. M., D' Ippolito G., Schiller P.C., Cheung H. S. Chondrogenesis of human bone marrow-derived mesenchymal stem cells in agarose culture. *The anatomical record. Part A, discoveries in molecular, cellular and evolutionary biology*, 278(1), (2004), 428-436.
- [50] Huber M., Trattng S., Lintner F. Anatomy, biochemistry, and physiology of articular cartilage. *Investigative Radiology*, 35(10), (2000), 573-580.
- [51] Hunziker E. B., Quinn T. M., Hauselmann H. J. Quantitative structural organization of normal adult human articular cartilage. *Osteoarthritis Cartilage*, 10, (2002) 564–72.
- [52] Ibusuki S., Papadopoulos A., Ranka M. P., Halbesma G. J. , Randolph M. A., Redmond R. W., Kochevar I. E., Gill T. J. Engineering cartilage in a photochemically crosslinked collagen gel. *Journal of knee surgery*, 22(1), (2009), 72-81.
- [53] Iwasa J, Ochi M, Uchio Y, et al. Effects of cell density on proliferation and matrix synthesis of chondrocytes embedded in atelocollagen gel. *Artificial Organs*. 27(3), (2003), 249-255.
- [54] James S. L., Abate D., Abate K. H., Abay S. M., ... Global, regional, and national incidence, prevalence, and years lived with disability for 354 diseases and injuries for 195 countries and territories, 1990–2017: a systematic analysis for the Global Burden of Disease Study 2017, *The Lancet*, 392(10159), (2018), 1789-1858.
- [55] Jensen E. C. Quantitative analysis of histological staining and fluorescence using ImageJ. *Anat Rec (Hoboken)*. 296(3), (2013), 378-381.
- [56] Jeon O, Alt D. S., Linderman S. W., Alsberg E. Biochemical and physical signal gradients in hydrogels to control stem cell behavior. *Advanced Materials*, 25(44), (2013), 6366-6372.
- [57] Jiang Y., Tuan R. S. Origin and function of cartilage stem/ progenitor cells in osteoarthritis. *Nature Reviews Rheumatology*, 11(4), (2015), 206–212.
- [58] Kačarević Ž. P., Rider P. M., Alkildani S., Retnasingh S., Smeets R., Jung O., Ivanišević Z., Barbeck M. An Introduction to 3D Bioprinting: Possibilities, Challenges and Future Aspects. *Materials (Basel)* 11(11), (2018), 2199.

- [59] Kang H. W., Lee S. J., Ko I. K., Kengla C., Yoo J. J., Atala A. A 3D bioprinting system to produce human-scale tissue constructs with structural integrity. *Nature Biotechnology*, 34, (2016), 312-319.
- [60] Katagiri H., Mendes L.F., and Luyten F.P.. Definition of a Critical Size Osteochondral Knee Defect and its Negative Effect on the Surrounding Articular Cartilage in the Rat, *Osteoarthritis Cartilage*. 25(9), (2017), 1531–1540.
- [61] Keriquel V., Oliveira H., Rémy M., Ziane S., Delmond S., Rousseau B., Rey S., Catros S., Amédée J., Guillemot F., Fricain J. C. In situ printing of mesenchymal stromal cells, by laser-assisted bioprinting, for in vivo bone regeneration applications. *Sci Rep*. 7(1), (2017), 1778.
- [62] Kim T.K., Sharma B., Williams C. G., Ruffner M. A., Malik A., McFarland E. G. and Elisseff J. H. Experimental Model for Cartilage Tissue Engineering to Regenerate the Zonal Organization of Articular Cartilage. *Osteoarthritis and Cartilage*, 11, (2003), 653–664.
- [63] Klein T.J., Rizzi S. C., Reichert J.C., Georgi N., Malda J., Schuurman W., Crawford R.W., Huttmacher D.W.. Strategies for Zonal Cartilage Repair using Hydrogels. *Macromolecular Bioscience*, 9, (2009), 1049-1058.
- [64] Klein T. J., Schumacher B. L., Schmidt T. A., Li K. W., Voegtline M. S., Masuda K., Thonar E. J.-M. A., Sah R. L. Tissue engineering of stratified articular cartilage from chondrocyte subpopulations. *Osteoarthritis Cartilage*.11(8), (2003), 595-602.
- [65] Lee J. S., J. H. 3D printing of composite tissue with complex shape applied to ear regeneration. *Biofabrication*, 6(1), (2014), 12.
- [66] Levato R, Webb W. R., Otto I. A., Mensinga A., Zhang Y., van Rijen M., van Weeren R., Khan I. M., Malda J. The bio in the ink: cartilage regeneration with bioprintable hydrogels and articular cartilage-derived progenitor cells. *Acta Biomaterialia*, 61, (2017), 41-53.
- [67] Li C., Faulkner-Jones A., Dun A. R., Jin J., Chen P., Xing Y., Yang Z., Li Z., Shu W., Liu D., Duncan R. R. Rapid Formation of a Supramolecular Polypeptide–DNA Hydrogel for In Situ Three-Dimensional Multilayer Bioprinting. *Angewandte Chemie International Edition*, 54(13), (2015), 3957-3961.
- [68] Lukanina K. I., Grigoriev T. E., Krashennikov S. V., Mamagulashvili V. G., Kamyshinsky R. A., Chvalun S. N. Multi-hierarchical tissue-engineering ECM-like scaffolds based on cellulose acetate with collagen and chitosan fillers. *Carbohydrate Polymers*, 191(1), (2018), 119-126.
- [69] Mandrycky C., Wang Z., Kim K., Kim D. H.. 3D bioprinting for engineering complex tissues. *Biotechnology Advances*. 34(4), (2016), 422-434.
- [70] Markstedt K, Mantas A, Tournier I, Martínez Ávila H, Hägg D, Gatenholm P. 3D Bioprinting Human Chondrocytes with Nanocellulose-Alginate Bioink for Cartilage Tissue Engineering Applications. *Biomacromolecules*. 16(5), (2015), 1489-1496.
- [71] Medvedeva, E. V., Grebenik, E. A., Gornostaeva, S. N., Telpuhov, V. I., Lychagin, A. V., Timashev, P. S., & Chagin, A. S. (2018). Repair of damaged articular cartilage: Current approaches and future directions. *International Journal of Molecular Sciences*, 19(8). Artn 2366
- [72] Mesallati T., Sheehy E. J., Vinardell T., Buckley C.T., Kelly D.J. Tissue Engineering Scaled-up, Anatomically Shaped Osteochondral Constructs For Joint Resurfacing. *European Cells and Materials*, 30, (2015), 163-186.

- [73] Monzón, M., Liu, C., Ajami, S., Oliveira M., Donate R., Ribeiro V., Reis R. L. Functionally graded additive manufacturing to achieve functionality specifications of osteochondral scaffolds. *Bio-Design and Manufacturing*, 1, (2018), 69-75.
- [74] Mouser V. H. M., Levato R., Mensinga A., Dhert W. J. A., Gawlitta D., Malda J. Bio-ink development for three-dimensional bioprinting of hetero-cellular cartilage constructs, *Connective Tissue Research*, 61(2), (2020), 137-151.
- [75] Mouw J. K., Case N. D., Guldborg R. E., Plaas A. H. K., Levenston M. E., Variations in matrix composition and GAG fine structure among scaffolds for cartilage tissue engineering. *Osteoarthritis and Cartilage* 13(9), (2005), 828-836.
- [76] Müller M, Öztürk E, Arlov Ø, Gatenholm P, Zenobi-Wong M. Alginate Sulfate-Nanocellulose Bioinks for Cartilage Bioprinting Applications. *Ann Biomed Eng.* 45(1), (2017), 210-223.
- [77] Murphy S.V., Atala. A. 3D bioprinting of tissues and organs. *Nature Biotechnology*, 32(8), (2014), 773–785.
- [78] Neuman M. G., Nanau R. M., Oruña-Sanchez L., Coto G.. Hyaluronic acid and wound healing. *Journal of pharmacy and pharmaceutical sciences*, 18(1), (2018), 53-60.
- [79] Nguyen, D., Hägg, D. A., Forsman, A., Ekholm J., Nimkingratana P., Brantsing C., Kalogeropoulos T., Zaunz S., Concaro S., Brittberg, M. Lindahl A., Gatenholm P., Enejder A., Simonsson S. Cartilage Tissue Engineering by the 3D Bioprinting of iPS Cells in a Nanocellulose/Alginate Bioink. *Scientific Reports* 7, (2017), 658.
- [80] Nooaeid P., Salih V., Beier J. P., Boccaccini A. R. Osteochondral tissue engineering: scaffolds, stem cells and applications, *J. Cell Mol. Med.* 16(10), (2012), 2247–2270.
- [81] Nowicki M. A., Castro N. J., Plesniak M. W., Zhang L. G. 3D printing of novel osteochondral scaffolds with graded microstructure. *Nanotechnology*, 27(41), (2016).
- [82] Nukavarapu S. P., Dorcenus D.L. Osteochondral tissue engineering: current strategies and challenges. *Biotechnol Adv.* 31(5), (2013), 706-721.
- [83] O’Connell G., Garcia J., Amir J. 3D Bioprinting: New Directions in Articular Cartilage Tissue Engineering. *ACS Biomater. Sci. Eng.* 3(11), (2017), 2657–2668.
- [84] O’Conor C. J., Case N., Guilak F. Mechanical regulation of chondrogenesis. *Stem Cell Research & Therapy* 4(4), (2013), 61.
- [85] Omelyanenko, N. P., Karalkin, P. A., Bulanova, E. A., Koudan, E. V., Parfenov, V. A., Rodionov, S. A., ... Mironov, V. A. Extracellular matrix determines biomechanical properties of chondrospheres during their maturation in vitro. *Cartilage.* (2018), 1947603518798890.
- [86] Panwar, A.; Tan, L.P. Current Status of Bioinks for Micro-Extrusion-Based 3D Bioprinting. *Molecules* 21, (2016), 685.
- [87] Parak A., Pradeep P., du Toit L.C., Kumar P., Choonara Y. E., Pillay V. Functionalizing bioinks for 3D bioprinting applications, *Drug Discovery Today* 24(1), (2019), 198-205.
- [88] Pati F., Cho D. W. Bioprinting of 3D Tissue Models Using Decellularized Extracellular Matrix Bioink. *Methods in Molecular Biology*, 1612, (2017), 381-390.

- [89] Peterson L., Brittberg M., Kiviranta I., Akerlund E.L., Lindahl A. Autologous chondrocyte transplantation. Biomechanics and long-term durability, *Am J Sports Med*, 30 (1), (2002), 2-12.
- [90] Pettit T., Kolvek T., Langworthy M. Cartilage damage: a review of surgical repair options and outcomes. *Physical Medicine and Rehabilitation Research*, 2(3), (2017), 1-10.
- [91] Quinn T.M., Häuselmann H.J., Shintani N., Hunziker E.B. Cell and matrix morphology in articular cartilage from adult human knee and ankle joints suggests depth-associated adaptations to biomechanical and anatomical roles, *Osteoarthr. Cart.* 21, (2013), 1904–1912.
- [92] Ren X., Wang F., Chen C., Gong X., Yin L., Yang L. Engineering zonal cartilage through bioprinting collagen type II hydrogel constructs with biomimetic chondrocyte density gradient. *BMC Musculoskeletal Disorders*, 17(1), (2016), p. 301.
- [93] Roseti L., Cavallo C., Desando G., Parisi V., Petretta M., Bartolotti I., Grigolo B. Three-Dimensional Bioprinting of Cartilage by the Use of Stem Cells: A Strategy to Improve Regeneration. *Materials (Basel.)*, 11(9), (2018), 1749.
- [94] Roseti L., Parisi V., Petretta M., Cavallo C., Desando G., Bartolotti I., Grigolo B. Scaffolds for Bone Tissue Engineering: State of the art and new perspectives. *Materials Science and Engineering C*, 78, (2017), 1246-1262.
- [95] Roseti, L., & Grigolo, B. Host environment: Scaffolds and signaling (Tissue Engineering) Articular Cartilage: Cells, Scaffolds, and Growth Factors. In: Gobbi A., Espregueira-Mendes J., Lane J., Karahan M. (eds), *Bio-Orthopaedics*, (2017), 87-103. Springer, Berlin, Heidelberg.
- [96] Rotbaum Y., Puiu C., Rittel D., Domingos M. Quasi-static and dynamic in vitro mechanical response of 3D printed scaffolds with tailored pore size and architectures. *Materials Science & Engineering C*, 96, (2019), 176–182.
- [97] Ruiz-Cantu L., Gleadall A., Faris C., Segal J., Shakesheff K., Yang J. Multi-material 3D bioprinting of porous constructs for cartilage regeneration. *Materials Science and Engineering: C*, (109), (2020), 110578.
- [98] Sakai S., Ohi H., Hotta T., Kamei H., Taya M. Differentiation potential of human adipose stem cells bioprinted with hyaluronic acid/gelatin-based bioink through microextrusion and visible light-initiated crosslinking. *Biopolymers*, 109(2), (2018).
- [99] Saris D.B., Vanlauwe J., Victor J., Almqvist K.F., Verdonk R., Bellemans J. Treatment of symptomatic cartilage defects of the knee: characterized chondrocyte implantation results in better clinical outcome at 36 months in a randomized trial compared to microfracture. *Am J Sports Med.* 37(1), (2009), 10s–19s.
- [100] Shepherd D., Seedhom B. Thickness of human articular cartilage in joints of the lower limb. *Annals of Rheumatic Diseases* 58(1), (1999), 27–34.
- [101] Shim J. H., Jang K. M., Hahn S. K., Park J. Y., Jung H., Oh K., Park K. M., Yeom J., Park S. H., Kim S. W., Wang J. H., Kim K., Cho D. W. Three-dimensional bioprinting of multilayered constructs containing human mesenchymal stromal cells for osteochondral tissue regeneration in the rabbit knee joint. *Biofabrication* 8(1), (2016), 014102.
- [102] Shomura Y. Advances in Composite Materials for Medicine and Nanotechnology, chapter 3: Natural polymers used in bone tissue engineering. Attaf B. (ed), *Technology and Engineering*, (2011), 40. Published by InTech, Croatia.

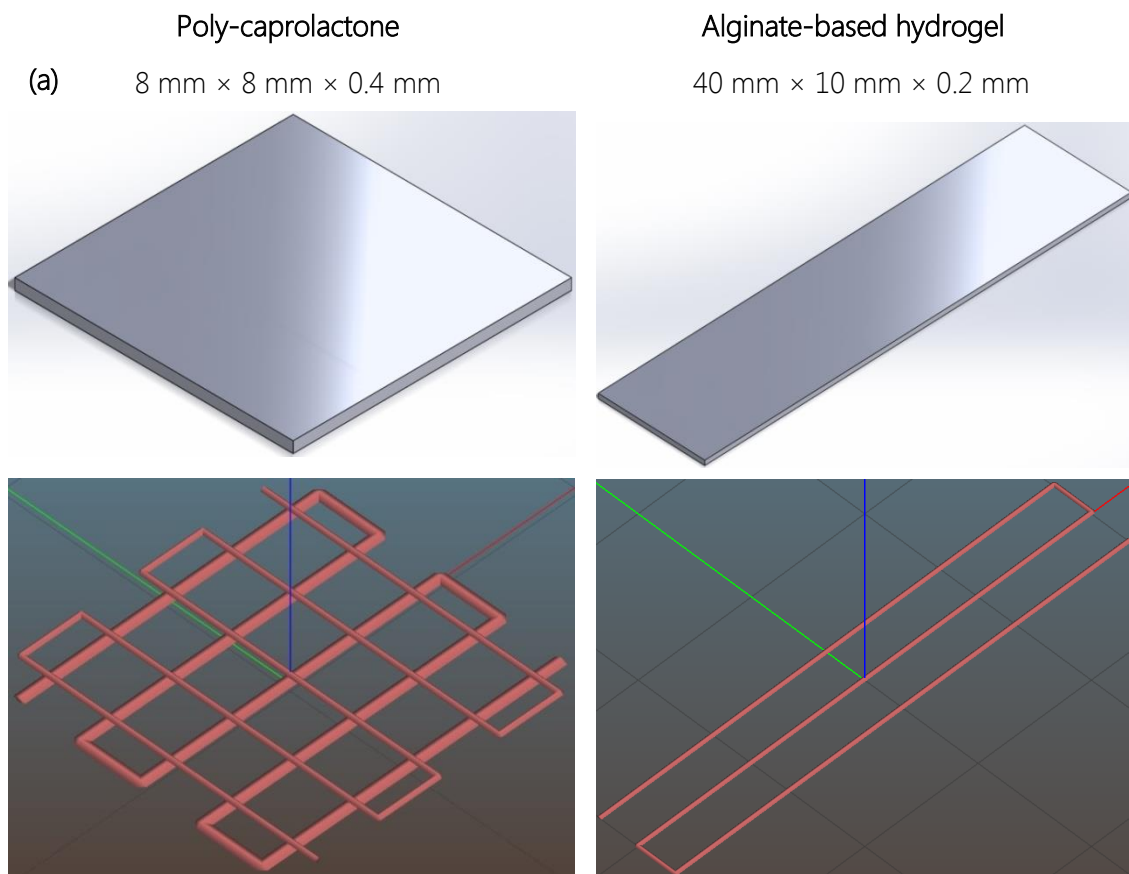
- [103] Temu T. M., Wu K. Y., Gruppuso P. A., Phornphutkul C. The mechanism of ascorbic acid-induced differentiation of ATDC5 chondrogenic cells. *Am J Physiol Endocrinol Metab* 299(2), (2010), E325–E334.
- [104] Theodoridis K., Aggelidou E., Vavilis T., Manthou M. E., Tsimponis A, Demiri E. C., Boukla A., Salpistis C., Bakopoulou A., Mihailidis A., Kritis A. Hyaline cartilage next generation implants from adipose-tissue-derived mesenchymal stem cells: Comparative study on 3D-printed polycaprolactone scaffold patterns. *J Tissue Eng Regen Med*.13(2), (2019), 342-355.
- [105] Unterman S.A., Matthew G., Lee J.H., Crist J., Chansakul T., B.S., Yang E.C., Elisseeff J.H. Hyaluronic Acid-Binding Scaffold for Articular Cartilage Repair. *Tissue Eng Part A*. 18(23-24), (2012), 2497–2506.
- [106] Van Assche D., Staes F., Van Caspel D., Vanlauwe J., Bellemans J., Saris D.B. Autologous chondrocyte implantation versus microfracture for knee cartilage injury: a prospective randomized trial, with 2-year follow-up. *Knee Surg Sports Traumatol Arthrosc.* 18, (2010), 486–495.
- [107] Vanlauwe J., Saris D.B., Victor J., Almqvist K.F., Bellemans J., Luyten F.P. Five-year outcome of characterized chondrocyte implantation versus microfracture for symptomatic cartilage defects of the knee: early treatment matters. *Am J Sports Med.* 39, (2011), 2566–2574.
- [108] Varady N. H., Grodzinsky A. J. Osteoarthritis year in review 2015: mechanics. *Osteoarthritis and cartilage*, 24(1), (2016), 27-35.
- [109] Wan Z., Zhang P., Liu Y., Lv L., Zhou Y. Four-dimensional bioprinting: Current developments and applications in bone tissue engineering, *Acta Biomaterialia* 101,(2020), 26-42.
- [110] Webb B., Doyle B. J., Parameter optimization for 3D bioprinting of hydrogels, *Bioprinting* 8, (2017), 8-12.
- [111] Yang J., Zhang Y. S., Yue K., Khademhosseini A. Cell-laden hydrogels for osteochondral and cartilage tissue engineering. *Acta Biomaterialia*, 57, (2017), 1-25.
- [112] Zhang L., Hu J., Athanasiou K. A., The role of tissue engineering in articular cartilage repair and regeneration, *Crit. Rev. Biomed. Eng.* 37, (2009), 1–57.
- [113] Zhou X., Castro N. J., Zhu W., Cui H., Aliabouzar M., Sarkar K., Zhang L. G. Improved Human Bone Marrow Mesenchymal Stem Cell Osteogenesis in 3D Bioprinted Tissue Scaffolds with Low Intensity Pulsed Ultrasound Stimulation. *Scientific Reports*, 6, (2016), 32876.

# APPENDIX A: Optimization of Printing Parameters

## Parameter Optimization of the PCL Framework

The BIO-X bioprinter has a maximum nozzle temperature of 250 °C for the thermoplastic nozzle, and a maximum pressure of 200 kPa (without the use of an external pump). From preliminary tests it was determined that a single PCL fiber could be printed in a continuous manner only when the print speed was smaller or equal to 5 mm/sec, for all different combinations of pressure and temperature. Finally, it was established that the best trade-off between speed and print quality, for the PCL, was given at 4 mm/sec and that was the speed chosen for the experiments. Taking into consideration the machine's capabilities, the preliminary tests for PCL, and the suggested parameter values provided by Cellink, the experimental conditions tested for the optimization study can be seen in Figure 21b. The corresponding designs used to test these conditions, are illustrated in Figure 21a, and the means strand measurements are presented in Table 10.

Based on the data from the graphs in Figure 23, the printed scaffold using 200 kPa and 210 °C conditions fulfils the requirements set for geometrical accuracy and constant thickness along the length of a printed fiber. Therefore, this combination of pressure and temperature, along with the 4 mm/sec speed, were selected for the printing of the PCL framework in the scaffolds.



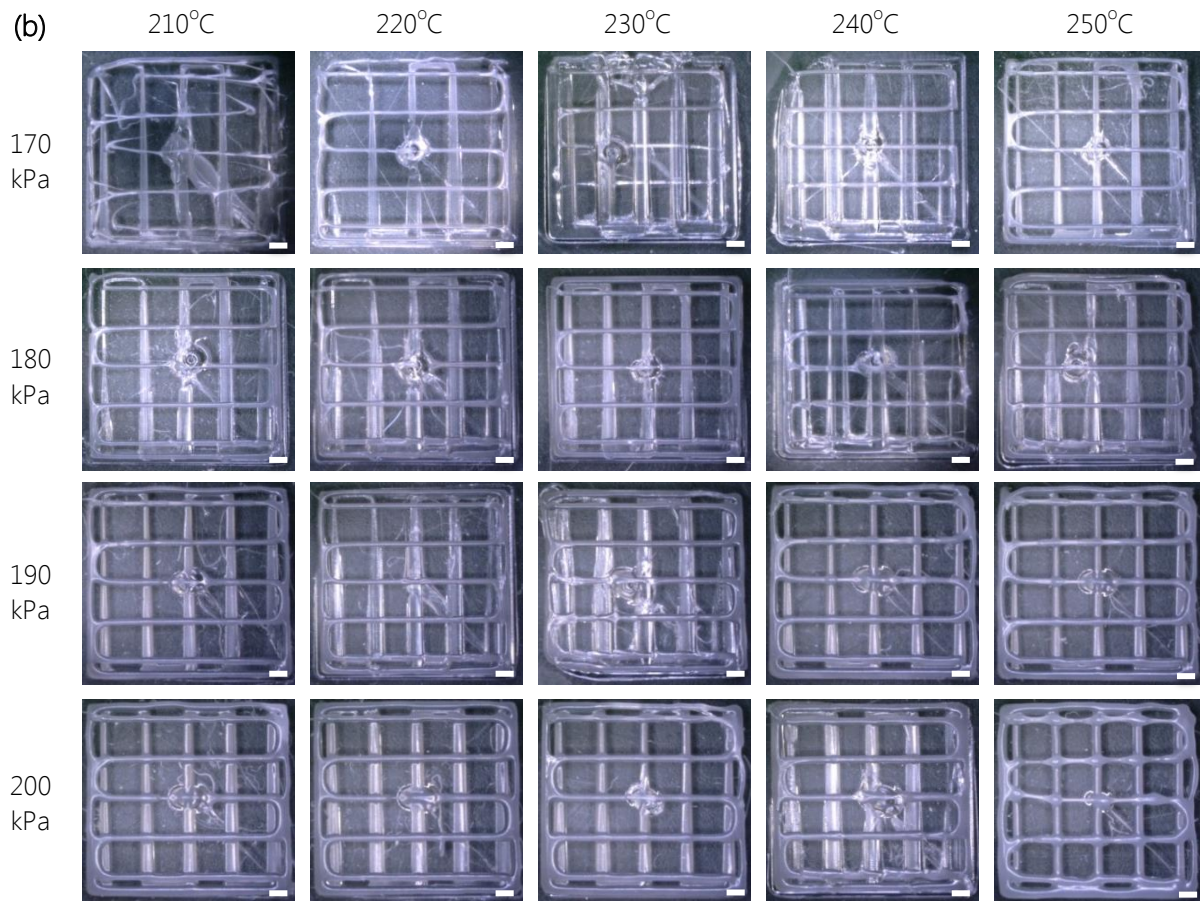


**Figure:** (a) The designs used for the optimization of the printing parameters for the PCL and the Alginate-based hydrogel, accordingly. (b) Images of the two-layered rectilinear PCL designs printed on a plastic petri-dish. The temperature ranged between 210 °C – 250 °C with a step of 10 °C and the pressure ranged from 170 kPa – 200 kPa with a step of 10 kPa. The constructs were designed with dimensions (l × w × h) = 10 mm × 10 mm × 0.4 mm and the layer height was set at 0.2 mm. The nozzle size and printing speed were set at Ø 0.2 mm and 4 mm/sec, respectively. All images were taken under the Keyence VHX-5000 microscope with the scale bar representing 1000 μm.

**Table:** Mean strand width ± sd measured for all configurations above, at a speed of 4 mm/sec. N/A denotes configurations that could not create adequate prints and the strand width shown in bold corresponds to the best configuration (geometrically accurate and uniform thickness along the fibers). The tested constructs were printed with a 0.2 mm nozzle. The highlighted value corresponds to the best condition as described above.

Pressure	210°C	220°C	230°C	240°C	250°C
170kPa	N/A	259.61 ± 34.21 μm	314.27 ± 51.50 μm	336.08 ± 57.10 μm	368.87 ± 63.83 μm
180kPa	210.12 ± 48.49 μm	269.35 ± 51.75 μm	316.53 ± 56.10 μm	349.78 ± 62.25 μm	375.33 ± 49.72 μm
190kPa	238.06 ± 73.60 μm	281.82 ± 66.40 μm	342.47 ± 47.97 μm	362.77 ± 63.46 μm	393.86 ± 45.35 μm
200kPa	<b>255.41 ± 47.10 μm</b>	315.82 ± 58.16 μm	357.00 ± 61.98 μm	403.59 ± 56.23 μm	437.42 ± 76.84 μm

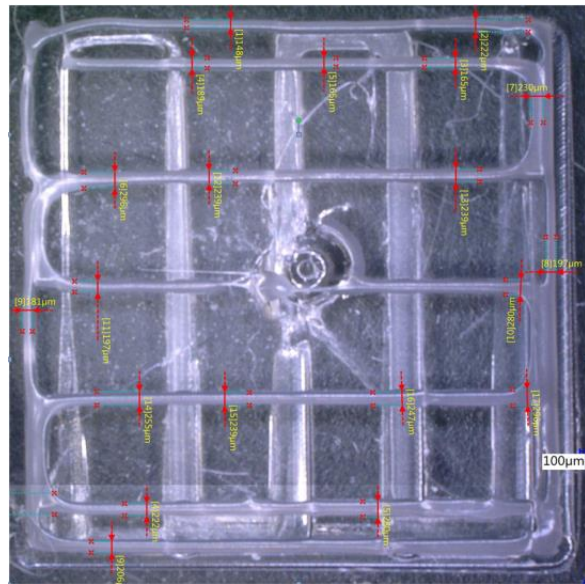
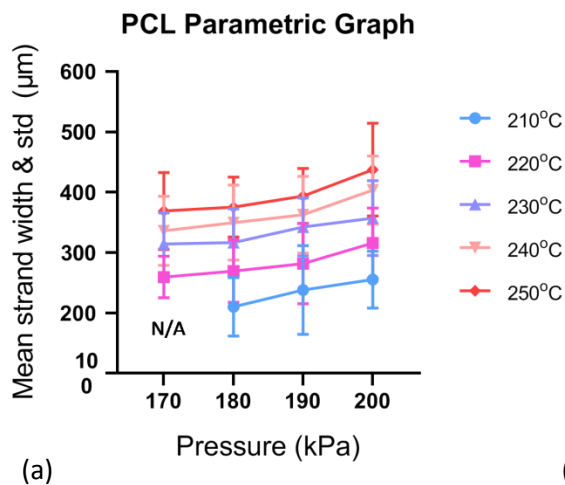


Figure: (a) Effect of pressure on the mean strand thickness of the PCL constructs, for different temperatures. The error bars show the standard deviation of each measurement. (b) Thickness measurement performed on 17 different points of a scaffold's fibers.

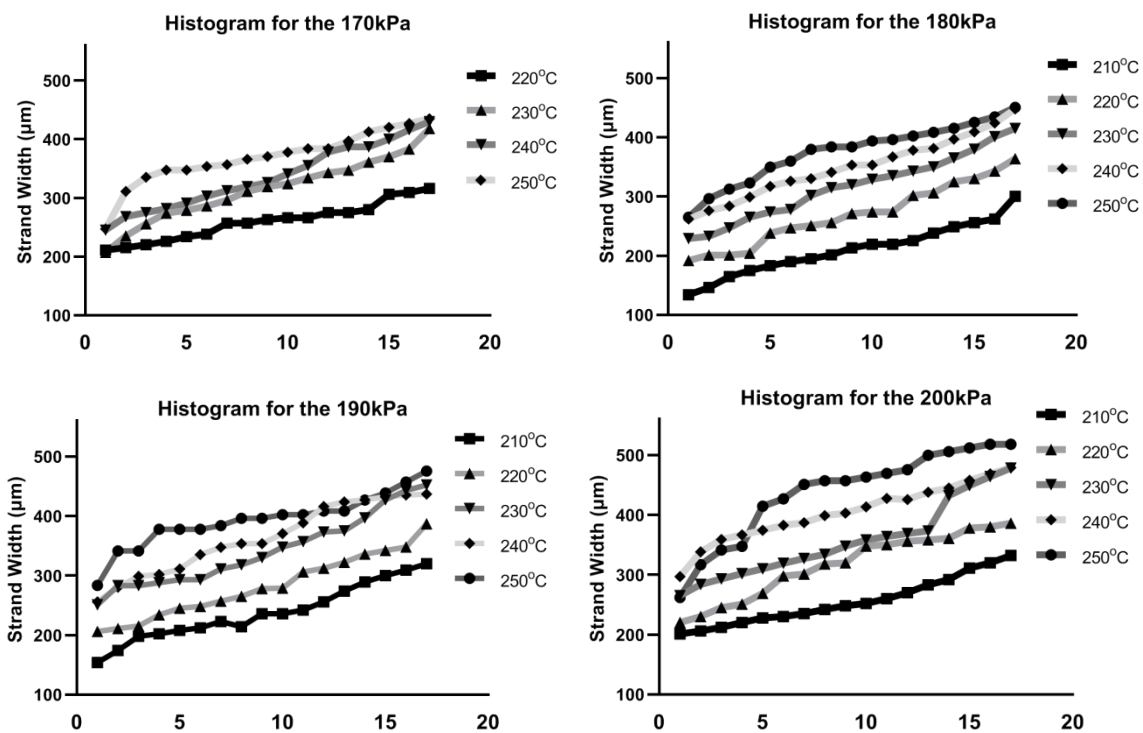


Figure: Each of the histograms includes 17 strand-thickness measurements of each of the constructs at a specific experimental condition (pressure, temperature). The histograms are grouped together according to the applied pressure during printing. The "best" condition is considered the one in which the thickness histogram remains as close to 200 µm as possible, and which remains almost constant across the measurements (small discrepancies between the thickness points).

## Parameter Optimization for the Alginate-based Hydrogel

It was determined that a single hydrogel fiber could be printed in a continuous manner only when the pressure was higher or equal to 12 kPa. Also, a 25 mm/sec and a 30 mm/sec speed could not always yield a continuous print when combined with a 12 kPa pressure. Based on the data from the Table 11 and Figure 24b, it is clear that the condition (12 kPa, 20 mm/sec) fulfils the requirements set for geometrical accuracy and constant thickness along the length of a printed strand. Therefore, this combination of pressure and speed, at room temperature speed, was selected for the printing of the alginate-based hydrogels in the scaffolds.

**Table:** Mean  $\pm$  sd of the measured strand width of all configurations tested for Bioink Cellink. The best configuration with the most accurate strand width is shown in bold. The tested constructs were designed with dimensions ( $l \times w \times h$ ) = 40 mm  $\times$  10 mm  $\times$  0.2 mm. The dimensions of the printed strands were measured after chemical crosslinking for 2'. All images were acquired with a Keyence VHX-5000 microscope.

Pressure	15mm/sec	20mm/sec	25mm/sec	30mm/sec
12kPa	698.77 $\pm$ 61.88 $\mu$ m	<b>638.40 <math>\pm</math> 66.22 <math>\mu</math>m</b>	632.68 $\pm$ 54.65 $\mu$ m	576.26 $\pm$ 30.17 $\mu$ m
15kPa	1089.66 $\pm$ 88.48 $\mu$ m	1867.08 $\pm$ 362.01 $\mu$ m	983.28 $\pm$ 163.80 $\mu$ m	952.34 $\pm$ 192.78 $\mu$ m
20kPa	2004.32 $\pm$ 205.60 $\mu$ m	1454.62 $\pm$ 193.85 $\mu$ m	1471.69 $\pm$ 151.37 $\mu$ m	1398.62 $\pm$ 150.01 $\mu$ m
25kPa	1281.54 $\pm$ 157.58 $\mu$ m	1814.76 $\pm$ 331.79 $\mu$ m	1357.57 $\pm$ 234.65 $\mu$ m	1592.34 $\pm$ 202.01 $\mu$ m
30kPa	2234.58 $\pm$ 224.58 $\mu$ m	2016.52 $\pm$ 360.55 $\mu$ m	1867.08 $\pm$ 96.10 $\mu$ m	1648.48 $\pm$ 278.52 $\mu$ m

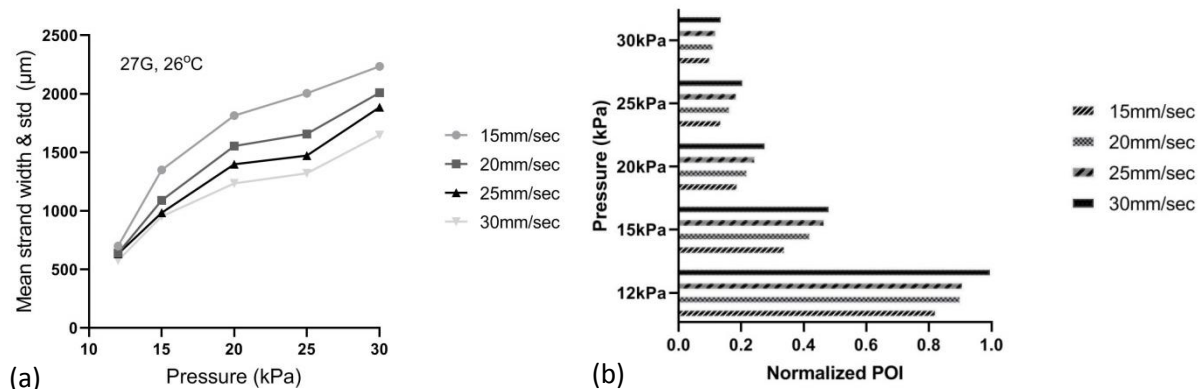


**Figure:** (a) Mean strand width vs. Pressure diagram of the Bioink Cellink for different printing speeds. All data were obtained using a 27G nozzle, at room temperature. Each data point is the mean of 14 measurements and for clarity the error bars are not shown. (b) Normalized POI for the combinations of printing parameters investigated for the Cellink Bioink.

# APPENDIX B: 2D Chondrocyte Culture

## Differentiation and Immunofluorescence results

The results showed that the re-differentiation of passage 3 CCs was achieved in 2D culture, after 10 days of in differentiation medium (Figure 28). The differentiated CCs, however, never reached the natural phenotype of passage 2 CCs (Figure 29). Collagen type II expression was also determined in the 2D *in vitro* culture. Chondrocytes were observed to deposit collagen type II from day 10 in chondrogenic conditions (Figure 30).

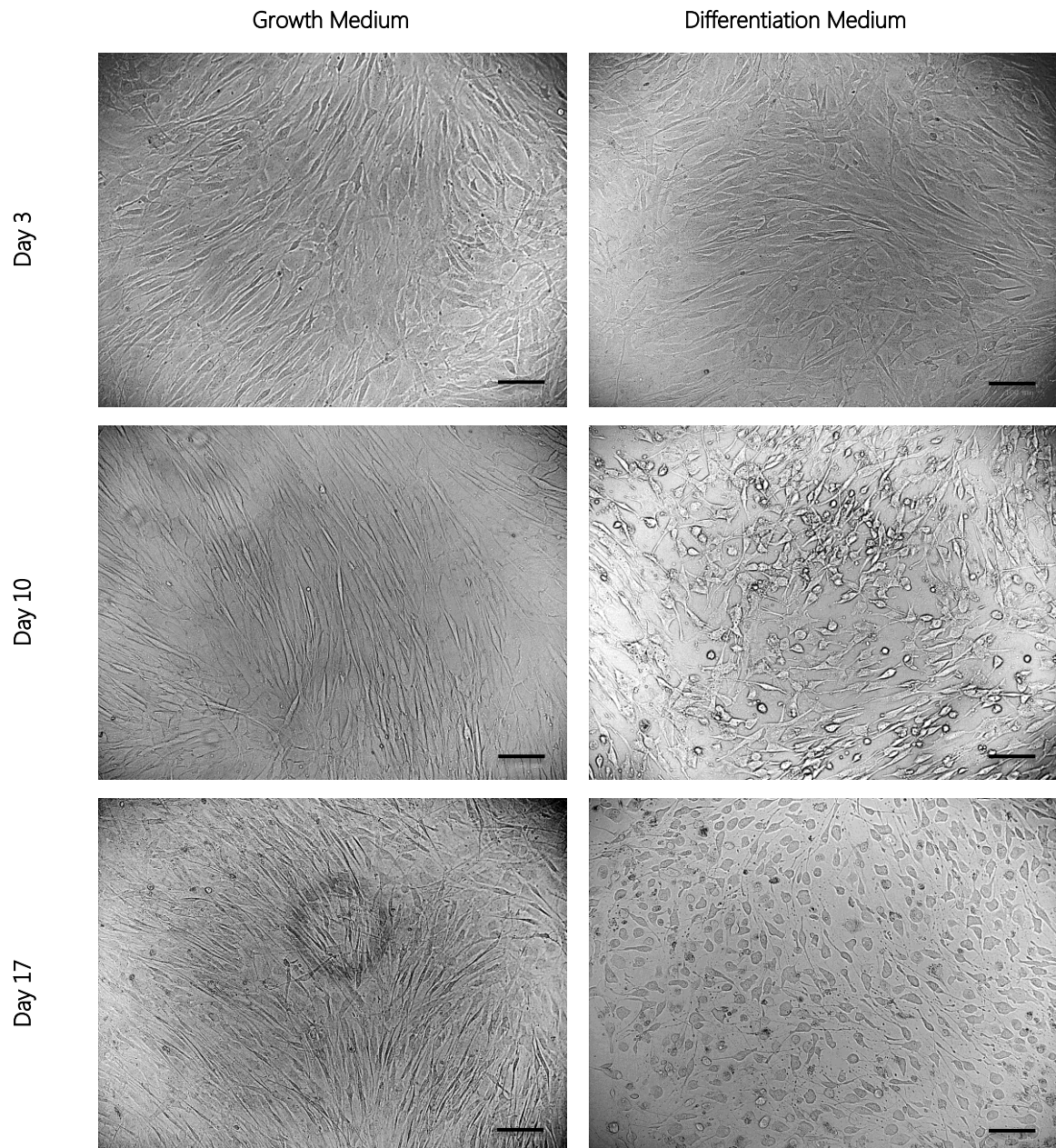


**Figure:** 2D culture of passage 3 chondrocytes cultured in growth and differentiation medium, respectively, for days 3, 5, 10 and 17. Scale bar = 100  $\mu$ m.

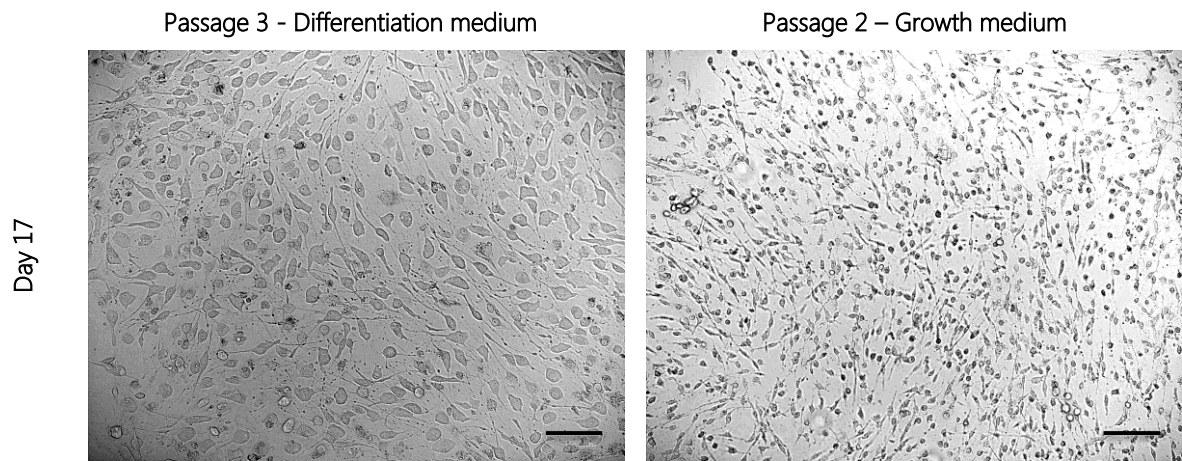


**Figure:** (Left image) 2D culture of passage-3 chondrocytes (re-differentiated) cultured in differentiation medium. (Right image) 2D culture of passage-2 (differentiated) chondrocytes cultured in growth medium. Even though the re-differentiation of passage 3 CCs is successful, there are still morphological differences between them and the lower passage CCs. The scale bar represents 100 $\mu$ m.

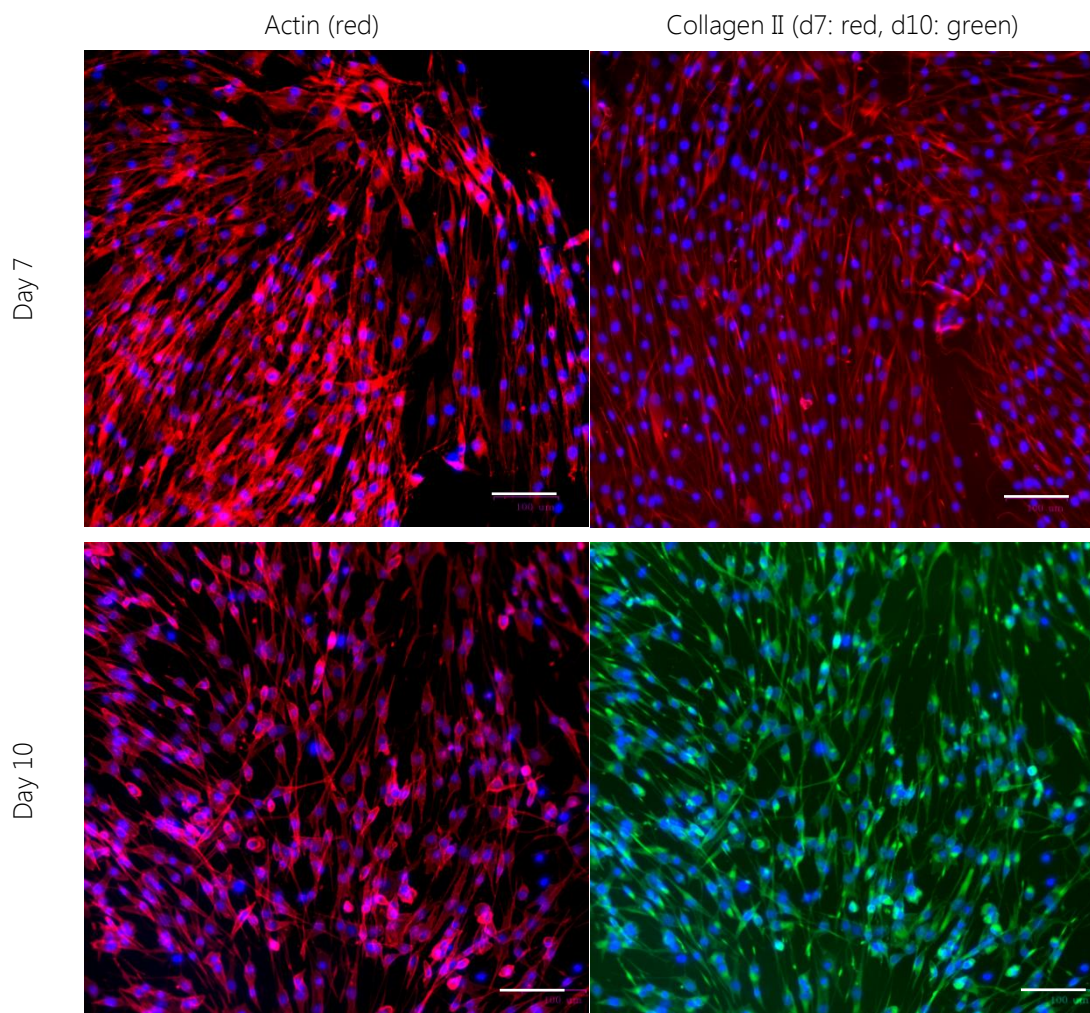


**Figure:** Immunofluorescent staining for Actin and Collagen II in 2D-cultured chondrocytes after 7 and 10 days of culture in differentiation medium (CDM) (without ascorbic acid). At the day 10 threshold (beginning of re-differentiation), chondrocytes still produce Collagen II (green). The scale bar represents 100 $\mu$ m.

# APPENDIX C: Comparison of the Scaffold's Designs

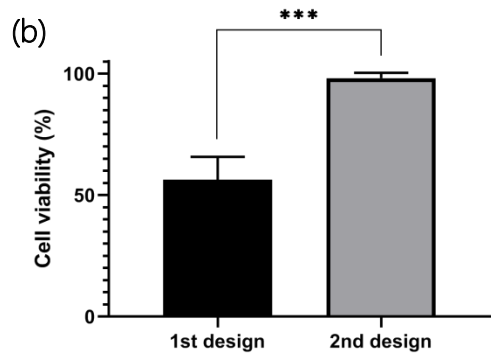
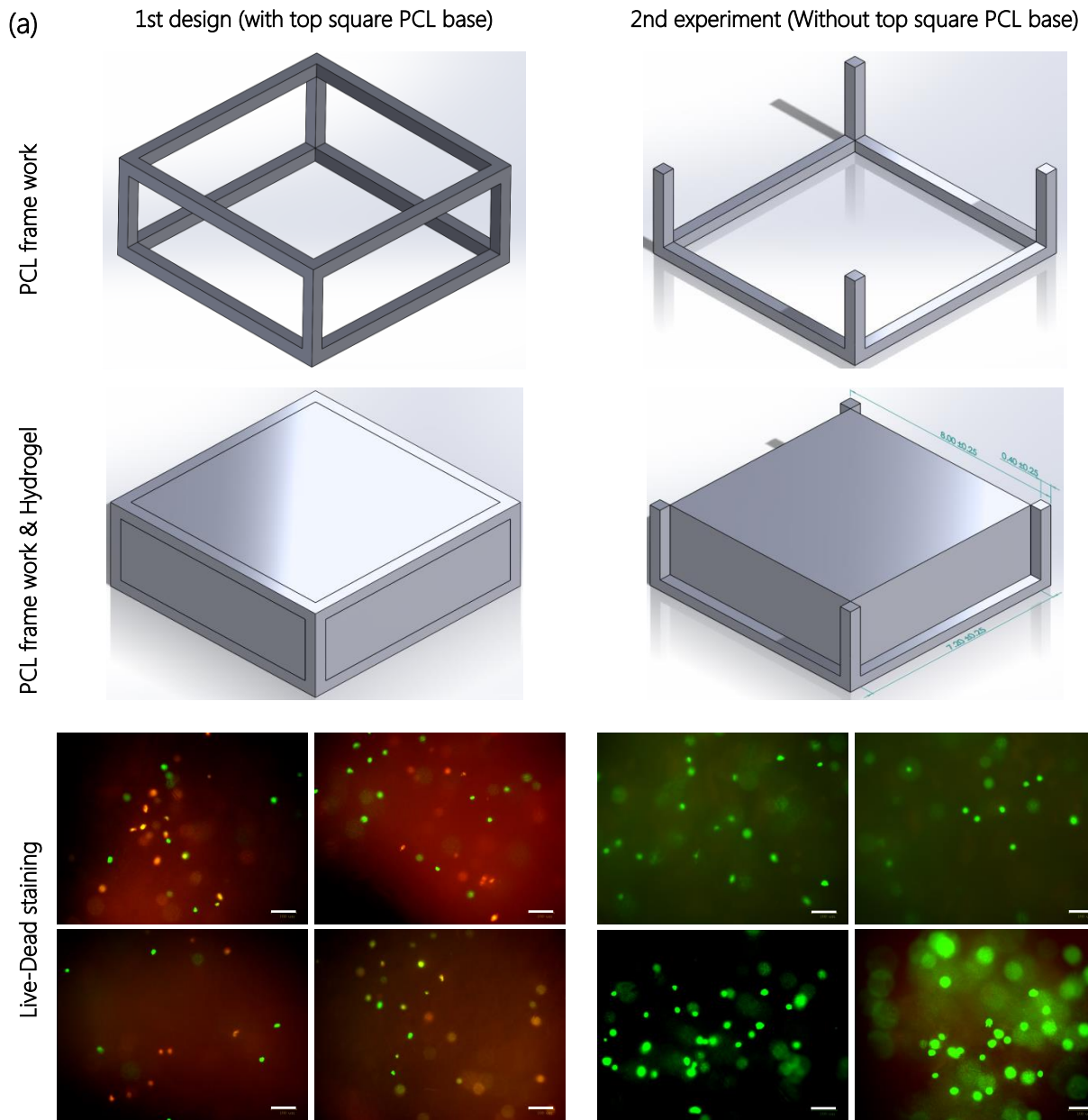


**Figure:** The two different designs tested for suitability for cartilage bioprinting. The assessment was performed based on the viability data of both scaffolds after bioprinting at day 0. The scale bars represent 100  $\mu$ m.

The best out of the two designs, separated in its individual parts, can be seen in detail in Figure 26.

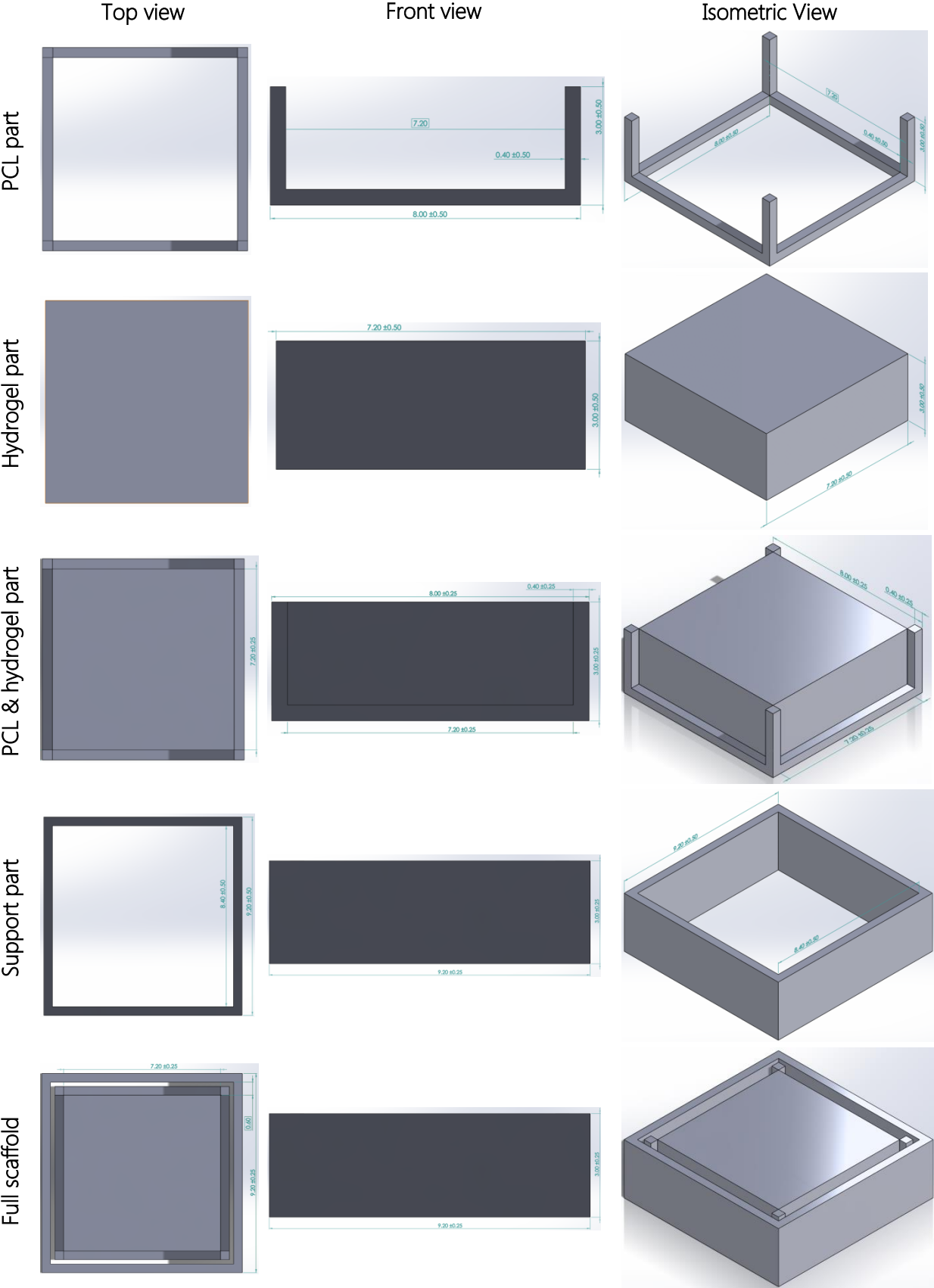


Figure: Designed parts (PCL, hydrogel, and support) and full scaffold in top, front, and isometric view.

## APPENDIX D: Images of the Bioprinted Scaffolds

Combining the design and slicing part, with the results of the optimization study and the preliminary cell experiments, the bioprinting of the cartilage scaffolds took place. Figure 31 shows the final bioprinted scaffolds.



Figure: Images of a batch of bioprinted scaffolds.

# APPENDIX E: Mechanical Characterization

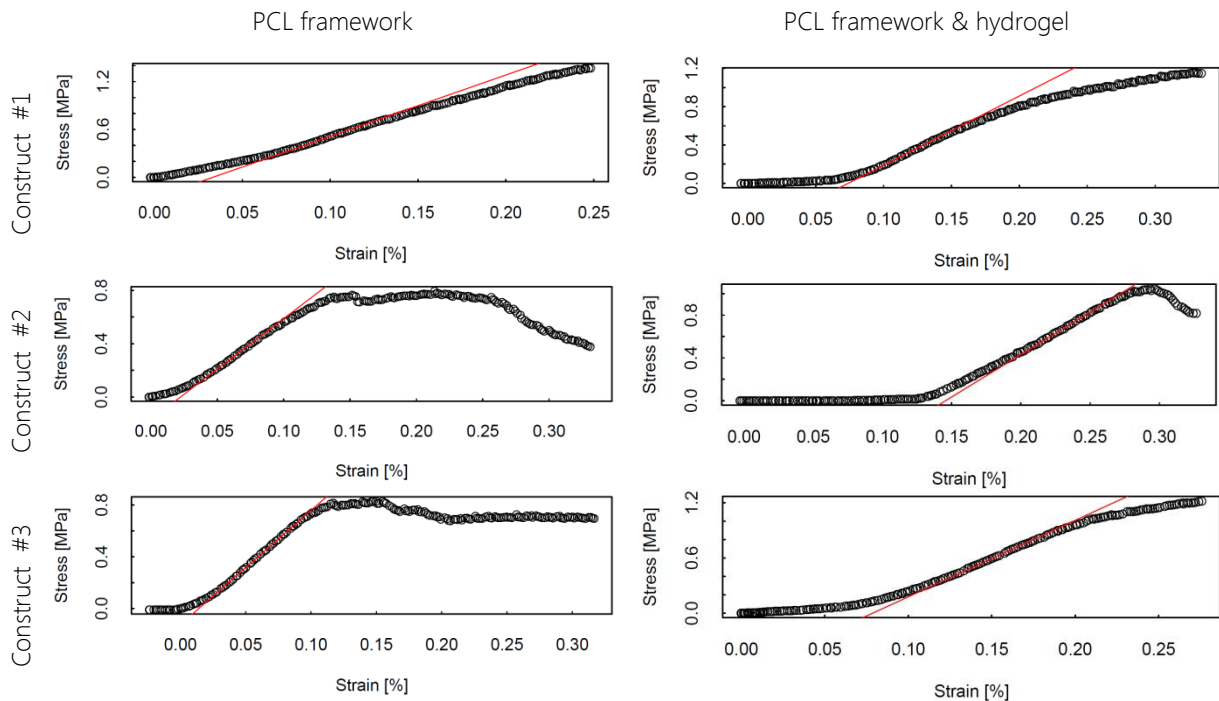
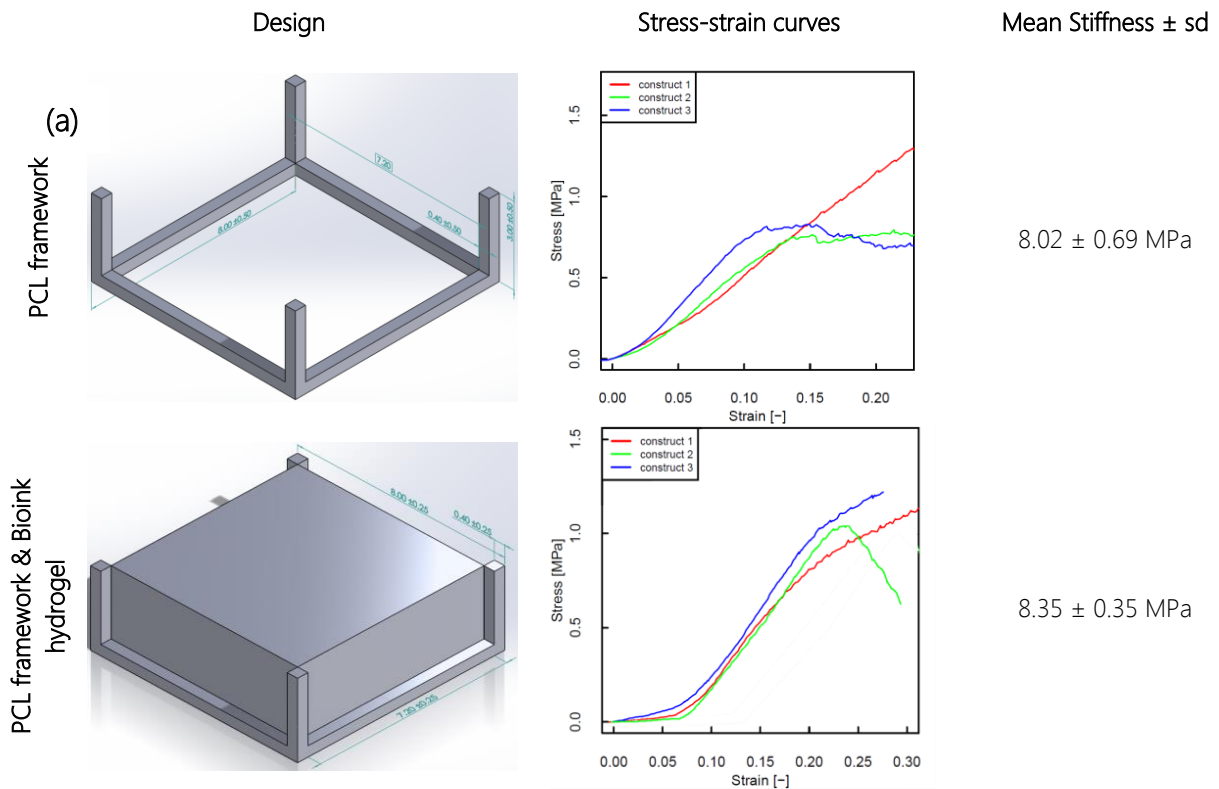


**Figure:** Graphical plots showing the Stress vs Strain for each individual construct of either the PCL framework, or PCL+hydrogel (n=3). Stiffness is calculated using the steepest line (red line) that fits the stress-strain data obtained by the compression test. The graphs were used to visually validate the stiffness calculation performed using the R code.